The Dissertation Committee for Hyun Jung Park

Certifies that this is the approved version of the following dissertation:

Interfacial properties of thin film hetero-structure:

Copper – Oxides of Hafnium-silicon

Committee:

John M. White, Supervisor

Dim Lee Kwong

Llewellyn K. Rabenberg

Russell D. Dupuis

John G. Ekerdt

Interfacial properties of thin film hetero-structure:

Copper – Oxides of Hafnium-silicon

by

Hyun Jung Park, B. S., M. S.

Dissertation

Presented to the Faculty of the Graduate School of

The University of Texas at Austin

in Partial Fulfillment

of the Requirements

for the Degree of

Doctor of Philosophy

The University of Texas at Austin

May, 2002

Dedication

For their patience, encouragement, and loving support, this dissertation is dedicated to my parents, parent-in-law, and my husband.

Acknowledgements

I extend my sincere gratitude to Dr. J. M. White. Dr. White has been an exceptional advisor, providing generous financial support, giving the opportunity for internship, and a splendid intellectual environment. It's been an honor to work with and to know him.

I would like to thank all of the members of the White group, present and past. Thanks to Yang-ming Sun for fruitful discussion and guidance in my work. Discussion, group meetings, and group seminar in our group have taught me to think critically about my data and know what questions to ask. I would like to thank Heyran Ihm for tutoring the basic UHV system, Qi Wang for solving instrument problems, Taeksoo Jeon and Jose Lozano for valuable discussion about my data.

I am at this point today because of the support of my entire family. I would like to thank my parent-in-law, sister-in-law, and brother-in-law for their love and encouragement. I especially like to thank brother who has always been a source of humor and friendship and my parent for their role in developing the person that I am today. In particular I would like to thank my father, who always encouraged me to study.

Finally, I would like to thank my husband. I thank him for thinking critically about issues that I was having and offering suggestions for

improvement. I thank him for his understanding and his emotional support, without which I may never have finished.

Interfacial properties of thin film hetero-structure:

Copper – Oxides of Hafnium-silicon

Publication No. _____

Hyun Jung Park, Ph. D.

The University of Texas at Austin, 2002

Supervisor: John M. White

This dissertation focuses on the properties of Cu / high-k oxide and high-k / Si (100) interfaces using surface analysis tools such as X-ray photoelectron spectroscopy (XPS), low-energy ion scattering (LEIS), transmission electron microscopy (TEM), and atomic force microscopy (AFM). In the first study, the growth and thermal annealing of Cu on HfO_2 surface were investigated using physical vapor deposition (PVD), *in-situ* XPS, *in-situ* LEIS, and *ex-situ* TEM. Growth of Cu on HfO_2 at 300 K involves initial formation of three-dimensional clusters without Cu oxidation. After thermal annealing at 673 K for 10 min, the Cu cluster size increases but there was no diffusion of Cu into the HfO_2 layer. STEM shows uniform Cu clusters (~11 nm diameter) after thermal annealing. The uniformity was attributed to self-limiting growth.

In the second study, the growth and thermal annealing of Cu on $HfSiO_4$ were studied using PVD, *in-situ* XPS, *in-situ* LEIS, and *ex-situ* AFM. Like Cu/HfO_2, the growth mode of Cu on $HfSiO_4$ at 300 K is three-dimensional. Using a CO_2 laser, the change of Cu morphology was monitored during thermal annealing by LEIS. During thermal annealing, Cu cluster size increased by combining small ones and Cu may diffuse into $HfSiO_4$ layer, although we do not have any evidence for the latter. AFM images of annealed samples show uniform diameter of Cu clusters.

In the third study, various compositions of hafnium silicide and hafnium silicate were formed on a Cu substrate, and the growth and thermal annealing of HfO_2 on Si (100) were studied using PVD, *in-situ* XPS and *in-situ* LEIS. At 300 K, there is no evidence for the formation of hafnium silicide at the interface between HfO_2 and Si (100). At 823 K, HfO_2 is thermodynamically stable upon contact with nonstoichiometric silicon oxide.

Table of Contents

List of Tables

List of Figures

CHAPTER 1

Introduction

1.1 BACKGROUND

1.1.1 Motivations for using HfO_2 and $HfSiO_4$ as gate dielectrics

As the CPU frequency of microprocessor increases, the device's vertical and lateral dimension have been shrunk with the scaling law to increase speed. According to International Technology Roadmap for Semiconductor (ITRS) '1999, for beyond 0.1 μm technology, the thickness of the gate dielectric needs to be very thin, below 10 Å equivalent oxide thickness (EOT), to get high drive current and low threshold voltage.

Silicon dioxide (SiO_2) has been used as the primary gate dielectric material in field-effect devices since 1957 due to good interface, low gate leakage currents, and excellent thermal (structural) stability at typical Si process temperatures. Since then, SiO_2 has been successfully scaled down for the device's high performance with much effort towards current technologies of 0.13 ~ 0.18 μm. It has been concluded that gate oxide scaling below 10 Å will be limited by direct tunneling currents, since the tunneling current (J) increases exponentially with decreasing physical thickness of SiO_2 [1]. Increased J could degrade standby-power dissipation, DRAM retention time, add to SRAM power consumption, offset designs of SRAM beta-ratio, reduce noise margin, and accelerate device degradation [2].

In addition to the tunneling current, thickness of control of SiO_2 is another issue, because SiO_2 of 10 Å physical thickness would be only three monolayers thick. Considering the manufacturing implications of producing devices having films with thickness on the order of a few monolayers, the variation of these films over a 200 nm or 300 nm silicon wafer is a substantial concern. A variation in thickness of only 1 Å could change the device operating conditions (capacitance), making it extremely difficult to maintain device margins [3].

Direct tunneling current (J) has the exponential relationship with the dielectric physical thickness (d), barrier height (Φ_B), and applied bias (V) as

$$J=\frac{A}{d^2}\cdot\left\{\left(\Phi_B-\frac{V}{2}\right)\cdot\exp\left(-B\cdot d\cdot\sqrt{\Phi_B-\frac{V}{2}}\right)-\left(\Phi_B+\frac{V}{2}\right)\cdot\exp\left(-B\cdot d\cdot\sqrt{\Phi_B+\frac{V}{2}}\right)\right\}$$

To reduce J, the most effect way is to use materials with higher dielectric constant (ε) than SiO_2 to increase the thickness while keeping high capacitance as

$$C=\frac{\varepsilon\cdot\varepsilon_o}{d}$$

Based on this idea, there are several proposed alternatives such as oxynitride and oxide/nitride stacks[4, 5], ferroelectric materials ($SrTiO_3$ and $Ba_xSr_{1-x}TiO_3$)[6, 7], and metal oxides such as Ta_2O_5[8], TiO_2[9], ZrO_2[10], HfO_2[11], Al_2O_3[12], Y_2O_3[13], and silicates ($HfSiO_4$ and $ZrSiO_4$)[14].

Among several candidates for a gate dielectric, HfO_2 is a promising candidate for replacement of SiO_2 because of its high dielectric constant up to 40, reasonable energy gap of 5.65 eV [15], and excellent thermal stability on Si. Additionally, HfO_2 has a lattice parameter similar to Si with small lattice misfit factor (<5 %) [16]. In the case of CVD HfO_2, the as-deposited film has an amorphous structure and starts to crystallize above 850^{o}C [17].

In addition to HfO_2 itself, $HfSiO_4$ has also been proposed for gate dielectrics because of its high dielectric constant (~11) and high thermal stability in direct contact with Si up to 1050 ^{o}C [14]. More importantly, in the case of CVD HfO_2, the possibility of forming an undesirable interfacial nonstoichiometric silicon oxide must be considered. If the structure contains several dielectrics in series, the lowest capacitance layer will dominate the overall capacitance and also set a limit on the minimum achievable EOT [1]. From the point of view of interfacial layer formation, $HfSiO_4$ has no undesirable interfacial layer. The study of interfaces between HfO_2 and Si is very important to learn how to control the interfacial layer formation and improve the EOT of dielectrics.

1.1.2 Motivations for using Cu as an interconnecting in ULSI structure

As chip size becomes smaller, the propagation delay time in a device is reduced. However, on-chip interconnect resistance capacitance (RC) delay becomes more important in determining chip performance and reliability. As interconnect feature sizes decrease and clock frequencies increase, RC time delays become the major limitation in achieving high circuit speeds [18]. To reduce RC delay, lower resistance metal and lower dielectric materials are being considered to replace current Al and SiO_2 interconnect materials. Among metals that have lower resistance than Al, Cu is promising since Cu interconnect lines have a high activation energy against electromigration, up to twice as large as that of aluminum [19].

Although Cu has advantages there are several critical issues. For examples, we need to obtain a high Cu deposition rate (> 250 nm/min), good step coverage, an optimum diffusion barrier and good adhesion. The study of the interface between Cu and diffusion barrier/gate dielectrics at the surface chemistry level will be very important to improve the adhesion in Cu-based metallization.

1.1.3 Wetting Criteria

When pure metal is grown on a pure oxide, we can decide whether the metal would, at equilibrium, form a continuous film on the oxide (i.e., wet the oxide) or form particles on the oxide surface characterized by some measurable contact angle between the metal/vacuum interface and the metal/oxide interface, where these two interfaces meet. "Wetting" is defined as the situation where the contact angle equals 0^o [20], i.e., spreading of a continuous multi-layer film.

The answer to whether wetting occurs at equilibrium lies in a comparison of the metal/oxide interfacial free energy, $\gamma_{m/ox}$, with the difference between the surface free energy of the clean oxide in vacuum, $\gamma_{v/ox}$, and that of the clean metal, $\gamma_{v/m}$. Fig. 1.1 shows the wetting criteria and three categories of hetero-epitaxy of the growth of metal films on oxide surfaces. If the metal wets the oxide, then $\gamma_{m/ox}$ is smaller than $\gamma_{v/ox} - \gamma_{v/m}$ at equilibrium and it is called "Frank- Van der Merwe (FM)" growth mode. If $\gamma_{m/ox}$ is almost equal to $\gamma_{v/ox} - \gamma_{v/m}$ at equilibrium, metal forms monolayer followed by three-dimensional particles. It is called "Stranski-Kranstanov (SK)" growth mode. If $\gamma_{m/ox}$ is larger than $\gamma_{v/ox} - \gamma_{v/m}$ at equilibrium, metal forms three-dimensional particles without intermediate monolayer and growth mode is called "Volmer-Weber (VW)" [21].

The interfacial free energy, $\gamma_{m/ox}$, includes any metal-oxide bonding as well as the bonding involves in any interfacial layers. All real interfacial energies γ are positive, and good bonding between the phases at the metal/oxide interface would lead to small positive values of $\gamma_{m/ox}$. Since the surface free energy of metals is usually larger than or comparable to that of oxides [22], for

wetting to occur, the metal/oxide interfacial free energy must be very small, or there must be very, good bonding at the metal/oxide interface.

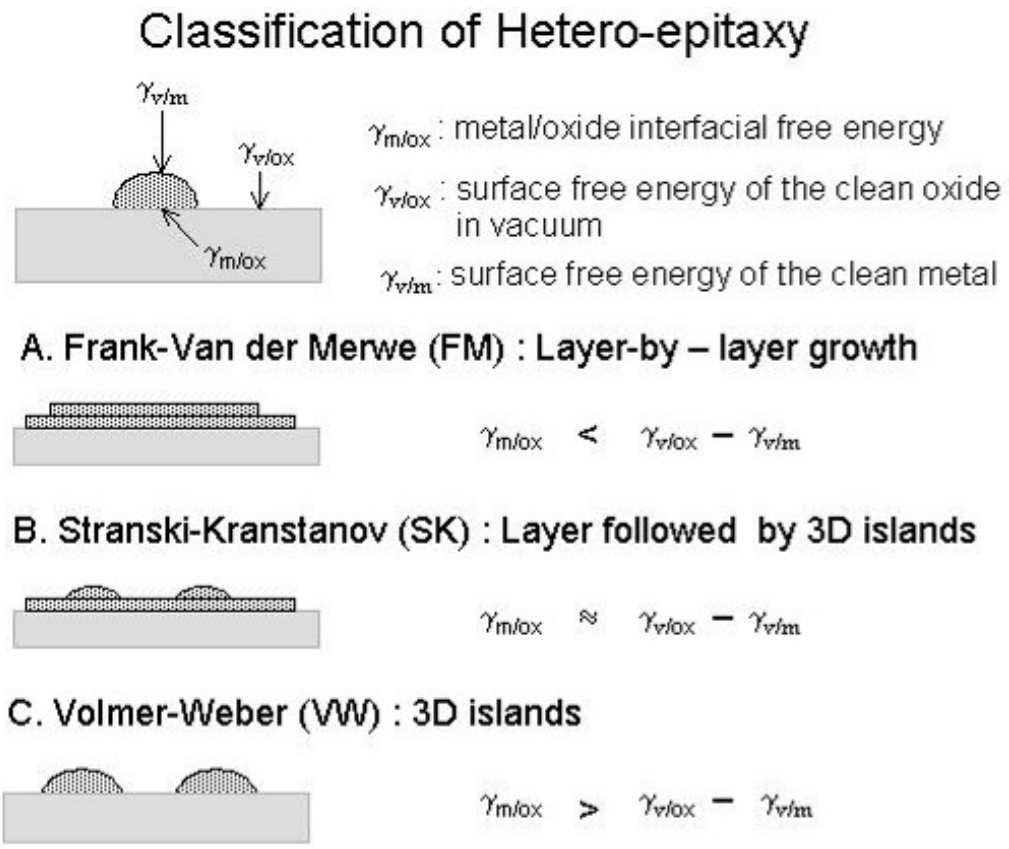

Fig. 1.1 The classification of hetero-epitaxy of the growth of metal film on oxide surface based on the wetting criteria.

1.2 EXPERIMENTAL

1.2.1 The system

Fig. 1.2 shows the schematic of the experimental system. The basic idea of the system is to perform the growth of sample and then to analyze the sample using one of the various instruments. Film growth is performed in the Chemical Vapor Deposition (CVD) chamber or the Physical Vapor Deposition Chamber (CVD). The samples are then transferred from CVD or PVD growth chamber to the analysis chamber equipped with X-ray Photoelectron Spectroscopy (XPS) and Low Energy Ion Scattering (LEIS). In addition, an external IR CO_2 laser is used to heat the sample inside analysis chamber so that we can perform XPS or LEIS during thermal annealing up to 400^{o}C under vacuum (~ 1×10^{-8} torr).

The PVD system is equipped with a main chamber, a load lock chamber, and three sputtering guns with one DC and two RF power supplies. The substrate could be heated to 773 K by a quartz lamp heater. The base pressure of the main chamber is ~ 5×10^{-8} torr). The sputtering is done with flowing, 20 sccm, ultrahigh purity Ar 99.999% that passed through a gas purifier prior to entering the chamber.

Once formed, the films were annealed in two ways. In the first, the sample was annealed in the CVD system using halogen lamp. The maximum temperature of sample was ~ 550^{o}C under vacuum (~ 1×10^{-6} torr). In this case, the sample was transferred from CVD chamber to analysis chamber after heating.

In the second method, sample was heated while in the analysis chamber by a continuous IR CO_2 laser. The laser beam entered the analysis chamber through a ZnSe mirror mounted on a flange at the bottom of the analysis chamber, was then reflected by a Cu total reflection mirror and irradiated the backside of the sample [23]. This in-situ thermal annealing make possible real time surface analysis at elevated temperatures.

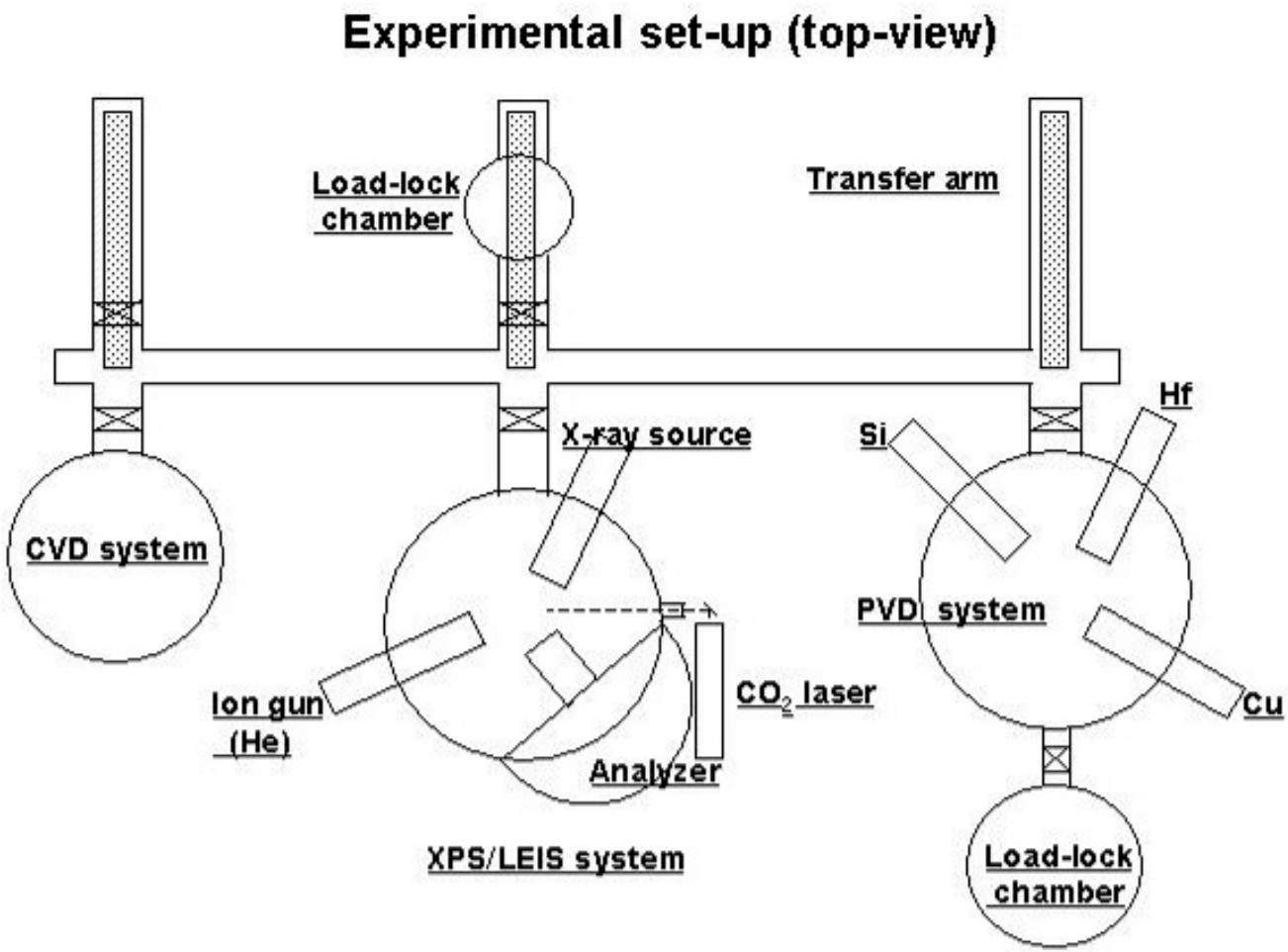

Fig.1.2 The schematic of the system

1.2.2 X-ray Photoelectron Spectroscopy (XPS)

Surface analysis by XPS is accomplished by irradiating a sample with monoenergetic soft x-rays and analyzing the energy of the detected electrons. Mg Kα (1253.6 eV) and Al Kα (1486.6 eV) x-rays are usually used. Fig. 1.3 shows how photoelectron is made by incident photon. These incident photons have limited penetrating power in a solid on the order of 1 –10 μm [24]. Detectable photoelectron interacts with atoms in the surface region (~ 70 Å), causing electrons to be emitted from core level orbital by the photoelectric effect. The emitted electrons have measured kinetic energies give by:

$$KE = h\nu - BE - \phi_s$$

where hν is the energy of the photon, BE is the binding energy of the atomic orbital from which the electron originates, and ϕ_s is the spectrometer work function.

The binding energy may be regarded as the energy difference between the initial and final states, the latter determined after the photoelectron has left the atom. The variety of kinetic energies of the emitted electrons corresponds to the variety of possible final states of the ions from each type of atom. Moreover, there is a different cross-section for each final state [24].

XPS can be used to identify and determine the concentration of the elements in the surface because each element has a unique set of binding energies and cross-section. Variations in the elemental binding energies (the chemical shifts) arise from differences in the chemical states.

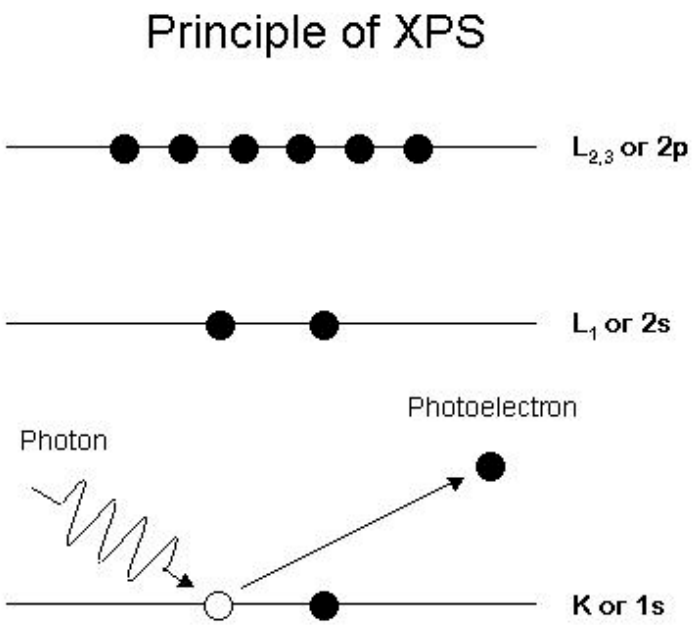

Fig. 1.3 The principle of XPS.

1.2.3 Low Energy Ion Scattering (LEIS)

Surface analysis by Ion Scattering Spectroscopy (ISS) is accomplished by elastic scattering of energetic ions at a the surface since the energy and angular distributions of scattered ions are a direct measure of the mass of atoms at the surface. There are two kinds of ISS according to the injection energy. If the energy of ion is larger than 10 keV, it is called medium energy ion scattering (MEIS). If the energy range of ion is from 100 eV to 10 keV, it is called low energy ion scattering (LEIS) [25]. LEIS is more surface sensitive than MEIS since LEIS has higher cross sections for the ion-mass interaction and high neutralization rate for noble-gas ion scattering [26].

In LEIS, ion surface scattering can be described by sequences of elastic two-body scattering events [26]. A single elastic-scattering event is determined by the energy transfer in the collision for a given scattering angle. Fig. 1. 4 shows the single-scattering geometry for laboratory system. Let us consider a hard-sphere collision between a primary particle with known mass M_1 and energy $E_o = 1/2M_1v_o^2$ and a surface atom at rest with mass M_2. After the collision into the scattering angle θ the final energy $E_1 = 1/2M_1v_1^2$ of the primary particle and the final energy $E_f = 1/2M_2v_2^2$ of the target are obtained from the conservation laws of energy and momentum (parallel and perpendicular to the direction of incidence):

$$1/2M_1v_o^2 = 1/2M_1v_1^2 + 1/2M_2v_2^2$$

$$M_1v_0 = M_1v_1\cos\theta + M_2v_2\cos\phi$$

$$0 = M_1v_1\sin\theta - M_2v_2\sin\phi$$

The elimination of the target-atom velocity components, i.e. recoil angle ϕ and recoil velocity ν_2 leads to an equation for the ratio of the primary particle velocities:

$$\nu_1 / \nu_o = (M_1 \cos\theta \pm \sqrt{M_2^2 - M_1^2 \sin^2\theta}) / (M_1 + M_2)$$

For comparison with the experimental data it is convenient to consider the energy ratio which be written after the substitution $A = M_2/M_1$

$$E_f/E_o = (\cos\theta \pm \sqrt{A^2 - \sin^2\theta})^2 / (1 + A)^2$$

For $A > 1$ only the plus sign applies while for $1 > A > \sin\theta$ both plus and minus are valid. Using the above equation, we can calculate E_f/E_o value of each mass ratio of incident ion to atom at the surface (A value) with fixed scattering angle θ.

Fig. 1. 5 shows that the geometry of LEIS in our system. Incident beam source is $^4He^+$ and the scattering angle θ is 115^o. We can calculate E_f/E_o value using A values for different surface components. For example, when ^4He is scattered by Cu atom on the surface, the calculated E_f/E_o value is 0.86.

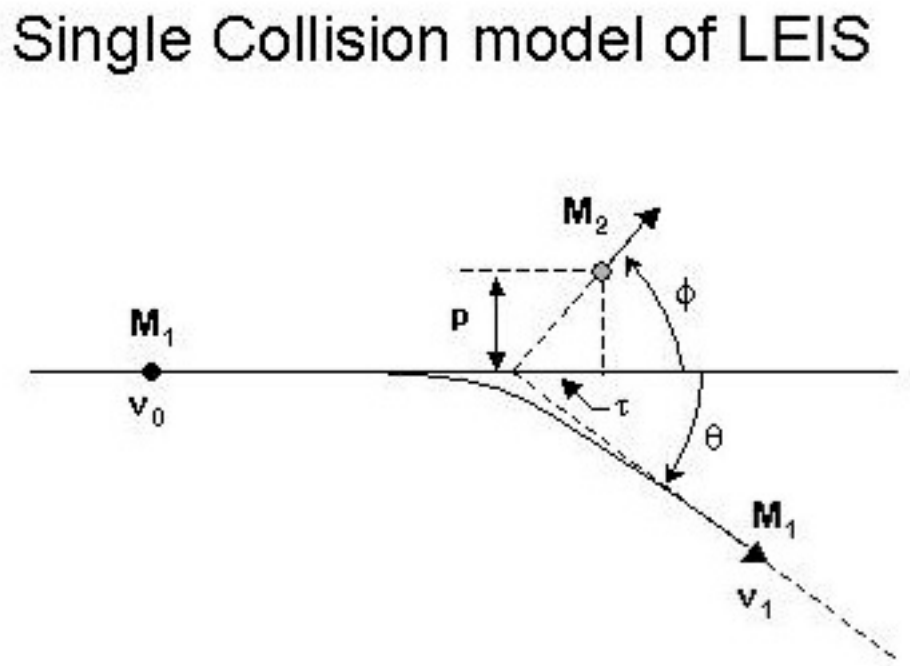

Fig. 1. 4 Single-scattering geometry in laboratory system. The projectile has the initial velocity v_o and an impact parameter p with the target particle. The projectile's final scattering angle is θ and its final velocity v_1. The target particle with the mass M_2, initially at rest, recoils at an angle ϕ with the velocity v_2.

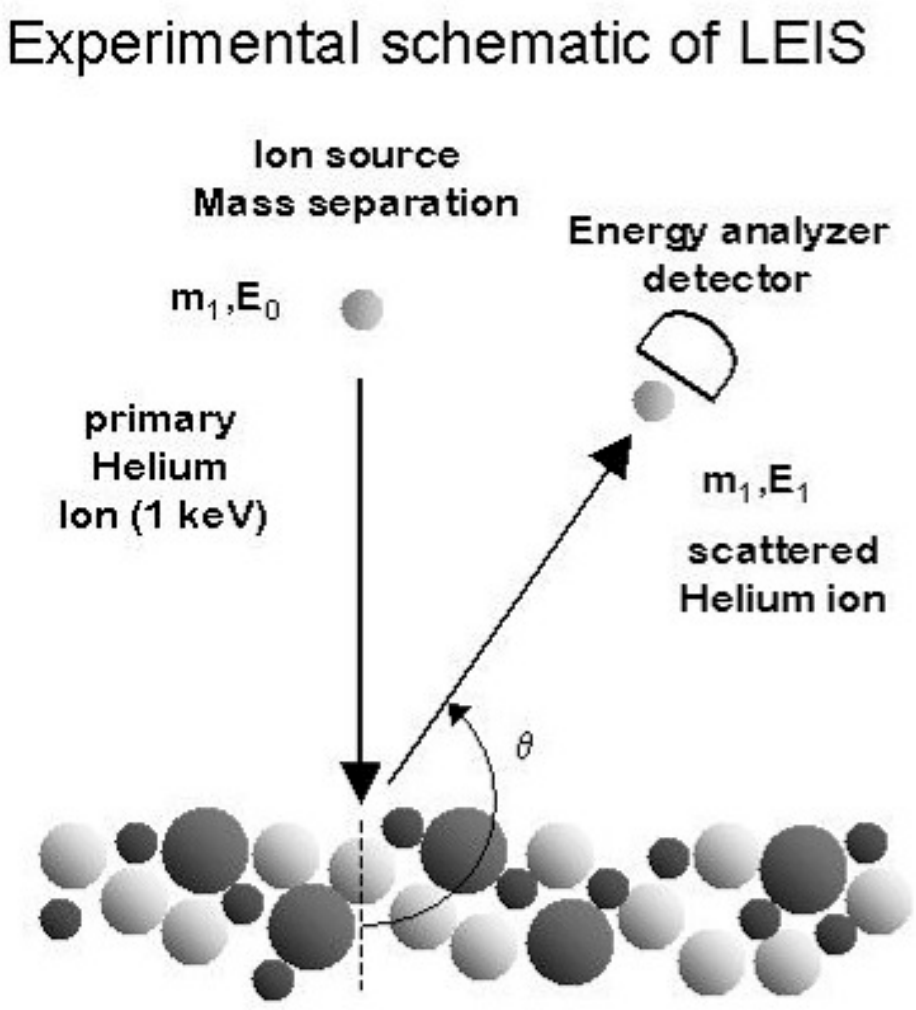

Fig. 1. 5 The geometry of LEIS in experiment. The scattering angle of θ is 115^{o} in our system. The kinetic energy of primary beam ($^{4}He^{+}$)is 1 keV.

1.3 REFERENCES

[1] T. Hori “Gate Dielectrics and MOS ULSIs”, Springer Series in Electronics and Photonics, Vol. 34, Springer, 1997

[2] C.T. Liu, Technical Digest of IEDM, (1998) 747.

[3] D.A. Buchanan, IBM J. Res. Develop., Vol 43, Iss 3, (1999) 245

[4] Y. Wu and G. Lucovsky, IEEE Electron Device Lett. Vol. 19, (1998) 367

[5] X. W. Wang, Y Shi, and T.P. Ma, VLSI Symp. Tech. Dig, (1995) 109

[6] Y. Abe, M. Kawamrua, and K. Sasaki, Jpn. J. Appl. Phys., Vol.36, Part I, (1997) 5175

[7] R.A. Mckee, F.J.Walker, and M.F. Chisholm, Phys. Rev. Lett. Vol. 81, (1998) 3014

[8] H. Luan, S. Lee, S. Song, Y. Mao, Y. Senaki, D. Roberts, and D.Kwong, Technical Digest of IEDM, (1999) 141

[9] D. Wicaksana, A. Kobayashi, and A. Kinbara, J. Vac. Sci. Tchnol. A 10(4) (1992) 1479

[10] W. J. Qi, Nieh, B.H.Lee, L.G. Kang, Y. Jeon, K. Onishi, T. Ngai, S. Banerjee, and J.C. Lee, Technical Digest of IEDM (1999) 145.

[11] L. Kang, B. Hun Lee, W.J. Qi, Y. Jeon, R. Nieh, S. Gopalan K. Onishi, and J.C.Lee, IEEE Electron Dev. Lett., Vol. 21, No. 4 (2000) 181

[12] L. Manchanda, W.H.Lee, J.E. Bower, F.H.Baumann, W.L.Brown, C. J.Case, R.C. Keller, Y.O. Kim, E.J. Laskowski, M. D. Morris, R.L. Opila, R.J. Silverman, T.W.Sorsch, and G.R.Weber, Technical Digest of IEDM (1998) 605

[13] L. Mannchanda, M. Gurvitch., IEEE Electron Dev. Lett. Vol.9 (1988) 180

[14] G.D. Wilk, R.M. Wallace, and J.M. Anthony, J. Appl. Phys., Vol. 87, No. 1 (2000) 484.

[15] M. Balog and M. Schieber, Thin Solid Films, Vol.41 (1997) 247

[16] H. Arashi, J. Am. Cera. Soc., Vol 75, (1992) 844.

[17] H. Treichel, A. Mitwalsky, G. Tempel, G. Zorn, D.A. Bohling, K.R. Coyle, B.S. Felker, M. George, W. Kern, A.P. Lane, N.P. Sandler, Advanced Materials for Optics and Electronics, Vol.5 (1995) 163

[18] J. Li, T. E. Seidel, and J. W. Mayer, MRS Bulletin, August, (1994) 15

[19] Y. Arita, Semiconductor World, December (1993) 158

[20] M. Schick, Les Houches, Session XL VIII, Liquids at Interfaces (1990) 415

[21] U. Diebold, J.-M Pan, T. E. Madey, Surf. Sci. 287/288 (1993) 896

[22] S.H. Overbury, P.A. Bertrand, and G.A.Somorjai, Chem, Rev. 75 (1975) 547.

[23] Q. Wang, Y.-M. Sun, W. Zhao, J. Campagna, J. M. White, submitted to Review of Scientific Instruments

[24] J. F. Moulder, W. F. Stickle, P. E. Sobol, and K. D. Bomben, *Handbook of X-ray Photoelectron Spectroscopy* (Physical Electronics, Inc. Eden Prairie, MN, 1995)

[25] H. Niehus, W. Heiland, and E. Taglauer, Surf. Sci. Rep. 17 (19930 213

[26] D.P.Smith, J. Appl. Phys. 18 (1967) 340

CHAPTER 2

Growth and thermal annealing of Cu on HfO_2

2.1 INTRODUCTION

The interface between Cu and oxide surfaces has been studied in several systems (TiO_2, ZrO_2, SiO_2, Al_2O_3) from the point of view of heterogeneous catalysis [1- 5], e.g., the reduction of nitric oxide on Cu/Al_2O_3 [6]. These interfaces are also important in microelectronics where Cu is being used to interconnect elements (ultra large scale integrated (ULSI) circuit). Since the resistivity of Cu (1.67 μΩ cm) is smaller than that of Al (2.66 μΩ cm) [7], better performance is plausible. HfO_2 is a promising candidate to replace the current SiO_2 gate dielectric materials in field-effect devices because it has large dielectric constant [8] and good thermal stability contact with silicon [9]. For example Cu on HfO_2 is potentially important for metal-insulator-metal (MIM) transistor development. Although the study of Cu growth on HfO_2 surfaces is very important in both the scientific and engineering areas, there are no fundamental surface science studies of the Cu growth and thermal properties on HfO_2.

The growth of thin metal films is usually described using three categories: (1) three-dimensional clustering ("Volmer-Weber", VW) where the overlayer does not wet the substrate; (2) complete wetting of the first monolayer followed by growth in three-dimensional clusters ("Stranski-Krastanov"); (3) and growth in

a layer-by-layer fashion ("Franck-van der Merwe") [1]. In previous studies on other oxide surfaces (TiO_2, ZrO_2, SiO_2, Al_2O_3), Cu typically forms three-dimensional clusters corresponding to the VW growth mode, and there is no reduction of the oxide. These phenomena are described using wetting criteria [10]. First, the surface free energy of Cu is larger than that of the oxide surfaces [11]. Second, the oxygen affinity of Cu is smaller than that of the metals composing the oxides [2].

In this paper, we report on the initial stages of Cu growth on HfO_2 surfaces and the effect of thermal annealing on the structure. We used physical vapor deposition (PVD), low-energy ion scattering spectroscopy (LEIS), X-ray photoelectron spectroscopy (XPS) and scanning transmission electron microscopy (STEM).

Growth of Cu on HfO_2 at 300 K involves initial formation of three-dimensional clusters (VW growth) without Cu oxidation. We propose a semi-quantitative model to explain the growth mode of Cu, and to calculate the fractional area covered by as Cu as the dosing time increases at 300 K and after thermal annealing at 673 K. At 300 K, as-deposited Cu covers no more than 90 % of the HfO_2 surface as two-dimensional islands. After thermal annealing at 673 K for 10 min under vacuum (1×10^{-8} torr) the Cu cluster size increases but there is no diffusion of Cu into the HfO_2 layer. STEM shows uniform Cu clusters (~ 11 nm diameter) after thermal annealing. The uniformity is attributed

to self-limiting growth [2]. TEM diffraction studies indicate that Cu is amorphous.

2.2 EXPERIMENTAL

Films were grown at 300 K in a physical vapor deposition system (AJA 1500H) described previously [12]. The load-lock system is equipped with a main chamber (base pressure ~ 5×10^{-8} torr), three sputtering guns, one DC and two with RF power supplies. HfO_2 (~15 nm) was deposited on a Ni substrate by plasma sputtering a Hf target (99.9%) (30 W DC plasma power, 20 W RF substrate bias and 10 mtorr of 10 % O_2 in Ar). To prepare HfO_2 on Cu, a thin HfO_2 film (~3 nm) was deposited on ~ 700 nm Cu on Si (100)) using the same condition. Copper was deposited by plasma sputtering a Cu target (99.99%) (10 W RF plasma power, 2 mtorr of Ar).

Vacuum annealing was done at 673 K, 10 min, and 1×10^{-8} torr in a second chamber connected to the preparation and analysis chambers by a transfer chamber (~1 x 10^{-8} torr).

For STEM a different substrate was used, namely, a 30 nm thick Si_3N_4 film (SPI Supplies) designed for mounting in the sample holder of the STEM. Using PVD, HfO_2 (~15 nm) and Cu were deposited as described above. The

sample was transported to the STEM system using an evacuated vessel to minimize oxidation the contamination.

The growth mode of Cu on HfO_2 was analyzed using LEIS and XPS. LEIS was used to identify the composition of topmost layer of the film. XPS was used to analyze the chemical composition of the surface and near-surface (~ 6 nm). These tools were installed in an ultrahigh vacuum (UHV) surface analysis chamber (base pressure ~ 1×10^{-9} torr) connected to the other chambers as described above. LEIS used a 1.0 keV He ion beam and a scattering angle of 115^{o}. For XPS, Mg Kα X-rays were used. Survey and the high-resolution scans were taken at 93.9 and 11.75 eV pass energy, respectively.

The transmission electron microscope used for the experiments was a TEM/STEM JEOL 2010-F equipped with a field emission source. The high angle annular dark field detector (HAADF) was used. This annular detector is located at an angle where the only contribution to the image is due to very high angle elastically incoherently scattered electrons. These are called Z–contrast images because the contrast is due to differences in the atomic number Z. For the situation described in this paper the Z number of the constituent elements of the sample (Cu, Hf and O) differ significantly and provide high contrast. The detector collects elastically incoherent scattered electrons in a full 360° ring, improving contrast, especially for amorphous materials.

2.3 RESULTS AND DISCUSSION

2.3.1 Growth at 300 K

Fig. 2.1 shows LEIS spectra for various Cu dosing time (t_{Cu}) at 300 K, (a-f), and finally, (g) after thermal annealing. The Cu and the Hf peaks are located at E/E_o = 0.86 and 0.78, respectively. As t_{Cu} increases, the area of the Cu peak first increases and the area of Hf peak decreases (up to t_{Cu} = 16 s). For higher doses, the Cu peak decreases while Hf peak area remains constant. These results suggest a change for two-dimensional layer to three- dimensional Cu growth at some point between 16 and 20 s.

XPS provides a second perspective (Fig. 2.2). The Cu $2p_{3/2}$ binding energy decreases from 934.7 eV to 934.0 eV as the t_{Cu} increases from 4 s to 24 s. Final-state screening effects can explain this shift as an increase of the Cu cluster size [5]. The full width half maximum (FWHM) narrows from 2.07 to 1.66 eV, consistent with a previous study of Cu on Al_2O_3 [5]. The narrowing is generally observed and attributed to better homogenity and core hole screening [13]. The important feature regarding Hf 4*f* is the absence of any evidence for reduced or partially reduced Hf. This is consistent with *bulk* thermodynamics; the Gibbs free energy of formation of HfO_2 is smaller than for the formation of Cu_2O (and CuO) [14]. In this context, however kinetics and *surface* thermodynamic consideration are, strictly speaking, more relevant.

The Hf 4*f* peak attenuates as Cu is deposited (dashed curve is the t_{Cu} = 0 s result placed over the t_{Cu} = 24 s data) and the calculated ensemble average thickness is ~ 0.35 nm [15]. The Cu 2 $p_{3/2}$ signal also provides insight (Fig. 2.2 a). The Cu peak increases linearly with t_{Cu} up to 16 s but not for larger times. Self-attenuation of the photoelectrons within three-dimensional Cu clusters is consistent with this behavior, i.e., two-dimensional growth below 16 s and three-dimensional growth for larger doses.

To compare LEIS and XPS, the relative intensity ratio of Cu/Hf is useful (Fig. 2.3). Between t_{Cu} = 4 s and 16 s, this Cu/Hf ratio increases linearly in both since the Cu covers the surface as isolated atoms or two-dimensional islands. In the second stage, clusters grow as indicated by the decreasing Cu/Hf ratio in LEIS and the slower increase in XPS.

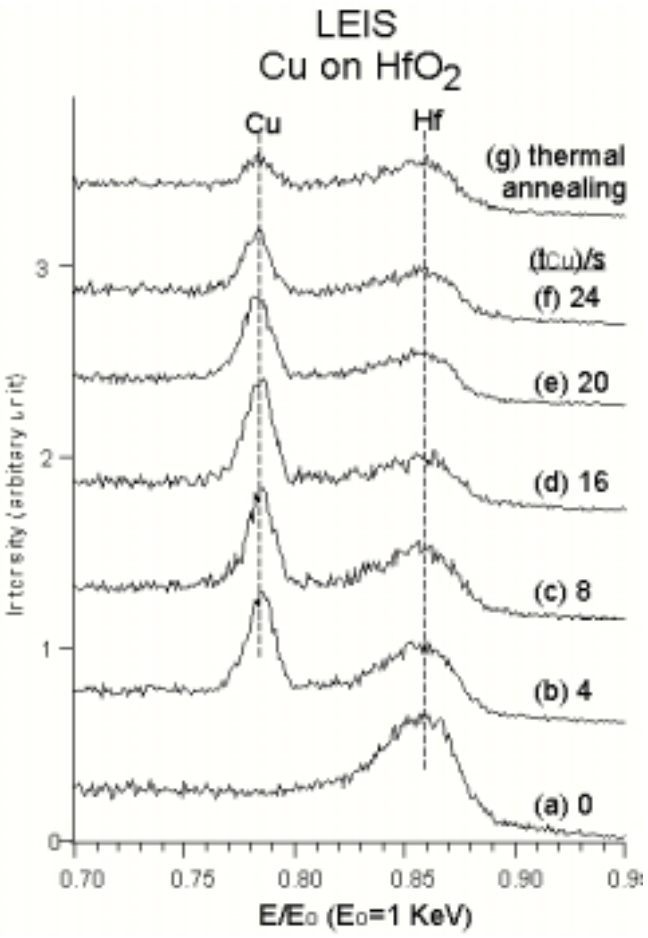

Fig. 2.1 LEIS results for Cu on HfO_2. The Cu dosing time (t_{Cu}) at 300 K are indicated (a-f). Curve (g) is the result of thermal annealing at 673 K for 10 min under vacuum (~1×10^{-8} torr). 1 keV of He^+ was used as primary beam

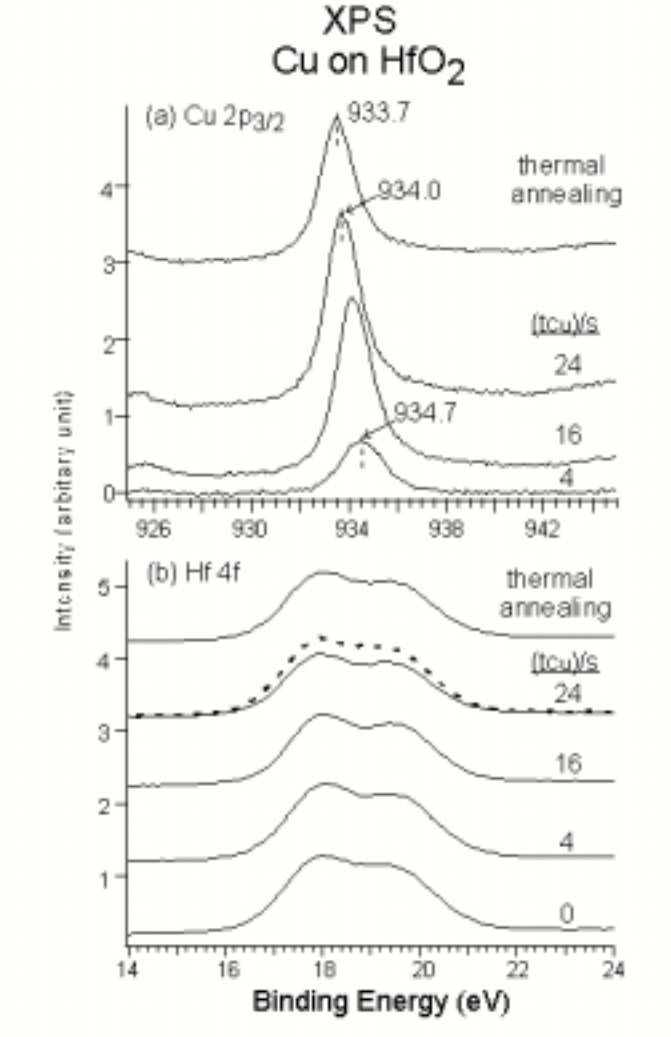

Fig. 2.2 XPS results for Cu on HfO_2 surface. Condition is same as in Fig. 1. In Fig. 2 (b), t_{Cu} = 0 s data (dashed curve) is placed over t_{Cu} = 24 s data for comparison

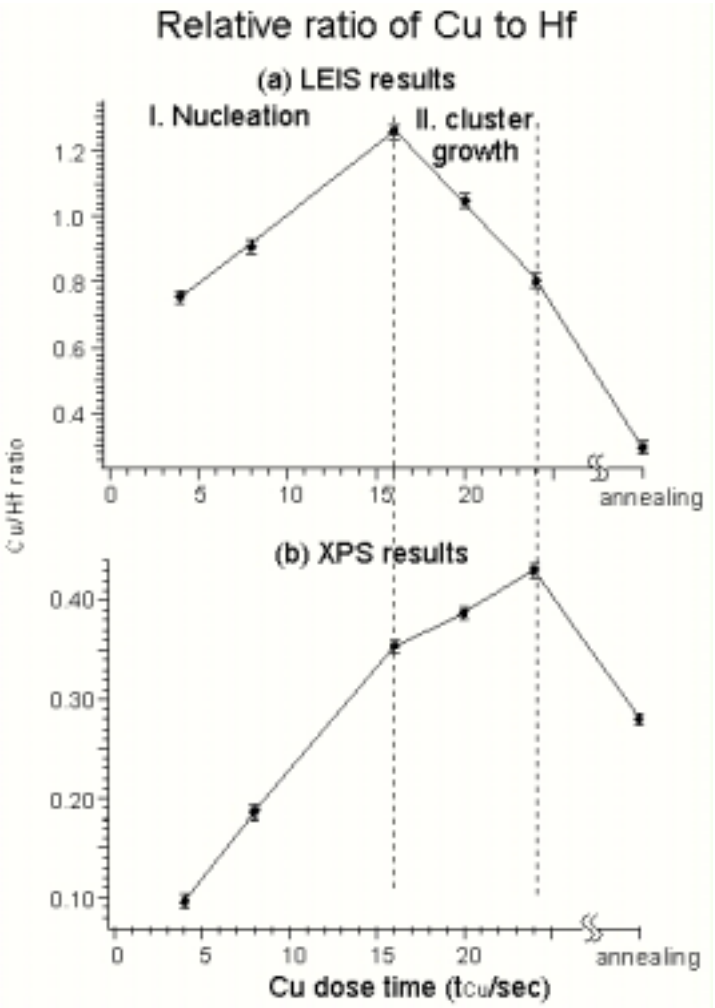

Fig. 2.3 The intensity ratio of Cu to Hf from LEIS and XPS data (Figs. 1 and 2)

2.3.2 Thermal annealing

Fig. 2.1 (g) shows the LEIS data after vacuum annealing at 673 K for 10 min. Clearly, the Cu/Hf ratio decreases because the Cu peak intensity decreases while Hf peak remains constant. There are three plausible explanations for the differential decreases: (1) small Cu clusters may combine to make larger 3-D clusters having less exposed area but shadowing the rougher HfO_2; (2) Cu atoms may diffuse into the HfO_2 layer; and (3) a combination of previous two.

The XPS data (Fig. 2.2a) shows that the Cu 2 $p_{3/2}$ binding energy decreases from 934.0 eV to 933.7 eV after upon thermal annealing. If the cluster size grows, final-state screening effects can explain at least part of the downward shift. The Cu/Hf ratio decreases results from a Cu peak intensity decrease (23 %) and a Hf peak intensity increase (6 %) upon thermal annealing. These changes are attributed to the same three possibilities as for LEIS.

To probe for diffusion into HfO_2, we inverted the structure by depositing a thin HfO_2 film (~3nm) on a 700 nm Cu substrate and annealing it at 673 K for 10 min under vacuum. If Cu atoms diffuse to the HfO_2 surface LEIS should detect them. As deposited and after annealing, LEIS shows (Fig. 2.4) only Hf indicating no detectable Cu migration onto the surface. However, the Hf intensity decreased probably due to increased surface roughness and to carbon contamination during annealing (see below). In any case the Cu signal is below the detection limit (~0.12 monolayer) after annealing.

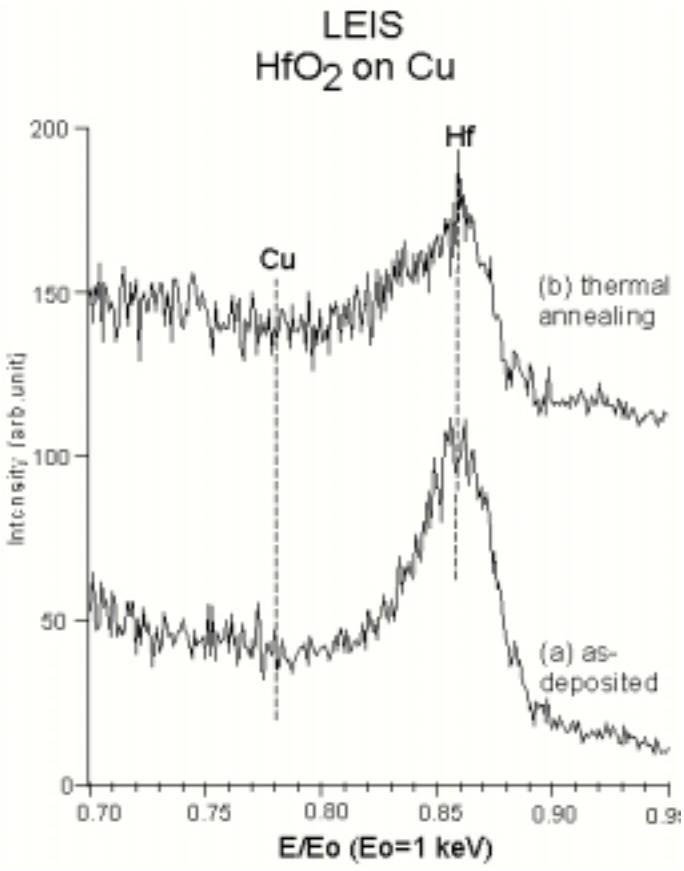

Fig. 2.4 LEIS results for a thin HfO_2 film (~ 3nm) on Cu substrate at 300 K and after thermal annealing at 673 K for 10 min under vacuum (~1×10^{-8} torr). 1 keV of He^+ was used as primary beam.

Fig. 2.5 shows the XPS spectra of Cu $2p_{3/2}$ (a), Hf 4*f* (b), and C 1 *s* (upper right inset box in (b)) before and after thermal annealing. The Cu and Hf integrated intensities decrease by 13% and 2%, respectively due in part to carbon contamination on the surface perhaps preferentially associated with Cu. Unfortunately, detecting C by LEIS has proven unreliable. Were Cu atoms diffusing into the HfO_2 layer but failing to reach the surface, the intensity of Cu 3*p* in the XPS spectra would increase and Cu/Hf XPS intensity ratio would increase, contrary to observation. In fact, the relative peak area ratio of Cu/Hf decreases from 0.19 to 0.17 after thermal annealing. Based on LEIS and XPS, we conclude that diffusion of Cu atoms into the HfO_2 layer is not detectable by either LEIS or XPS. The detection limit is insufficient (~ 5 % of a layer) to draw more than modest conclusion.

To investigate the presence, size and morphology of Cu clusters, two Cu/HfO_2 samples were prepared and analyzed by STEM. One was annealed at 673 K for 10 min under vacuum. From Hf attenuation in XPS, the ensemble average Cu thickness was ~ 1.3 nm. Prior to STEM, LEIS and XPS data were gathered and established that the Si_3N_4 base did not alter overall picture (Fig. 2.6). LEIS, Fig. 2.6 (a), exhibits Hf before annealing, indicating that the HfO_2 surface is not completely covered by Cu. After thermal annealing, the Cu peak intensities in both LEIS and XPS spectra decrease and the binding energy of Cu $2p_{3/2}$ in XPS shifted lower as in Figs. 2.1 and 2.2.

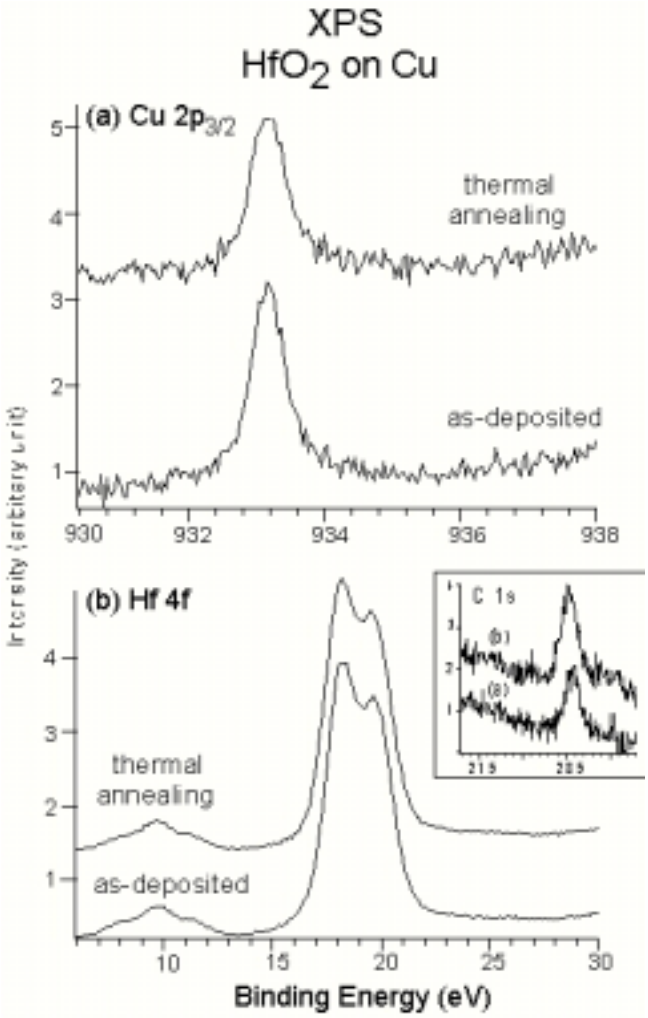

Fig. 2.5 XPS for Cu 2 $p_{3/2}$ (a) and Hf 4f (b) of a thin HfO_2 film (~3nm) on a Cu substrate at 300 K and after thermal annealing at 673 K for 10 min under vacuum (~1×10^{-8} torr). The C 1s spectra of Cu/HfO_2 sample are shown in the upper right inset box in Fig. 5 (b).

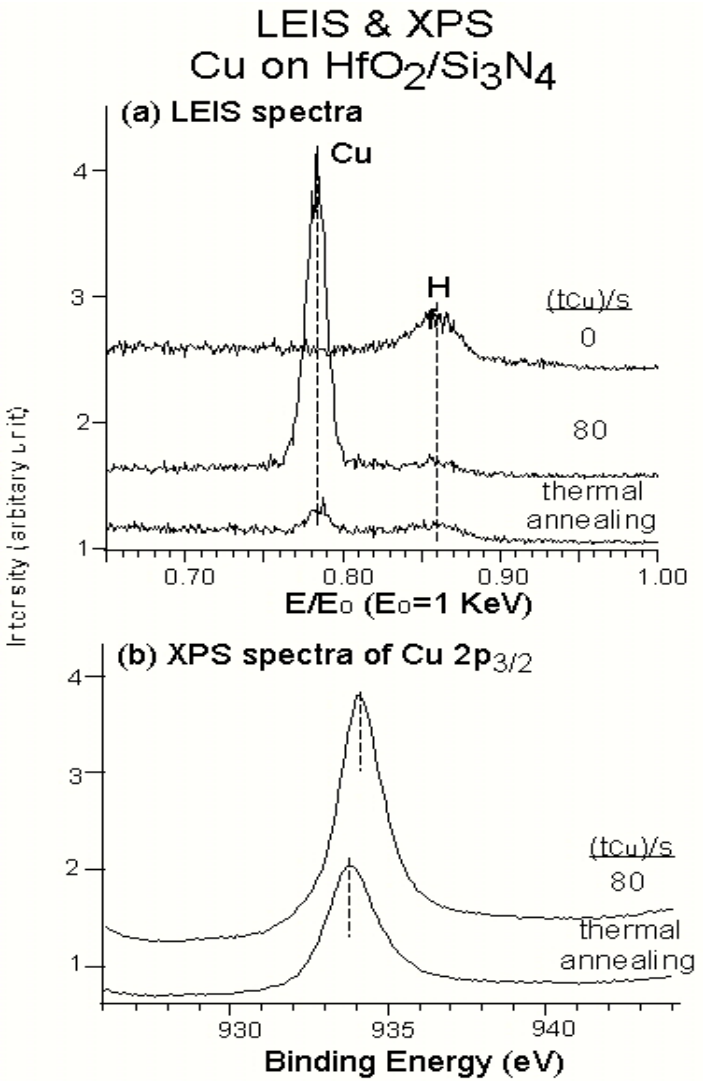

Fig. 2.6 LEIS and XPS spectra for Cu on HfO_2/Si_3N_4 at 300 K and after thermal annealing at 673 K for 10 min under vacuum (~1×10^{-8} torr).

STEM of the unannealed sample showed no Cu clusters because both the diameter and thickness lie below the detection limit. We do not know the precise detection limit but experience suggests that the diameter of Cu clusters is less than 5 nm. Fig. 7 (a) shows a dark field STEM image of the annealed sample. The brighter areas are thicker. The higher electron scattering in this area is due to increased (mass×thickness). Combined with XPS, LEIS and STEM images indicate that these brighter zones (B) correspond to the Cu clusters. The area between the clusters (A) presents a "sponge – like" structure due to the presence of Cu. Transmission images cannot distinguish whether the Cu is located on or inside the HfO_2 structure but from LEIS and XPS little Cu, if any, diffused into the HfO_2. We conclude that the sponge – like region in Fig. 7 (a) represents small Cu clusters. A cluster diameter distribution histogram, Fig. 7 (b), gives an average diameter of 11.0 ± 0.2 nm.

Diffraction experiments (TEM) showed no crystallographic features, indicating that Cu is amorphous. The high contrast in Fig. 7 is consistent with amorphous copper; the detector gathers many Rutherford scattered electrons in all directions.

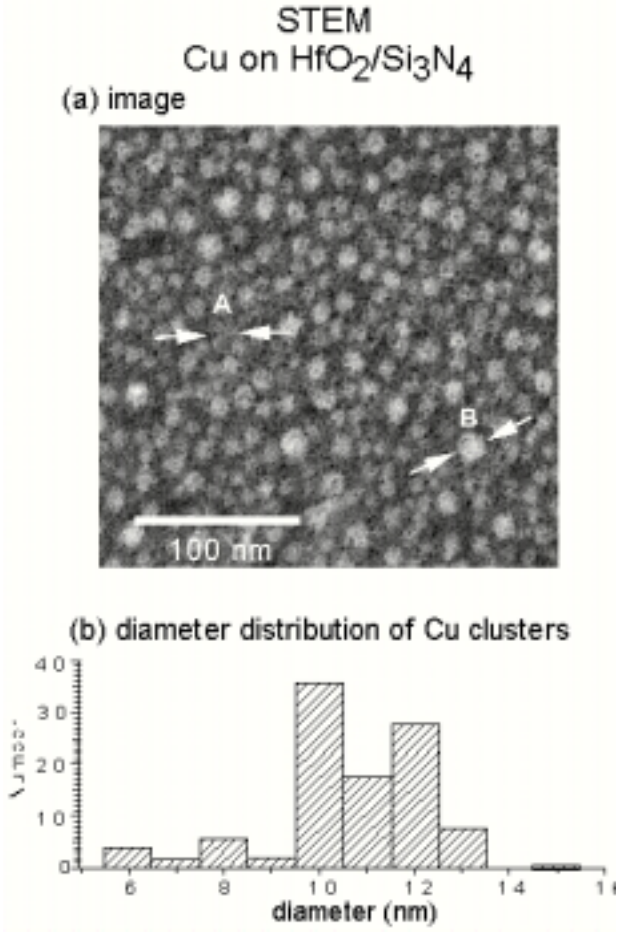

Fig. 2.7 STEM image of Cu on HfO_2/Si_3N_4 after thermal annealing at 673 K for 10 min under vacuum (~1×10^{-8} torr). Fig. 2.7 (a) shows the image of sample and Fig. 2.7 (b) shows the histogram for the cluster distribution form Fig. 2.7 (a). In Fig. 2.7 (a), the zone between arrows marked as A shows a sponge - like region and the zone between arrows marked as B defines a typical Cu cluster. The white bar in the figure corresponds to 100 nm

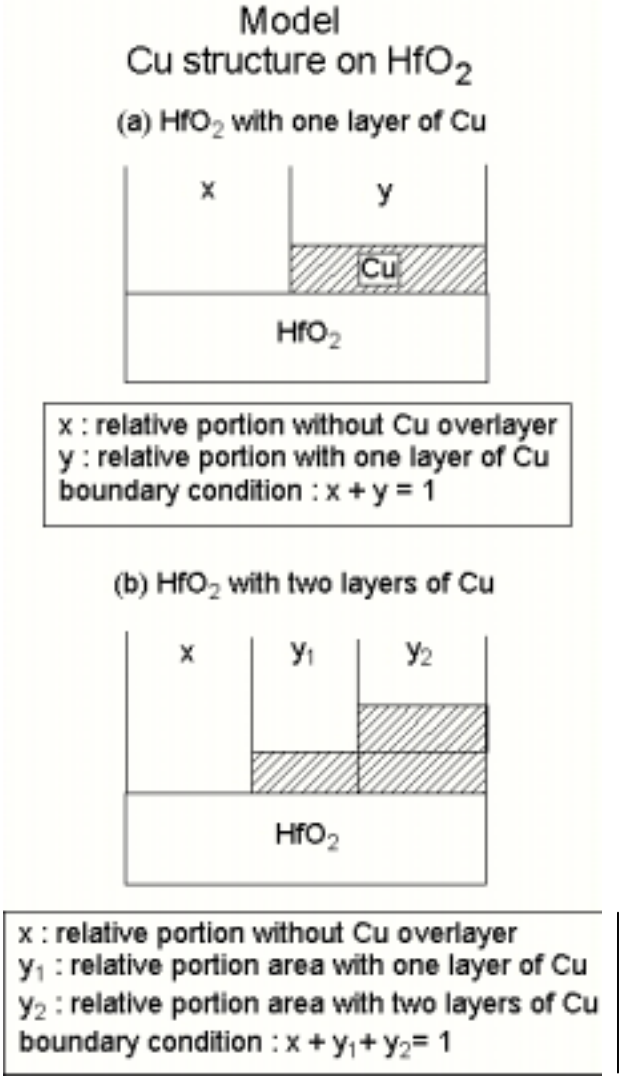

Fig. 2.8 Schematic of structure used to model Cu on HfO_2.

2.3.3 Proposed phenomenological model

Based on the reduction of the Hf 4 *f* peak intensity by Cu, we build a model expression by modifying a standard attenuation equation [15].

$$N = N_o \cdot \exp\left[-L/\left(\lambda_{Cu} \cdot \sin\theta\right)\right] \quad (1)$$

Where N is the Hf 4*f* peak area with Cu overlayer, N_o is the Hf 4*f* peak area without Cu overlayer, L is the thickness of Cu overlayer, λ_{Cu} is the mean free path of Hf electron passing through Cu (1.9 nm) [16], and θ is the angle between analyzer and sample (60^o). The basic notion, Fig. 2.8, is that the total intensity of the photoelectrons from Hf (per unit area) can be found by summing on a layer – by – layer basis Hf photoelectrons passing through *n* Cu layers. While surface roughness variations are not taken into account, this model does account for variation of the Cu thickness. For the case of only one Cu (Fig. 2.8 (a)), we calculate the relative portion of Hf without a Cu overlayer (x) and Hf with Cu overlayer (y) using eq. (2) and one boundary condition ($x + y = 1$) as total area of Hf is constant.

$$N / N_o = x + (1-x) \cdot \exp\left[-L_1/\left(\lambda_{Cu} \cdot \sin\theta\right)\right] \quad (2)$$

Where L_1 is the thickness of monolayer of Cu (0.2 nm).

When accounting for two layers of Cu, Fig. 2.8(b), the analogous equation is:

$$N / N_o = x + y_1 \cdot \exp\left[-L_1/\left(\lambda_{Cu} \cdot \sin\theta\right)\right] + y_2 \cdot \exp\left[-2 \cdot L_1/\left(\lambda_{Cu} \cdot \sin\theta\right)\right] \quad (3)$$

Clearly, the relative portion of each Cu multi-layer can not be calculated with only one boundary condition ($x + y_1 + y_2 = 1$). Instead, we estimated the attenuation of the Hf intensity ($(N/N_o)_{cal}$) based on model structure. The procedure for evaluation of model structure is: (1) build several acceptable Cu structures consistent with the LEIS data, (2) determine x, y_1, and y_2 for each Cu structure, (3) calculate $(N/N_o)_{cal}$ for each model from eq. (3) using x, y_1, and y_2, and (4) compare $(N/N_o)_{cal}$ with $(N/N_o)_{exp}$ determined from XPS to determine the optimum, but not necessarily unique, model.

For an n-layer case, we expand eq. (3) as:

$$N / N_o = x + \sum_{i=1}^{n} y_i \cdot \exp\left[-i \cdot L_1 / \left(\lambda_{Cu} \cdot \sin\theta\right)\right] \qquad (4)$$

Where n is the number of Cu layers, and the boundary condition is:

$(x + \sum_{i=1}^{n} y_i = 1)$.

Table 2.1
The summary of proposed Cu structure based on LEIS and XPS results

t_{Cu}	**Model**	**Mechanism**	# of Cu atom detected by LEIS	XPS results	
				Experiments	Calculation
4 s	⊗ :exposed Cu, ○ :covered Cu ○ :Hf, ° :O, ⁘ :vacated Cu site 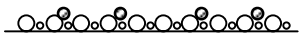 HfO_2	nucleation stage ↑	4	$(N/N_o)_{exp}$ = 0.965	x = 0.74, y = 0.26
8 s	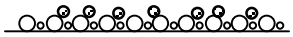		8	$(N/N_o)_{exp}$ = 0.935	x = 0.52, y = 0.48
16 s	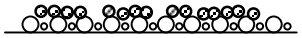	nucleation stage ↓	16	$(N/N_o)_{exp}$ = 0.875	x = 0.1, y = 0.9
20 s	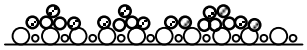	Mechanism I (see text)	12	$(N/N_o)_{exp}$ = 0.82-0.85	x = 0.1, y_1 = 0.675, y_2 = 0.225 => $(N/N_o)_{cal}$ = 0.85
	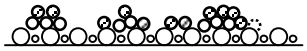	Mechanism I & II (see text)	11		x = 0.2, y_1 = 0.264, y_2 = 0.528 => $(N/N_o)_{cal}$ = 0.82
24 s	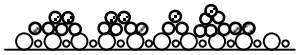	Mechanism I	10	$(N/N_o)_{exp}$ = 0.77-0.79	x = 0.1, y_1 = 0.342, y_2 = 0.396, y_3=0.162 => $(N/N_o)_{cal}$ = 0.80
		Mechanism I & II	9		x = 0.2, y_1 = 0.168, y_2 = 0.4, y_3=0.132 => $(N/N_o)_{cal}$ = 0.80
Thermal annealing	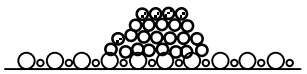	Three Cu islands make one Cu isalnd	5	$(N/N_o)_{exp}$ = 0.85-0.87	x = 0.5, y_1 = 0.065, y_2 = 0.065, y_3=0.19, y_4=0.19 => $(N/N_o)_{cal}$ = 0.80

Based on the LEIS measurements and on the results obtained from the modified attenuation equation using XPS data, we propose a Cu structure and possible mechanisms for the nucleation and cluster growth stages. Table 2.1 summarizes. The 2nd column shows schematic side-views, the 3rd column describes proposed contributing mechanisms, the 4th column shows the number of Cu atoms that can be detected by LEIS in the model structure and the 5th column shows, for XPS, the calculated and experimental results. Assuming no multilayer of Cu for $t_{Cu} \leq 16$ s, the relative coverage of Cu on the HfO_2 surface increases from 26% to 90% using eq. (2).

Upon further dosing of Cu, clusters are proposed consistent with data in Fig. 2.3. There are three possibilities: (I) Cu atoms add to existing layer, (II) Cu atoms adsorb on HfO_2 and diffuse laterally to make 2nd layer (diffusion-mediated growth), and (III) Cu atoms migrate from the 1st layer into the 2nd (self-growth). In case (I), the relative percentage of HfO_2 surface without Cu overlayer does not change since there are no added Cu atoms on HfO_2 surface. Case (III) is indistinguishable from case (I). Thus, we only case I and a combination of cases I and II. At t_{Cu} = 20 and 24 s, the number of exposed Cu atoms (detected by LEIS) decreases due to the formation of clusters, as observed by decaying Cu/Hf ratio in Fig. 2.3 (a). At t_{Cu} = 20 s, the $(N/N_o)_{cal}$ values for both cases are within our experimental data range. At t_{Cu} = 24 s, the $(N/N_o)_{cal}$ values in both cases using eq. (4) are same although the relative percentage of each Cu layer differs.

Currently, we cannot determine which mechanism is dominant. Nevertheless, formulation can be applied to model the Cu structure since the $(N/N_o)_{cal}$ values within 5 % of $(N/N_o)_{exp}$.

After thermal annealing, we propose that small Cu clusters agglomerate and there is no Cu diffusion into the HfO_2 layer. The calculated attenuation of the Hf 4*f* intensity, based on the larger Cu cluster forming from the three Cu small clusters (column 2 of Table 2.1) matches the experimental data and is consistent with the STEM image (Fig. 2.7).

We propose that self-limiting growth leads to the narrow distribution of cluster size observed by STEM after thermal annealing. Were there no limitation on the growth of the Cu clusters, broader diameter dispersion and no inter-cluster sponge – like regions are expected. Self-limiting growth of Cu clusters has been reported on another oxide surface (TiO_2) [2]. Two possible mechanisms were suggested. First, the rate at which adatoms attach to existing clusters decreases rapidly as the cluster size increases, due to the existence of strain fields originating in the lattice mismatch at the interface between the Cu clusters and TiO_2 substrate. In other words, the total strain energy is proportional to the interfacial area so that larger Cu clusters subject to a larger strain field. Second, the rate at which added adatoms reach the existing clusters decreases rapidly as the Cu coverage increases. In our thermal annealing case, no Cu is added so we favor the first mechanism.

2.4 CONCLUSION

The growth of Cu on HfO_2 surfaces at 300 K as a function of Cu dose and the effect of thermal annealing were investigated using *in-situ* LEIS, *in-situ* XPS, and *ex-situ* STEM. There are two growth stages of Cu on HfO_2 at 300 K: two-dimensional island until no more than 90 % of the HfO_2 is covered and three-dimensional cluster growth thereafter. The HfO_2 is not reduced at its interface with Cu. A model is presented that rationalizes the growth and effect of thermal annealing. After thermal annealing at 673 K for 10 min under vacuum ($\sim 1 \times 10^{-8}$ torr), the Cu cluster size increases but there is no evidence of diffusion across Cu – HfO_2 interfaces. After annealing, STEM images confirm the presence of Cu clusters and a narrow Cu cluster diameter distribution (11 ± 1 nm). We propose that strain fields at the Cu / HfO_2 interface limit growth of Cu clusters. TEM diffraction studies indicate that Cu is amorphous.

2.5 REFERENCES

[1] U. Diebold, J.-M Pan, T. E. Madey, Surf. Sci. 287/288 (1993) 896

[2] D. A. Chen, M. C. Bartelt, R. Q. Hwang, K.F. MaCarty, Surf. Sci. 450 (2000) 78

[3] Q. Ge, P. Møller, Thin Solid Films 254 (1995) 10

[4] X. Xu, J.-W. He, D.W. Goodman, Surf. Sci. 284 (1993) 103

[5] Y. Wu, E. Garfunkel, T. E. Maday, J. Vac. Sci. Technol. A 14 (1996) 1662

[6] M-C Wu, D. W. Goodman, J. Phys. Chem. 98 (1994) 9874

[7] Jian Li, Tom E. Seidel, Jim W. Mayer, MRS bulletin/August (1994) 15

[8] M. Balog and M. Schieber, Thin Solid Films 41, 247 (1977)

[9] K.J. Hubbard and D.G. Schlom. J. Mater. Res. 11(11), 2757 (1996)

[10] A. W. Adamson, "Physical Chemistry of Surfaces", New York (1990)

[11] S. H. Overbury, P. A. Bertrand, G. A. Somorjai, Chem. Rev. 75 (1975) 547

[12] Y. -M Sun, J. Lozano, H. Ho, H. J. Park, S. Veldman, J. M. White, Appl. Surf. Sci. 161 (2000) 115

[13] W. F. Egelhoff, Jr., Surf. Sci. Rep. 6 (1987) 253

[14] Ihsan Barin, Gregor Platzki, "Thermochemical Data of Pure Substances", 3rd edition, VCH Inc., (1995)

[15] A.Y.Mao, K.-A.Son, D.A.Hess, L.A. Brown, J.M.White, D.L. kwong, D.A. Roberts, R.N.Vritis, Thin Solid Films 349 (1999) 230

[16] S. Tanuma, C. J. Powell, Surf. Interface Anal. 17(13) (1991) 911

CHAPTER 3

Growth and thermal annealing of Cu on $HfSiO_4$

3.1 INTRODUCTION

The interface between Cu and oxide surfaces has been studied in several systems (TiO_2, ZrO_2, SiO_2, Al_2O_3) from the point of view of heterogenous catalysis [1-5], e.g., the reduction of nitric oxide on Cu/Al_2O_3 [6]. These interfaces are also important in microelectronics where Cu is being used to interconnect elements (ultra large scale integrated (ULSI) circuit). $HfSiO_4$ is a promising candidate to replace the current SiO_2 gate dielectric materials in field-effect devices because it has a large dielectric constant and good thermal stability in contact with silicon [7]. For example, Cu on $HfSiO_4$ is potentially important for metal-insulator-metal (MIM) transistor development. Although the study of Cu growth on $HfSiO_4$ surfaces is very important in both the scientific and engineering areas, there are no fundamental surface science studies of the Cu growth and thermal properties on $HfSiO_4$.

Previously, Cu on HfO_2 was investigated with same reason as $Cu/HfSiO_4$ since HfO_2 was also one of promising candidate to replace SiO_2 gate dielectrics [8]. In that case, it was shown that Cu forms two-dimensional islands up to a surface coverage of 90 % followed by three-dimensional growth. Upon thermal annealing at 673 K, Cu clusters combined to form larger ones based on XPS,

LEIS and TEM results before and after thermal annealing. No evidence was found for Cu diffusion into the HfO_2 substrate. Previous studies of Cu deposition on other oxide surfaces (TiO_2, ZrO_2, SiO_2, Al_2O_3) show that Cu typically forms three-dimensional clusters corresponding to the VW growth mode, and there is no reduction of the oxide. The formation of Cu clusters is explained using wetting criteria [9] by the fact that the surface free energy of Cu is larger than that of the oxide surfaces [10]. Since the oxygen affinity of Cu is smaller than that of the metals in the oxide substrate, the Cu does not reduce the oxide [2].

In this work, we studied the structure of submonolayer coverage of Cu on $HfSiO_4$ surfaces and the effect of thermal annealing on the structure with real time scale. We used physical vapor deposition (PVD) to prepare the films and *in-situ* low-energy ion scattering spectroscopy (LEIS), *in-situ* X-ray photoelectron spectroscopy (XPS), and *ex-situ* atomic force microscopy (AFM). For vacuum annealing experiments, A CO_2 laser beam was used to heat the sample for obtaining LEIS analysis at high temperature (> 300 K).

We found that growth of Cu on $HfSiO_4$ at 300 K involves initial formation of three-dimensional clusters (VW growth) without Cu oxidation. We proposed a semi-quantitative model to explain the growth mode of Cu, and the fractional area covered by Cu as the dosing time increases at 300 K and the change of Cu structure during thermal annealing at 573 K. At 300 K, as-deposited Cu covers

no more than 85 % of $HfSiO_4$ surface as two-dimensional islands, as determined by XPS Hf and Si signal attenuation. During thermal annealing at 573 K for 27 min under vacuum (~ 7×10^{-9} torr), the Cu cluster size increases and Cu may diffuse into $HfSiO_4$ layer, although we do not have any evidence for the latter. AFM images of annealed samples show uniform Cu clusters (9.6 ± 0.3 nm), this uniformity is ascribed to a self-limiting growth [2, 8].

3.2 EXPERIMENTAL

Films were grown at 300 K in a physical vapor deposition system described previously [11]. The main chamber (base pressure ~ 5×10^{-8} torr) is equipped with a load-lock chamber and three sputtering guns with one DC and two RF power supplies. The Si (100) substrates (25× 25× 1 mm) were dipped in a 3% HF solution to remove the native oxide layer and contaminants. The samples were then mounted on a hollow stage and introduced into the PVD system. $HfSiO_4$ (~ 15 nm as determined by XPS signal attenuation) was deposited on a Si (100) substrate by plasma sputtering a Hf target (99.9 %) with 15 W DC plasma power and Si target (99.9 %) with 50 W RF plasma power under 10 mtorr of 10 % O_2 in Ar. The stoichiometry of the hafnium silicate films and the reproducibility of the films thickness were confirmed by XPS. Copper was also deposited by plasma sputtering a Cu target (99.9 %) with 5 W DC power under 2 mtorr of Ar. The Cu dosing time (t_{Cu}) is the elapsed time in

which the surface is exposed to the Cu ions from the target. Based on our XPS data, the amount of copper deposited per second, in terms of surface coverage, is about 5.3% of a monolayer.

Once prepared, the films were transferred through a UHV system into an analysis chamber (base pressure ~ 1×10^{-9} torr) for LEIS and XPS. LEIS was used to identify the composition of the topmost layer of film. The primary ion beam energy E_o used in this work was 1 keV. The pressure in the analysis chamber was ~ 7×10^{-9} torr during LEIS. XPS was used to analyze the composition of the surface and near - surface region (~6 nm).

Atomic Force Microscopy (AFM) was performed *ex-situ* under ambient conditions using a CP Research Autoprobe (Thermomicroscopes) with high aspect ratio silicon tips (radius of curvature of ~ 10 nm.) The probe was operated in non-contact mode (NCM) at a resonant frequency between 80 and 115 kHz. The roughness was calculated using Autoprobe Image processing software provided by Thermomicroscopes. The RMS roughness values reported in this work are the average of the values obtained over several 2x2 μm^2 regions of each sample.

Sample heating was achieved by introducing a continuous IR CO2 laser beam (wavelengths between 10.57 and 10.63 micron) into the analysis chamber through a ZnS window. Once inside the chamber, the beam was directed towards the back of the sample by a Cu total reflection mirror mounted

underneath the hollow sample stage. The sample temperature was monitored by a thermocouple coated with graphite placed in the laser beam pathway. The reading obtained from this thermocouple was calibrated to the temperature of the sample as described by Wang et al. [12]. By heating the sample in the analysis chamber it was possible to obtain LEIS data at elevated temperatures, instead of only being able to obtain post-anneal data as in the previous work done on Cu deposited on HfO_2 [8].

3.3 RESULTS AND DISCUSSION

3.3.1 Growth at 300 K

Fig. 3.1 shows the Cu $2p_{3/2}$, Hf 4f and Si 2p XPS signals for various Cu dosing times (t_{Cu}) at 300K. As the Cu dosing time increases, the intensity of the Cu peak increases while the intensity of the Si and Hf peaks decrease. The O1s signal (not shown) followed the same trend as the Hf and Si signals. A small amount of carbon was also detected on the surface (~8%) possibly due to contamination from filaments in the chamber. The carbon content did not seem to change with Cu dosing time. The ensemble thickness of the Cu layer was calculated using the Hf XPS signals shown in Fig. 1 and the standard attenuation equation [13]. The ensemble thickness of the Cu layer as a function of Cu dosing time is shown in Fig. 3.2. By including the point at the origin corresponding to zero thickness at $t_{Cu} = 0$, we observe a linear increase in Cu

thickness up to a dosing time of 16 seconds. The calculated ensemble coverage at this dosing time was ~85% of a monolayer. Between 16s and 32s, a change in the slope of the line takes place, followed by a linear increase in Cu thickness with increasing dosing time. This change indicates that the amount of substrate area covered by the incoming Cu atoms did not increase as much as it should have, given the fact that the Cu dosing time was doubled. By extrapolating the line across the last 3 data points (dosing time > 32s) we see that the time axis is intersected at t = 5s. This suggests that a de-wetting of the surface might have taken place between 16 and 32 seconds. To illustrate the point, a wetting effect would increase the coverage of the substrate, in which case, a line over the data points after the wetting took place would intersect the time axis at negative values.

Fig. 3.1 also shows two important changes in the $Cu2p_{3/2}$ signal as the dosing time is increased. The First, the full width at half maximum (FWHM) narrows from 2.0 to 1.75eV, consistent with a previous study of Cu on Al_2O_3 [5]. This narrowing is generally attributed to improved homogeneity and core hole screening [14] as the origin of the XPS signal changes from single atoms to bulk-like configurations. Second, the bonding energy of $Cu2p_{3/2}$ shifts to a lower binding energy from 934.4 to 934.0eV (Fig. 1). This shift can be explained by final-state screening effect due to an increase in the Cu cluster size [5]. The largest shift in the peak position takes place between 16 and 32 sec., when the

change in binding energy is about 0.2eV, compared to 0.1eV or less at all other intervals and it is consistent with the changes observed in the rate of Cu growth shown in Fig. 3.2.

Fig. 3.3 shows LEIS data of Cu on $HfSiO_4$ for various Cu dosing times. On the clean $HfSiO_4$ surface (that is, t_{Cu} = 0s) the Hf and Si peaks are located at E/E_o = 0.56 and 0.86, respectively. As the dosing time increases, a peak appears at at E/E_o = 0.78, which corresponds to Cu. Up to 16s, the intensity of the Cu peak increases while the intensity of the Si and Hf peaks decreased as the dosing time increased. For higher doses, the intensity of the Cu peak decreased even though more Cu was added to the surface. The Hf and Si peaks also decreased but did not vanish, indicating that even at the longest dosing times, the hafnium silicate substrate was not completely covered by Cu. The decrease in the intensity of all LEIS signals observed at high dosing times may be attributed to surface roughening; therefore, it is useful to plot the ratio of the peak intensities to visualize changes in the signals relative to each element. Fig. 3.4 shows such plot for the Cu/Hf XPS and LEIS signal ratio. The Cu/Hf (both LEIS and XPS) ratio increases as the dosing time is increased up to 16s, which corresponds to a surface coverage of about 85%, as mentioned above. At higher dosing times, the Cu/Hf ratio in the LEIS data starts to decrease, indicating an increase in the area of hafnium silicate exposed. Similarly, for dosing times greater than 16s, the Cu/Hf XPS ratio undergoes a change in the rate of increase, as indicated by the

decrease in the slope of the line between the points for t_{Cu}> 32s compared to the points for t_{Cu} < 16s. This effect can be explained by self-attenuation of $Cu2p_{3/2}$ photoelectrons as a result of Cu cluster formation at t_{Cu} > 16s. Using the XPS data, we calculated that this dosing time corresponds to a surface coverage of ~85%.

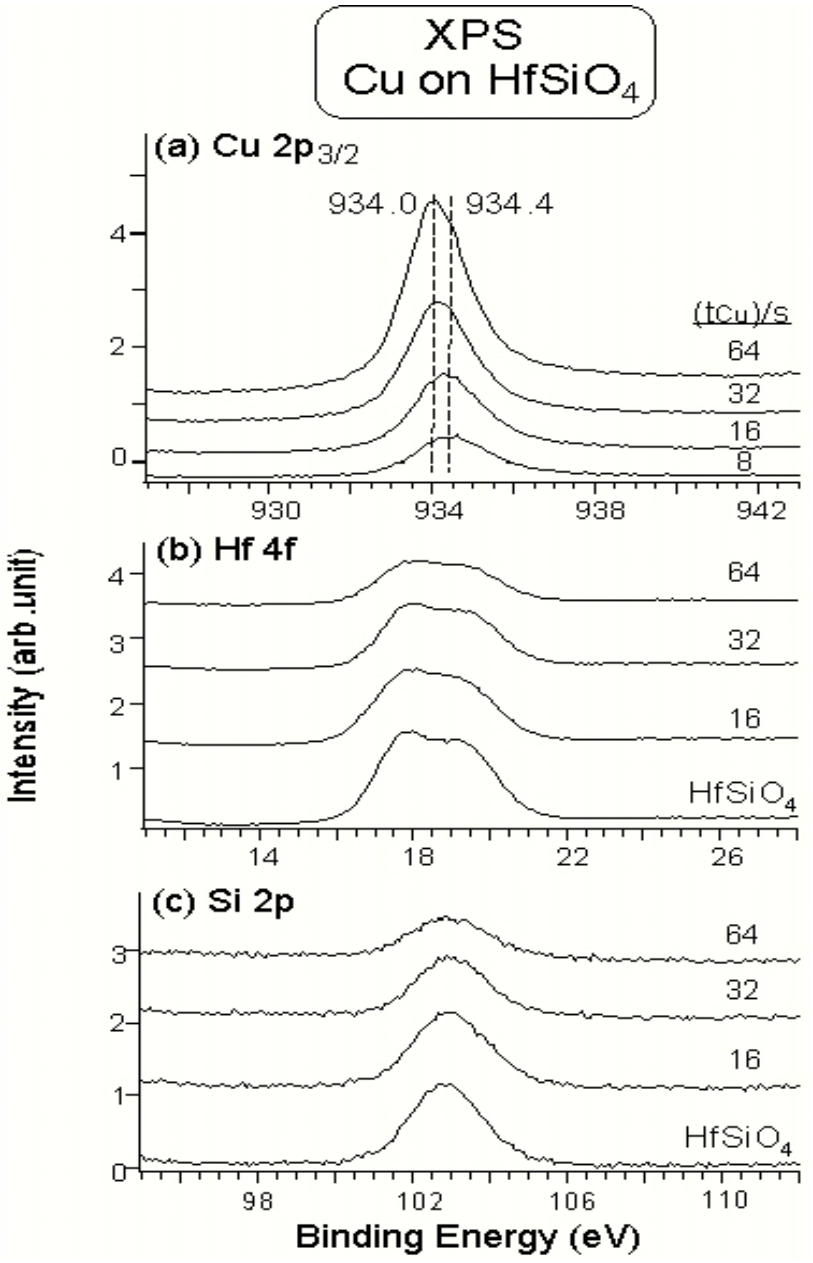

Fig. 3.1 XPS data for Cu on $HfSiO_4$ at 300 K as a function of Cu dosing time.

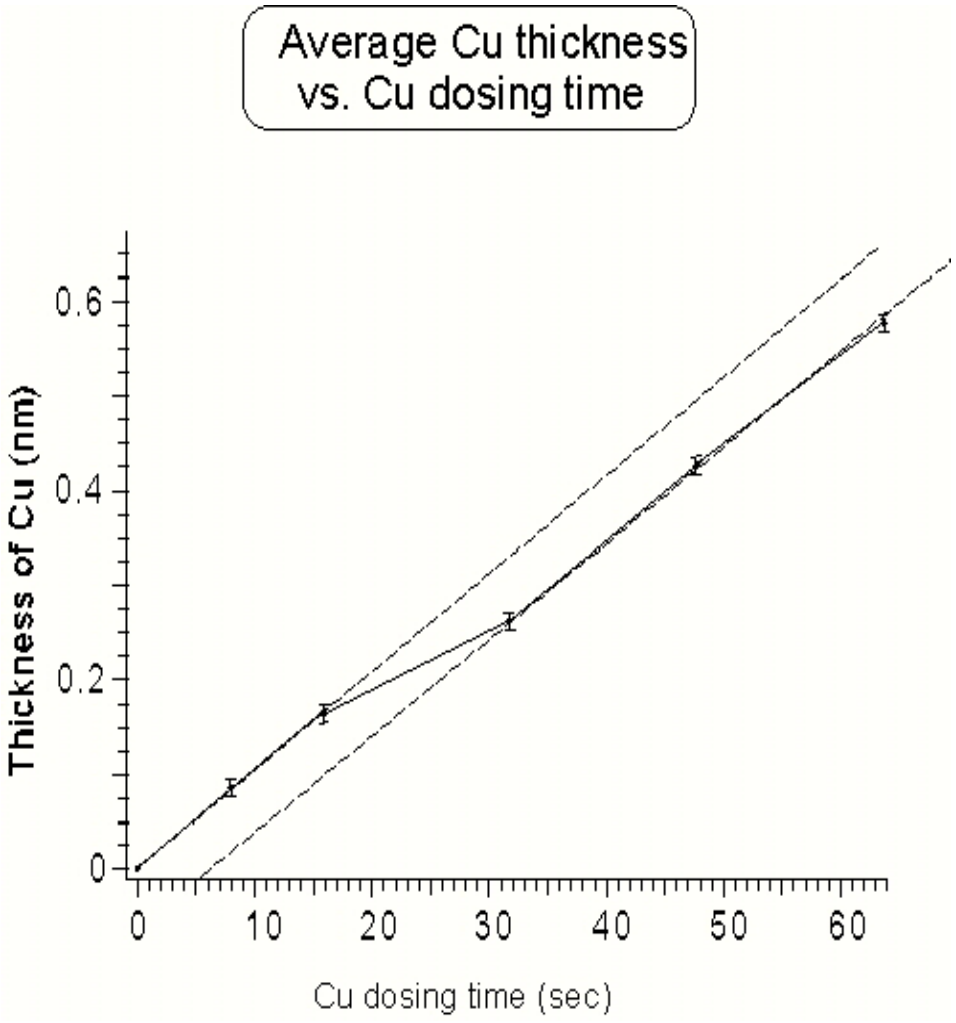

Fig. 3.2 Ensemble average Cu thickness at 300 K as a function of Cu dosing time.

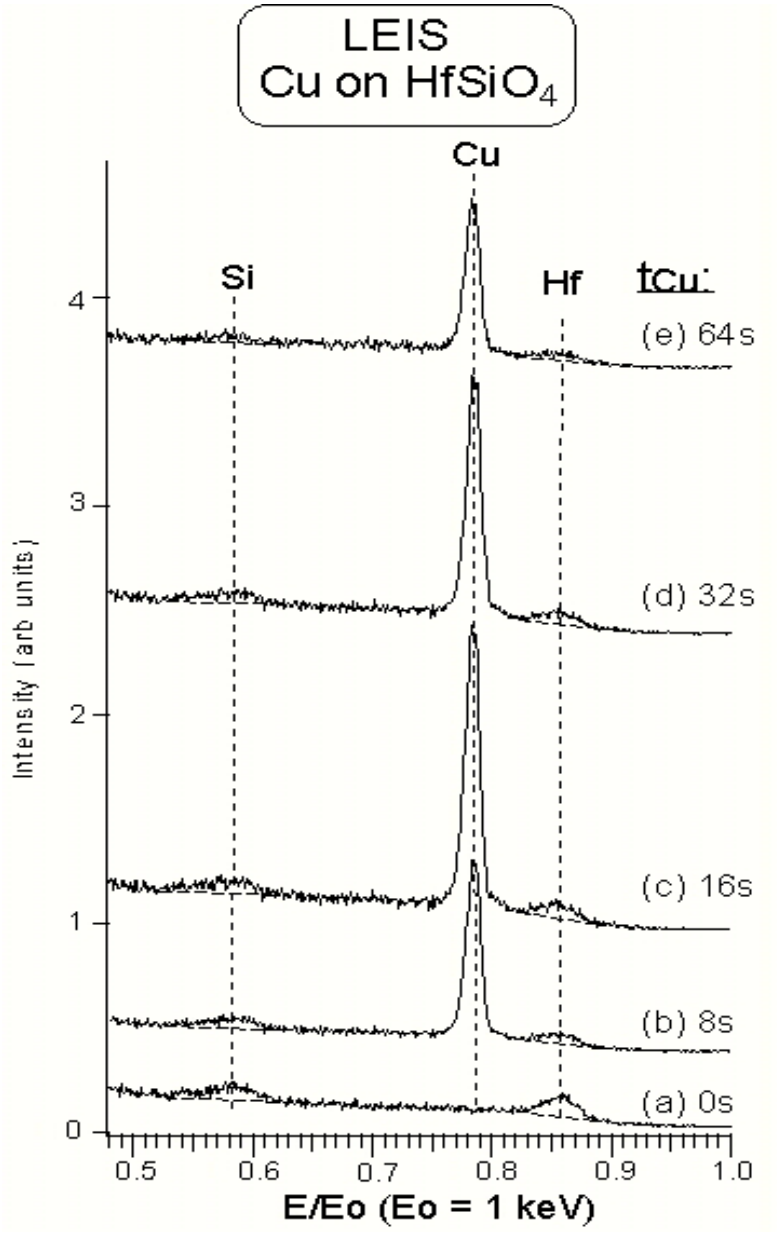

Fig. 3.3 LEIS data for Cu on $HfSiO_4$ at 300 K as a function of Cu dosing time. 1 keV of He^+ was used as primary beam.

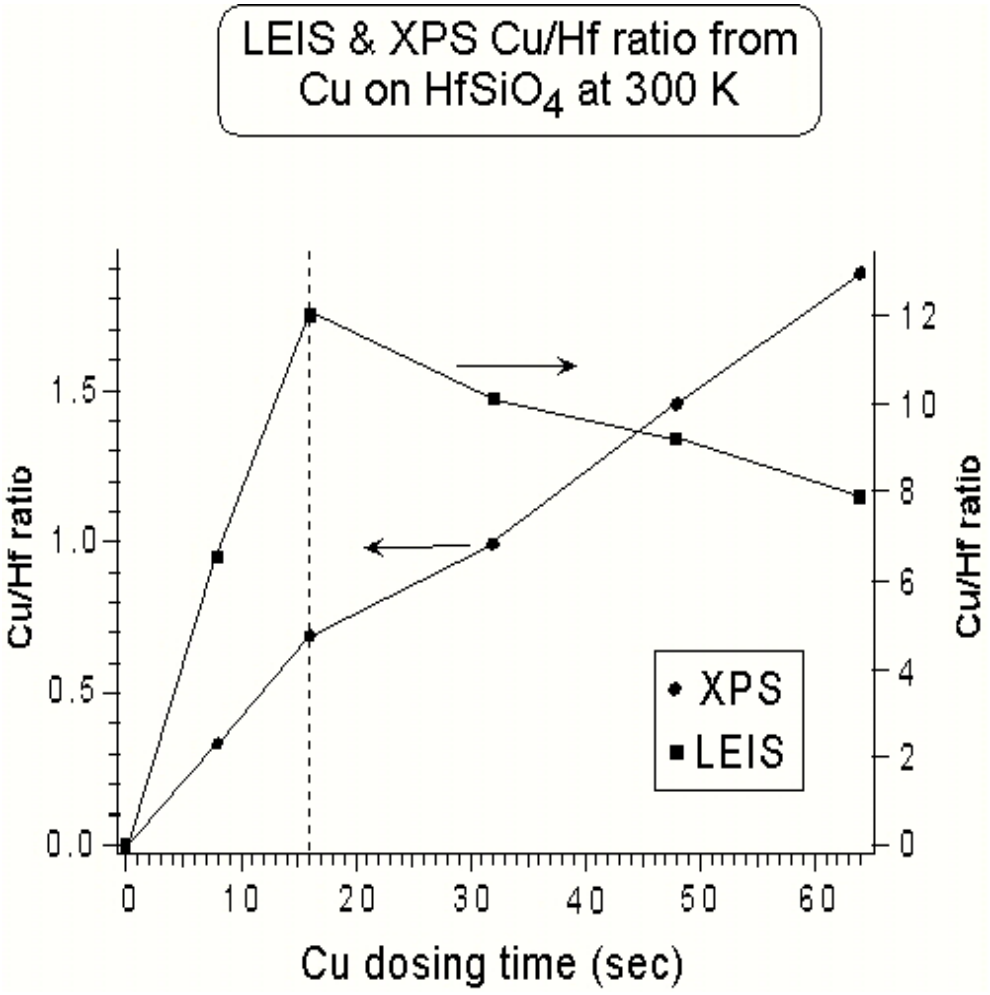

Fig. 3.4 The intensity ratio of Cu to Hf of LEIS and XPS data from Cu on $HfSiO_4$ at 300 K according to Cu dosing time.

3.3.2 Thermal annealing

The samples were prepared by exposing the hafnium silicate surface to Cu for 64s. The ensemble thickness of the deposited Cu layer before annealing was 0.56 nm, based on the attenuation of the Hf XPS signal. Fig. 3.5 shows the LEIS data during vacuum annealing at 573 K for 27 min. For the reference, LEIS data at 300 K is shown, and $t_{an} = 0$ was defined by 2 min after laser beam turned on, which actual sample temperature reached at 573 K. Since LEIS scan takes 3 min, spectra at each time is average value for 3 min. As the annealing time (t_{an}) increases from 0 to 12 min, the Cu peak intensity continuously decreases while both Hf and Si peak intensities continuously increase. After further annealing, Cu peak intensity decreases slowly and then remains constant, and both Hf and Si peak intensities increase slowly and then remain constant. To analyze this behavior, the intensity of Cu, Hf, and Si peaks and relative intensity ratio of Cu/Hf are calculated as a function of t_{an} (Fig. 3.6). In Fig. 3.6 (a), Cu peak intensity decreases by 38 % for $t_{an} \leq 3$ min and slowly decreases with further annealing. In the case of Hf peak, the intensity increases by 2 times large for $t_{an} \leq 3$ min and slowly increases with further annealing. For convenience, we divide three stages of Cu peak area according to the slope: (1) fast decrease for first 3min; (2) intermediate decrease for the next 9 min, and (3) saturation after further annealing. In Fig. 3.6 (b), for the fast stage, relative ratio of Cu peak area to Hf peak area decreases by 56 %. For the intermediate stage,

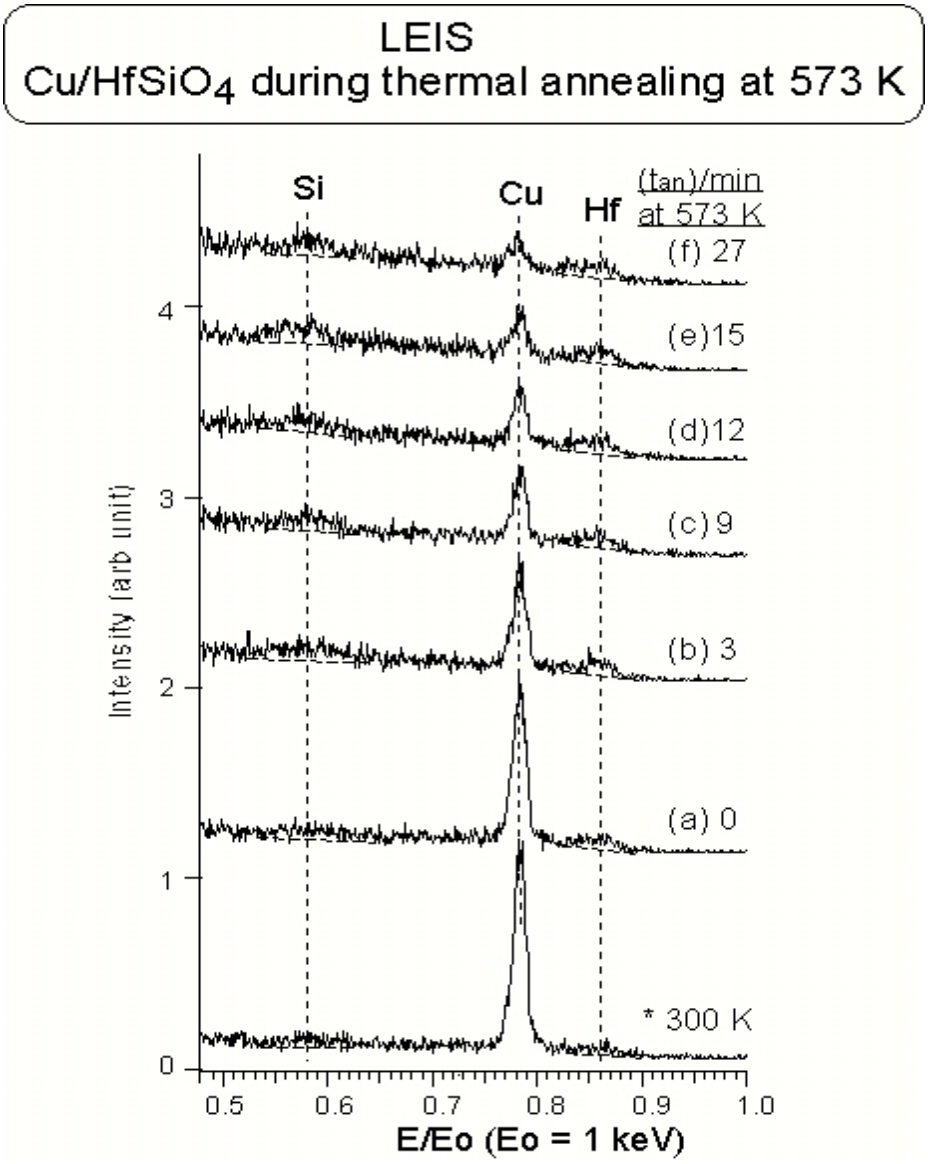

Fig. 3.5 LEIS spectra of Cu on $HfSiO_4$ (a- f) during thermal annealing at 573 K for 27 min under vacuum (< 7×10^{-9} torr). For reference, LEIS spectrum at 300 K is shown (*300K).

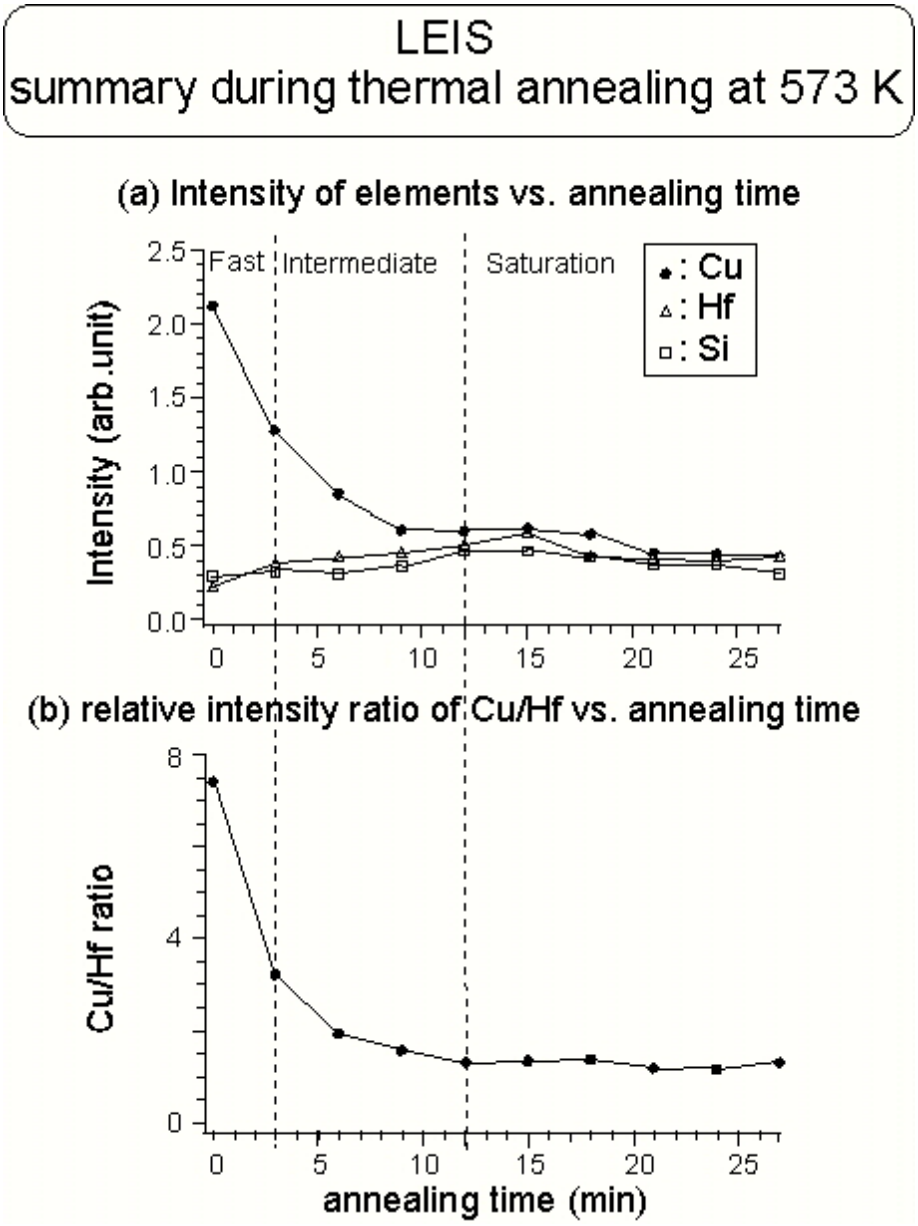

Fig. 3.6 The intensity of Cu, Hf, and Si (a) and intensity ratio of Cu to Hf (b) as a function of annealing time (t_{an}) from LEIS data (Fig.3.5).

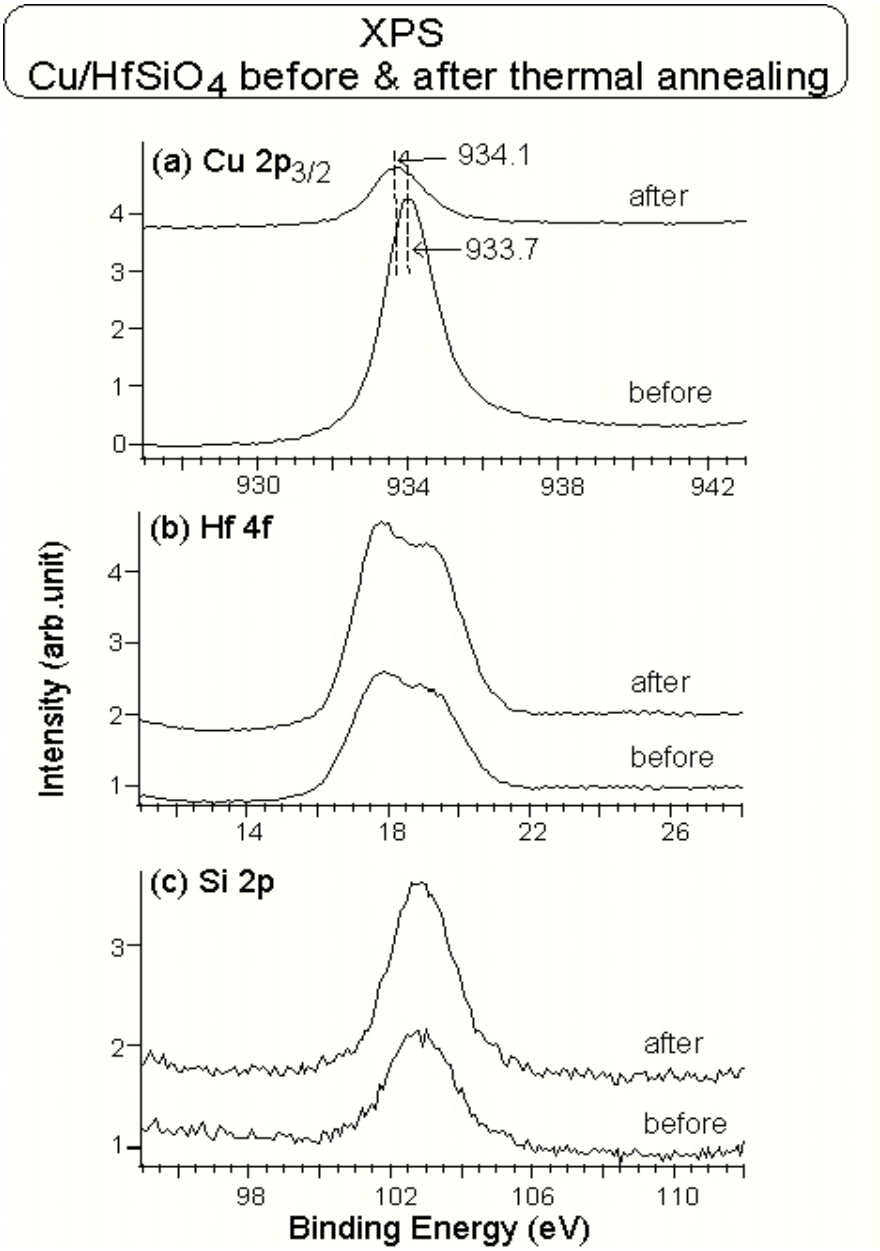

Fig. 3.7 XPS spectra of Cu on $HfSiO_4$ before and after thermal annealing at 573 K for 27 min under vacuum (< 7×10^{-9} torr).

Cu/Hf ratio decreases to 19 % of original intensity and remain constant further annealing (saturation stage).

The XPS data (Fig. 3.7) shows that the Cu 2 $p_{3/2}$ binding energy decreases from 934.1 to 933.7 eV after thermal annealing. If the cluster size grows, final-state screening effects can explain at least part of the downward shift. After thermal annealing, the Cu peak intensity decreases and both Hf and Si peak intensities increase. From these changes, ensemble average Cu thickness (based on the attenuation of Hf signal in XPS) decreases from 0.56 to 0.21 nm after thermal annealing. Based on the results from LEIS and XPS, we propose three plausible explanations for the decrease of Cu/Hf ratio: (1) small Cu clusters may combine to make larger three-dimensional clusters having less exposed area; (2) Cu atoms may diffuse into the $HfSiO_4$ layer, and (3) a combination of the previous two. If there were a taller Cu clusters after annealing, shadowing effect would be considered for both XPS and LEIS.

To investigate the size and morphology of Cu clusters, three samples were prepared and analyzed by AFM (Fig. 3.8): (1) Cu/$HfSiO_4$ sample after vacuum annealing at 573 K for 27 min (8a); (2) Cu/$HfSiO_4$ sample without vacuum annealing (8b); and, for comparison, (3) clean $HfSiO_4$ sample after vacuum annealing at 573 K for 27 min (8c). To determine actual lateral size of the features in the AFM images, we obtain AFM tip deconvolution graph with radius of curve from tip (10 nm) and standard sample. Fig. 3.8 shows the relationship

between measured size and actual size. For all AFM images, we convert measured diameter of Cu cluster from line-profile to actual diameter of Cu cluster using the equation shown in Fig. 8.

AFM images were obtained in at least 3 regions of each sample; the images shown in fig. 3.9 are representative of each of the surfaces. The profiles of the lines shown on the AFM images are displayed on the right side of each image. In $Cu/HfSiO_4$ sample after annealing, (a), there are bright areas (thicker areas) and rough background. The roughness of entire image is 0.87 nm. From the line-profile of all dots, the average diameter and height are 22.2 nm and 3.6 nm respectively. In the line-profile of the surface, Line 2, the distance from top to bottom is ~ 1.9 nm.

To confirm the bright dots are Cu clusters and investigate whether surface roughness is related with Cu over-layer, a $Cu/HfSiO_4$ sample without annealing ((b)) and a $HfSiO_4$ sample ((c)) were analyzed same way as (a). For the $Cu/HfSiO_4$ sample without annealing, (b), there are no distinct bright dots and the surface is smooth compared to (a). This implies that the diameter and height of Cu clusters at 300 K are below the detection limit (~ 3nm). Line profile shows that the distance from top to bottom is ~ 0.9 nm and RMS roughness is 0.15 nm. This suggests that thermal annealing leads to formation of large Cu clusters on the surface and roughening of surface. In $HfSiO_4$ sample after annealing, (c), line

profile shows that the distance from top to bottom is ~ 0.7 nm and RMS roughness is 0.14 nm.

To know whether all Cu clusters before annealing became large clusters after annealing, in Fig. 3.9 (a), total volume of all bright dots with diameter and height assuming ellipsoid ("oblate") shape. For the comparison, total volume of Cu overlayer using ensemble average thickness (0. 56 nm) from XPS data. Total volume of bright dots and Cu overlayer are 4,050 nm^3 and 140,000 nm^3 respectively. From this estimation, total volume of bright dots after annealing is only 3 % of Cu overlayer before annealing. This suggests that 97 % of Cu make rough surface as shown in Line 2 and/or diffuse into $HfSiO_4$ layer.

From all three images, we propose the following: (1) bright dots are Cu clusters; (2) rough surface is related with Cu clusters not from $HfSiO_4$ surface itself; and (3) most of Cu exists on the surface and not inside $HfSiO_4$ layer since Cu inside $HfSiO_4$ layer could not change surface roughness by a factor of 6.

To investigate the distribution of Cu cluster size, 1×1 μm^2 area of $Cu/HfSiO_4$ after thermal annealing was analyzed. The image is shown in Fig. 3.10 (a) and the diameter distribution of Cu clusters (bright dots) is shown in Fig. 3.10 (b). Actual diameter distribution (converted from measured values using AFM tip deconvolution curve), (b), shows narrow distribution (9 ± 2 nm) and average diameter is 9.6 ± 0.3 nm. The average height is 0.7 ± 0.08 nm. This narrow distribution can be explained by self-limiting growth. Self-limiting

growth of Cu clusters has been reported on another oxide surface (TiO_2, HfO_2) [2, 8]. The suggested mechanism was that the rate at which adatoms attach to existing clusters decreases rapidly as the cluster size increases, due to the existence of strain fields originating in the lattice mismatch at the interface between the Cu clusters and HfO_2 substrate during thermal annealing.

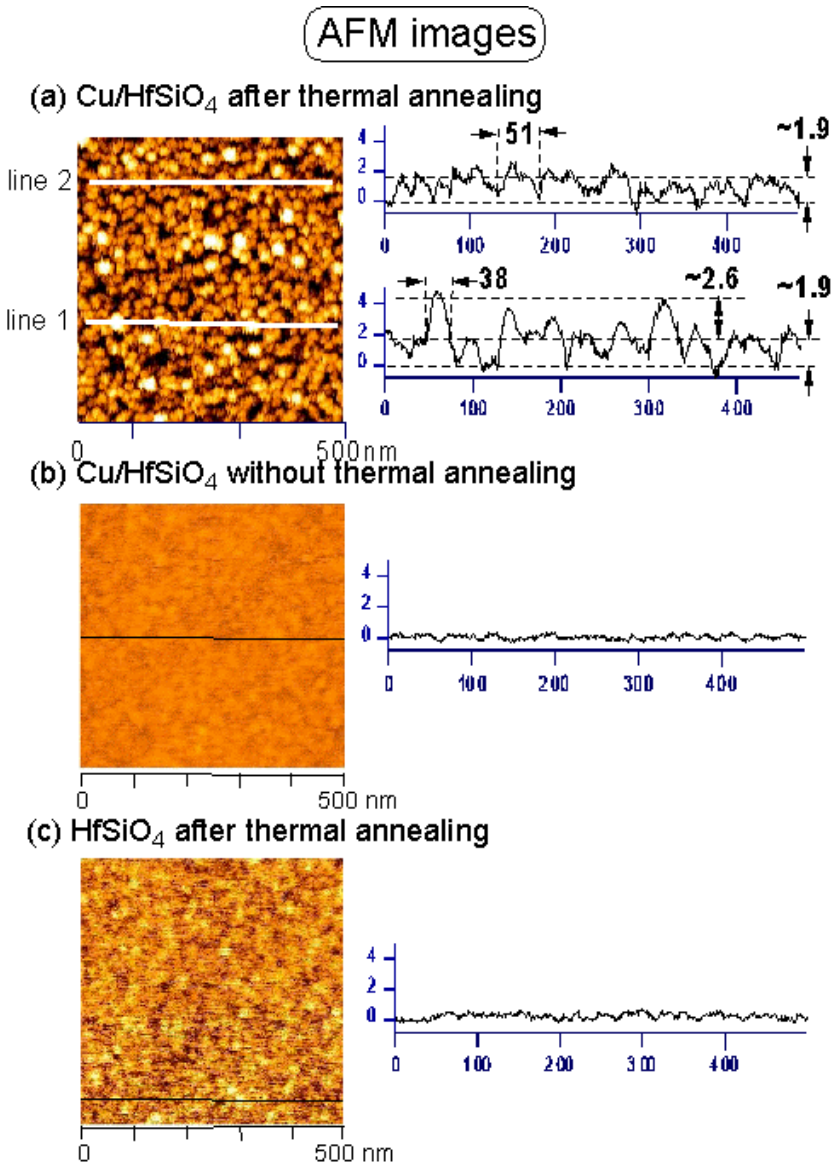

Fig. 3.8 AFM images of three samples: (a) $Cu/HfSiO_4$ sample after vacuum annealing at 573 K for 27 min; (b) $Cu/HfSiO_4$ sample without vacuum annealing; and, (c) clean $HfSiO_4$ sample after vacuum annealing at 573 K for 27 min.

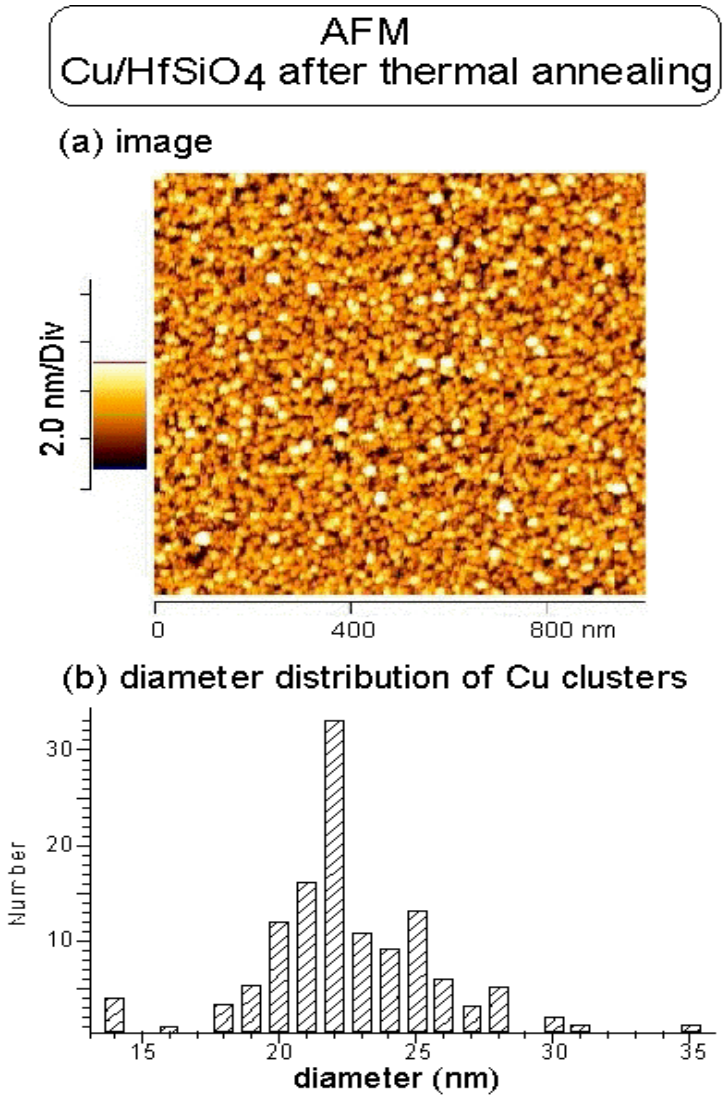

Fig. 3.9 AFM images of $Cu/HfSiO_4$ sample after vacuum annealing at 573 K for 27 min. (a) shows the image and (b) shows the histogram for the cluster diameter distribution from (a).

3.3.3 Proposed phenomenological model

3.3.3.1 At 300 K

Based on the reduction of the Hf 4 *f* peak intensity by Cu, we used a model proposed previous paper (Cu on HfO_2) [8]. This model was built by modification of a standard attenuation equation [13].

$$N = N_o \cdot \exp\left[-L/\left(\lambda_{Cu} \cdot \sin\theta\right)\right] \quad (1)$$

Where N is the Hf 4*f* peak area with Cu overlayer, N_o is the Hf 4*f* peak area without Cu overlayer, L is the thickness of Cu overlayer, λ_{Cu} is the mean free path of Hf electron passing through Cu (1.9 nm) [15], and θ is the angle between analyzer and sample (60^o). The basic idea is that the total intensity of the photoelectrons from Hf (per unit area) can be estimated by summing Hf photoelectrons passing through n Cu layers. This model does account for variation of the Cu thickness while surface roughness variations are not taken into account. For the case of only one Cu layer, we calculate the relative portion of Hf without a Cu overlayer (x) and Hf with Cu overlayer (y) using eq. (2) and one boundary condition ($x + y = 1$) as total area of Hf is constant.

$$N / N_o = x + (1-x) \cdot \exp\left[-L_1/\left(\lambda_{Cu} \cdot \sin\theta\right)\right] \quad (2)$$

Where L_1 is the thickness of monolayer of Cu (0.2 nm).

When accounting for two layers of Cu, the analogous equation is:

$$N / N_o = x + y_1 \cdot \exp\left[-L_1/\left(\lambda_{Cu} \cdot \sin\theta\right)\right] + y_2 \cdot \exp\left[-2 \cdot L_1/\left(\lambda_{Cu} \cdot \sin\theta\right)\right] \quad (3)$$

For a *n*-layer case, we expand eq. (3) as:

$$N / N_o = x + \sum_{i=1}^{n} y_i \cdot \exp\left[-i \cdot L_1 / \left(\lambda_{Cu} \cdot \sin\theta\right)\right] \qquad (4)$$

Where n is the number of Cu layers, and the boundary condition is: $(x + \sum_{i=1}^{n} y_i = 1)$.

The relative portion of each Cu multi-layer can not be calculated with only one boundary condition $(x + \sum_{i=1}^{n} y_i = 1)$. Instead, we estimated the attenuation of the Hf intensity ($(N/N_o)_{cal}$) based on model structure. The evaluation procedure for model structure is: (1) build several possible Cu structures consistent with the LEIS data, (2) determine x, y_1, $\cdot\cdot$ y_n for each Cu structure, (3) calculate $(N/N_o)_{cal}$ for each model from eq. (3) using x, y_1, $\cdot\cdot$ y_n and (4) compare $(N/N_o)_{cal}$ with $(N/N_o)_{exp}$ determined from XPS to determine the optimum, but not necessarily unique, model.

Based on the LEIS measurements and on the results obtained from the modified attenuation equation using XPS data, we propose a Cu structure and possible mechanisms for the nucleation and cluster growth stages. Table 3.1 summarizes. The 2nd column shows schematic side-views of Cu structure on Si, there are three kinds of Cu sites in the model: (1) Cu site detected by LEIS, i.e., top layer of island, (2) Cu site not detected by LEIS, i.e., inside island, and (3) vacated Cu site due to migration of Cu. The 3rd column describes proposed

contributing mechanisms, the 4th column shows the number of Cu atoms that could be detected by LEIS in the model structure and the 5th column shows, for XPS, the calculated and experimental results. Assuming no multi-layer of Cu for $t_{Cu} \leq 16$ s, the relative coverage of Cu on the HfO_2 surface increases from 44% to 85% from eq. (2).

Upon further dosing of Cu, clusters are proposed based on data in Fig. 3. There are three plausible mechanisms: (I) Cu atoms add only to existing Cu layer, (II) Cu atoms adsorb on HfO_2 and diffuse laterally to make 2nd layer (diffusion-mediated growth), and (III) Cu atoms migrate from the 1st layer into the 2nd (self-growth). In case (I), the percentage of HfO_2 surface without Cu overlayer to total HfO_2 surface remains constant since there are no added Cu atoms on HfO_2 surface. Case (III) is indistinguishable from case (I). Thus, we only consider case I and a combination of cases I and II. At t_{Cu} = 32 and 48 s, the number of exposed Cu atoms (detected by LEIS) decreases due to the formation of clusters, as observed by decaying Cu/Hf ratio in Fig. 3 (b). At t_{Cu} = 32 and 48 s, the $(N/N_o)_{cal}$ values for both cases are within our experimental data range. At t_{Cu} = 64 s, the $(N/N_o)_{cal}$ values in both cases using eq. (4) are same although the relative percentage of each Cu layer differs. Currently, we cannot determine which mechanism is dominant. Nevertheless, formulation can be applied to model the Cu structure since the $(N/N_o)_{cal}$ values within 5 % of $(N/N_o)_{exp}$.

3.3.3.2 At 573 K

We propose the change of Cu structure based on LEIS and AFM results (Figs.3.5 and 3.9). Fig. 11 shows the proposed structure at 300 and 573 K. Basic idea of our model is that the intensity of LEIS data is proportional to the total exposed surface area of Cu with following assumptions: (1) total Cu volume is constant (no vertical diffusion into HfO_2 occurs during annealing process); (2) uniform Cu clusters size at 300 and 573 K; (3) roughness of $HfSiO_4$ surface is neglected; and (4) initial exposed Hf surface area per unit area ($^{o}A_{Hf}$) at 300 K is from proposed model at 300 K. Fig. 3.11 shows the proposed model at 300 and 573 K. Using above boundary conditions and experimental data (LEIS, AFM), we calculate the ratio of total number of cluster at 573 K to total number of cluster at 300 K ($^{cal}R_{num} = m/n$) and ratio of total exposed Cu surface area at 573 K to total exposed Cu surface area at 300 K ($^{cal}R_{Cu} = {}^{573}A_{Cu} / {}^{0}A_{Cu}$).

At 573 K, total covered Hf surface by Cu cluster is:

$$^{573}A_{int} = {}^{cal}R_{int} \cdot {}^{o}A_{int} \qquad (5)$$

where $^{o}A_{int} = n \cdot 4 \cdot \pi \cdot r_o^2$, $^{573}A_{int} = m \cdot 4 \cdot \pi \cdot r^2$, and $^{cal}R_{int}$ is calculated from $^{o}A_{Hf}$ (from proposed Cu structure at 300 K) $^{exp}R_{Hf}$ (from LEIS data).

From eq. (5), the diameter of Cu clusters at 573 K is:

$$r = \{ (^{cal}R_{num})^{-1} \cdot R_{int} \}^{1/2} \cdot r_o \qquad (6)$$

From the constant of total Cu volume ($^{573}V_{Cu} = {}^{o}V_{Cu}$) and eq. (6), the height of cluster is:

$$m \cdot (0.5) \cdot \{(4/3)\pi \cdot r^2 \cdot h\} = n \cdot (0.5) \cdot \{(4/3)\pi \cdot r_o^3\}$$

$$h = r_o \,/\, {}^{cal}R_{int} \qquad (7)$$

Using the ratio of radius to height ($^{exp}R_{r/h}$) from the AFM image, eq. (10), and eq. (7) the $^{cal}R_{num}$ is:

$$^{exp}R_{r/h} = \quad r / h$$

$$= {}^{cal}R_{int} \cdot \{(^{cal}R_{num})^{-1} \cdot {}^{cal}R_{int}\}^{1/2}$$

$$^{cal}R_{num} = (^{cal}R_{int})^3 \cdot (^{exp}R_{r/d})^{-2} \qquad (8)$$

Using the equation of surface area for ellipsoid ("oblate" shape), $^{573}A_{Cu}$ is:

$$^{573}A_{Cu} = m \cdot (0.5) \cdot \{2\pi \cdot r^2 + 2\pi \cdot (r \cdot h / e) \cdot \sin^{-1}(e)\} \qquad (9)$$

where e is the eccentricity of the ellipse ($e \equiv (1 - h^2 / r^2)^{1/2}$).

Using $^0A_{Cu}$ (= $n\, 2\pi \cdot r_o^2$), eq. (6), (7), (8), and (9), the $^{cal}R_{Cu}$ is:

$$^{cal}R_{Cu} = {}^{573}A_{Cu} / {}^0A_{Cu}$$

$$= {}^{cal}R_{num} \cdot (0.5) \cdot \{{}^{cal}R_{num}{}^{-1} \cdot {}^{Cal}R_{int} + e^{-1} \cdot {}^{Cal}R_{int}{}^{-1/2} \cdot {}^{cal}R_{num}{}^{-1/2} \cdot \sin^{-1}(e)\} \qquad (10)$$

Table 3.2 shows the summary of the calculation values of $^{cal}R_{int}$ and $^{cal}R_{Cu}$ using eq. (8) and (10) according to two initial exposed Hf surface area using above equations and experimental values. The 1st column shows two different exposed Hf surface at 300 K according to growth mechanisms described in Table 1. The 2nd column shows the experimental values ($^{exp}R_{Hf}$, $^{exp}R_{Cu}$, $^{exp}R_{r/d}$), form LEIS (Fig. 6) and AFM (Fig. 10). The 3rd column shows the calculation values of $^{cal}R_{int}$, $^{cal}R_{num}$, and $^{cal}R_{Cu}$. Compared with two cases, $^{cal}R_{Cu}$ from case 2 is closer to $^{exp}R_{Cu}$ than that from case 1. This suggests that the combination of self-

growth and diffusion-mediated growth is the more dominant mechanism at 300 K. From the case 2, ${}^{cal}R_{Cu}$ is 0.5 times larger than ${}^{exp}R_{Cu}$ and ${}^{cal}R_{num}$ is 0.007, i.e., only 0.7 % of total number of Cu clusters is left on surface after thermal annealing. Based on our model and experimental data, we propose three plausible explanation for the difference between ${}^{cal}R_{Cu}$ and ${}^{exp}R_{Cu}$: (1) Although AFM results support no Cu diffusion into $HfSiO_4$ layer, there are still possibility of Cu diffusion, contributing the decrease of ${}^{exp}R_{Cu}$; (2) As the height of cluster increases, shadowing effect of the other side of cluster increases, contributing the decrease of ${}^{exp}R_{Cu}$; (3) Not all Cu clusters make large Cu clusters as shown in Figs. 3.9 and 10, there are small Cu clusters on the $HfSiO_4$ surface due to self-limiting growth mechanism, contributing to the increase of ${}^{exp}R_{Cu}$. Consequently, we propose that the decrease of Cu/Hf ratio during thermal annealing is due to the combination of making large clusters by combining smaller ones and the diffusion of Cu into $HfSiO_4$ layer, but the dominant mechanism is first one. Compared with previous study of Cu on HfO_2 surface, we can not determine which one is dominant growth mechanism only from XPS data. Combined with XPS, LEIS, and AFM results, we propose that the dominant growth mechanism of Cu on $HfSiO_4$ surface at 300 K is combination of self-growth and diffusion-mediated growth.

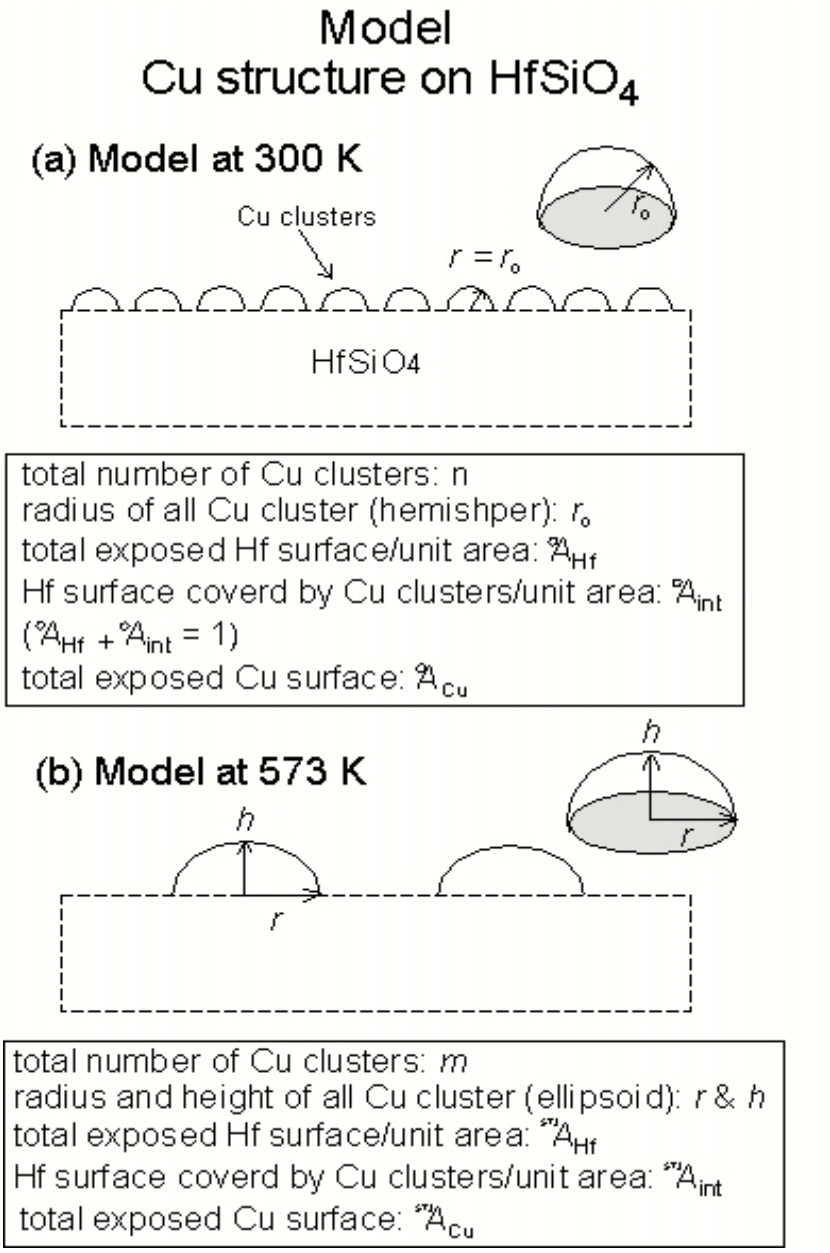

Fig. 3.10 Proposed model for Cu structure on $HfSiO_4$ at 300 K and 573 K.

Table 3.1.
The summary of proposed Cu structure at 300K based on LEIS and XPS results

t_{Cu} (s)	**Model**	**Mechan-ism**	# of Cu detected by LEIS	XPS results	
				Experiments	Calculation
8	◉:Detected Cu, ○:undetected Cu, ◯: Hf, ∘ : O, ⁘ :vacated Cu site 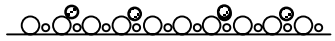 HfO_2	Nucleation stage	5	$(N/N_o)_{exp}$ = 0.938	x = 0.56, y = 0.44
16			10	$(N/N_o)_{exp}$ = 0.885	x = 0.15, y = 0.85
32	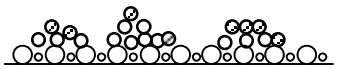	Mechanism I (see text)	8	$(N/N_o)_{exp}$ = 0.83-0.85	x = 0.15, y_1 = 0.28, y_2 = 0.43 y_3 = 0.14 => $(N/N_o)_{cal}$ = 0.83
	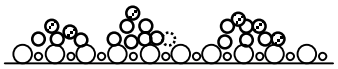	Mechanism I & II (see text)	6		x = 0.24, y_1 = 0.19, y_2 = 0.38 y_3 = 0.19 => $(N/N_o)_{cal}$ = 0.84
48	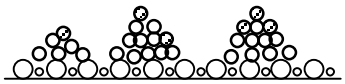	Mechanism I	6	$(N/N_o)_{exp}$ = 0.74-0.76	x = 0.15, y_1 = 0.21, y_2 = 0.22, y_3=0.28,y_4=0.14 => $(N/N_o)_{cal}$ = 0.75
	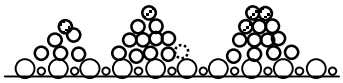	Mechanism I & II	5		x = 0.24, y_1 = 0.13, y_2 = 0.25, y_3=0.19,y_4=0.19 => $(N/N_o)_{cal}$ = 0.76
64	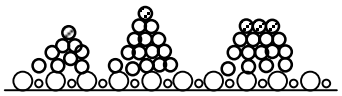	Mechanism I	5	$(N/N_o)_{exp}$ = 0.67-0.70	x = 0.15, y_1 = 0.08, y_2 = 0.21, y_3=0.21,y_4=0.28 y_5=0.07 => $(N/N_o)_{cal}$ = 0.70
	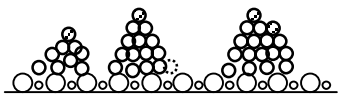	Mechanism I & II	4		x = 0.24, y_1 = 0, y_2 = 0.19, y_3=0.19,y_4=0.25 y_5=0.13 => $(N/N_o)_{cal}$ = 0.70

Table 3.2
Summary of proposed Cu structure at 573 K based on LEIS and AFM results

Two initial conditions	Experiments Total surface area of Hf: 1.0			Calculation		
Exposed Hf surface per unit area ($^{o}A_{Hf}$)	LEIS data		AFM data	$^{cal}R_{int}$ ($^{573}A_{int}/^{0}A_{int}$)	$^{cal}R_{num}$ (m/n)	$^{cal}R_{Cu}$ ($^{573}A_{Cu}/^{0}A_{Cu}$)
	$^{exp}R_{Hf}$ ($^{573}A_{Hf}/^{0}A_{Hf}$)	$^{exp}R_{Cu}$ ($^{573}A_{Cu}/^{0}A_{Cu}$)	$^{exp}R_{r/d}$ (r/d)			
Case 1: 0.15 (Mechanism I)	2.60	0.20	6.86	0.70	0.007	0.43
Case 2: 0.24 (Mechanism I & II)	2.60	0.20	6.86	0.49	0.003	0.30

3.4 CONCLUSION

The growth of Cu on $HfSiO_4$ at 300 K involves initial formation of three-dimensional clusters (VW growth) without Cu oxidation. We proposed a semi-quantitative model to explain the growth mode of Cu, the fractional area covered by Cu as the dosing time increases at 300 K, and the change of Cu structure during thermal annealing at 573 K based on XPS, LEIS, and AFM results. At 300 K, as-deposited Cu covers no more than 85 % of $HfSiO_4$ surface as two-dimensional islands, as determined by XPS Hf and Si signal attenuation. During thermal annealing at 573 K for 27 min under vacuum ($\sim 7 \times 10^{-9}$ torr), the Cu cluster size increases by combining smaller ones and Cu may diffuse into $HfSiO_4$ layer, although we do not have any evidence for the latter. AFM images of annealed samples show uniform Cu clusters (9.6 ± 0.3 nm), this uniformity is ascribed to a self-limiting growth [2, 8].

3.5 REFERENCES

[1] U. Diebold, J.-M Pan, T. E. Madey, Surf. Sci. 287/288 (1993) 896

[2] D. A. Chen, M. C. Bartelt, R. Q. Hwang, K.F. Macarty, Surf. Sci. 450 (2000) 78

[3] Q. Ge, P. Møller, Thin Solid Films 254 (1995) 10

[4] X. Xu, J.-W. He, D.W. Goodman, Surf. Sci. 284 (1993) 103

[5] Y. Wu, E. Garfunkel, T. E. Maday, J. Vac. Sci. Technol. A 14 (1996) 1662

[6] M-C Wu, D. W. Goodman, J. Phys. Chem. 98 (1994) 9874

[7] G. D. Wilk, R. M. Wallace, J. M. Anthony, J. Appl. Phys. 87 (2000) 484

[8] H. J. Park, Y.-M. Sun, H. Troiani, P. Santiago, M. J. Yacaman, J. M. White, *submitted to* Surface Science

[9] A. W. Adamson, "*Physical Chemistry of Surfaces*", New York (1990)

[10] S. H. Overbury, P. A. Bertrand, G. A. Somorjai, Chem. Rev. 75 (1975) 547

[11] Y. -M Sun, J. Lozano, H. Ho, H. J. Park, S. Veldman, J. M. White, Appl. Surf. Sci. 161 (2000) 115

[12] Q. Wang, Y.-M. Sun, W. Zhao, J. Campagna, J. M. White, submitted to Review of Scientific Instruments

[13] A. Y. Mao, K.-A. Son, D. A. Hess, L. A. Brown, J. M. White, D. L. Kwong, D. A. Roberts, R. N. Vritis, Thin Solid Films 349 (1999) 230

[14] W. F. Egelhoff, Jr., Surf. Sci. Rep. 6 (1987) 253

[15] S. Tanuma, C. J. Powell, Surf. Interface Anal. 17(13) (1991) 911

CHAPTER 4

Growth and thermal annealing of HfO_2 on Si (100)

4.1 INTRODUCTION

Silicon dioxide (SiO_2) has been successfully used as the primary gate dielectric material in field-effect devices and scaled down for the device's high performance with much effort towards current technologies of 0.13~0.18 μm. However, the technology beyond 0.1 μm requires further thickness scaling of SiO_2, but the thickness of SiO_2 is approaching its scaling limit. Among many high-k dielectric candidates for replacing SiO_2, HfO_2 is promising because of its high dielectric constant (~ 30) and thermodynamic stability in contact with Si [1]. An important parameter to control is its chemical reaction with silicon, since those two materials are usually in direct contact in metal-oxide technology [2]. The possible interfacial material between HfO_2 and Si are nonstoichiometric silicon oxide and hafnium silicate. The dielectric constant of both materials is smaller than that of HfO_2, so these materials reduce the total capacitance. The study of the interface between HfO_2 and Si is very important to control the interfacial layer formation and improve the equivalent oxide thickness (EOT) of dielectrics.

Generally, to make hafnium silicate, there are three possible ways: (1) $HfSi + O_2 \Rightarrow HfSiO_4$, i.e., oxidation of hafnium silicide; (2) $HfO_2 + SiO_2 \Rightarrow HfSiO_4$, i.e., HfO_2 is deposited on SiO_2 substrate; and (3) $HfO_2 + Si + O_2 \Rightarrow HfSiO_4$, i.e., Si atom and extra oxygen are supplied to HfO_2. Among the three methods, the first method is easy to utilize to make hafnium silicate using physical vapor deposition [3]. Cosnier *et al.* made interfacial hafnium silicate between HfO_2 and SiO_2 substrate using the second method [4]. In the case of third method, we need very high temperature annealing for migration of Si atom from Si substrate. Previously, we reported that the migration of Si atom from Si substrate occurred at 1073K [5].

In this paper, we studied various compositions of hafnium silicide and hafnium silicate on Cu substrates, and the growth and thermal annealing effects on HfO_2 on Si (100) using *in-situ* physical vapor deposition (PVD), *in-situ* X-ray photoelectron spectroscopy (XPS) and *in-situ* low energy ion scattering (LEIS). For vacuum annealing experiments, a CO_2 laser beam was used to irradiate the back of the samples, allowing us to obtain XPS and LEIS data at high temperature (823 K).

We obtained XPS spectra of various compositions of hafnium silicide and hafnium silicate on Cu substrates for standard binding energy in XPS spectra according to composition. To minimize the formation of interfacial silicon oxide between HfO_2 and the Si substrate, we deposited Hf layer first and then oxidized

the Hf layer using an oxygen plasma source at 300 K. We observed that there is no hafnium silicide formation during deposition of Hf layer on Si (100). We confirmed that the Hf layer on the Si substrate plays a role as an oxygen diffusion barrier with two different structures of Hf on Si. LEIS confirmed the structures of two samples: (1) Si substrate fully covered by Hf overlayers (sample A); and (2) Si substrate partially covered by Hf (sample B). During oxidation of the Hf layer at 300 K, both samples showed the formation of interfacial silicon oxide, but the relative amount of interfacial silicon oxide inside HfO_2 in sample A is smaller than in sample B. During vacuum annealing at 823 K, there was no change of chemical states of elements and no evidence for the formation of hafnium silicate at the interface between HfO_2 and nonstoichiometric silicon oxide. Based on the thermal annealing results, we suggest that HfO_2 is thermodynamically stable in contact with nonstoichiometric silicon oxide at 823 K

4.2 EXPERIMENTAL

4.2.1 Film deposition

Films were deposited in a physical vapor deposition system equipped with a main chamber (base pressure ~ 5×10^{-8} torr), a load lock chamber, and three sputtering guns with one DC and two RF power supplies. The detail of the PVD system was described previously [6]. Metallic Hf target (99.9%) was purchased

from Kurt Lesker. Sputtering was done with flowing, 20 sccm, ultrahigh purity Ar (99.999%) that passed through as gas purifier prior to entering the chamber. Hafnium silicide and hafnium silicate were deposited on Cu substrate using sputtering Hf and Si targets simultaneously. DC and RF plasma sources were used for deposition of Hf and Si, respectively. Plasma oxygen (10% diluted with argon) was used to oxidize Hafnium films using 10 W of RF power and 10 sccm of flow rate of oxygen under 2 mtorr of chamber pressure. The $25 \times 25 \times 1$ mm^3 boron-doped Si (100) substrates were cleaned using the follow procedure: surface hydrocarbons were removed using acetone, iso-propyl alcohol, and deionized water in sequential washings, the native oxide was removed by rinsing in HF solution (H_2O: HF = 40:1).

4.2.2 Analysis

Once prepared, the films were transferred through a UHV system into an analysis chamber (base pressure ~ 1×10^{-9} torr) for LEIS and XPS. LEIS was used to identify the composition of the topmost layer of film. The primary ion beam energy E_o used in this work was 1 keV. The pressure in the analysis chamber was ~7×10^{-9} torr during LEIS. XPS was used to analyze the composition of the surface and near-surface region (~6 nm). Mg Kα X-ray source was used to take survey and high-resolution spectra. Survey and high resolution scans were taken at 93.9 and 50.0 eV pass energy, respectively.

4.2.3 Thermal annealing

Sample heating was achieved by introducing a continuous IR CO_2 laser beam (wavelengths between 10.57 and 10.63 microns) into the analysis chamber through a ZnS window. Once inside the chamber, the beam was directed towards the back of the sample by a Cu total reflection mirror mounted underneath the hollow sample stage. The sample temperature was monitored by a thermocouple coated with graphite placed in the laser beam pathway. The reading obtained from this thermocouple was calibrated to the temperature of the sample as described by Wang *et al*. [7]. By heating the sample in the analysis chamber it was possible to obtain LEIS data at elevated temperatures.

4.3 RESULTS AND DISCUSSION

4.3.1 At 300K

4.3.1.1 Hafnium silicate on Cu

To identify the interfacial layer between HfO_2 and Si substrate, two possible materials (hafnium silicide, hafnium silicate) with various compositions were investigated by XPS. First, various compositions of HfSix were deposited on Cu substrates. Fig. 4.1 shows the XP spectra of Hf 4f (a) and Si 2p (b) with various atomic ratios of Hf to Si. Although $HfSi_x$ was deposited without supplied oxygen, oxygen exists in the $HfSi_x$ film, giving rise to a high BE

shoulder in the Hf 4f spectra. We suspect that the oxygen may have come from metallic targets (Hf and Si), even though the targets were pre-sputtered to clean their surface. In $HfSi_{0.07}$ sample, the BE of Hf 4f is almost identical to that of metallic Hf 4f (14.5 eV), while the BE of Si 2p is ~ 1.0 eV smaller than that of metallic Si (99.9 eV) [8]. As the atomic ratio of Si increases up to 1.5, the BE of both Hf 4f and Si 2p peaks increases; however, the BE of Si 2p is still smaller than that of metallic Si 2p. These changes can be explained by comparing the electronegativity of Hf and Si. The electronegativity of Si is larger than that of Hf, as a result, the electron density shifts toward the Si atom when they form a chemical bond. Therefore, the BE of Hf 4f is larger than that of its metallic state while BE of Si 2p is smaller than that of its metallic state.

Second, various compositions of $HfSi_xO_y$ were deposited on Cu substrates. Fig. 4.2 shows the XP spectra of Hf 4f, Si 2p, and O 1s for various atomic ratios of Hf to Si. In the spectra of Hf 4f and Si 2p, (Figs. 4.2 (a) and (b)), corresponding to hafnium rich and stoichiometric hafnium silicate, $Hf_1Si_{0.5}O_3$ and $HfSiO_4$, the BE of Hf 4f and Si 2p are smaller than that of HfO_2 and SiO_2, respectively. On the other hand, in the case of silicon-rich hafnium silicate, $Hf_1Si_{17}O_{36}$, the BE of Hf 4f and Si 2p is larger than that of HfO_2 and SiO_2, respectively. In the spectra of O 1s, (Fig. 4.2 (c)), the BE is close to that of HfO_2 in hafnium rich silicate ($Hf_1Si_{0.5}O_3$) while BE is close to that of SiO_2 in silicon rich silicate ($Hf_1Si_{17}O_{36}$). These trends in the changes of BE of Hf 4f, Si 2p, O

1s can also be explained by comparing the electronegativity of Hf, Si, and O. The order of their electronegativities is O > Si > Hf.

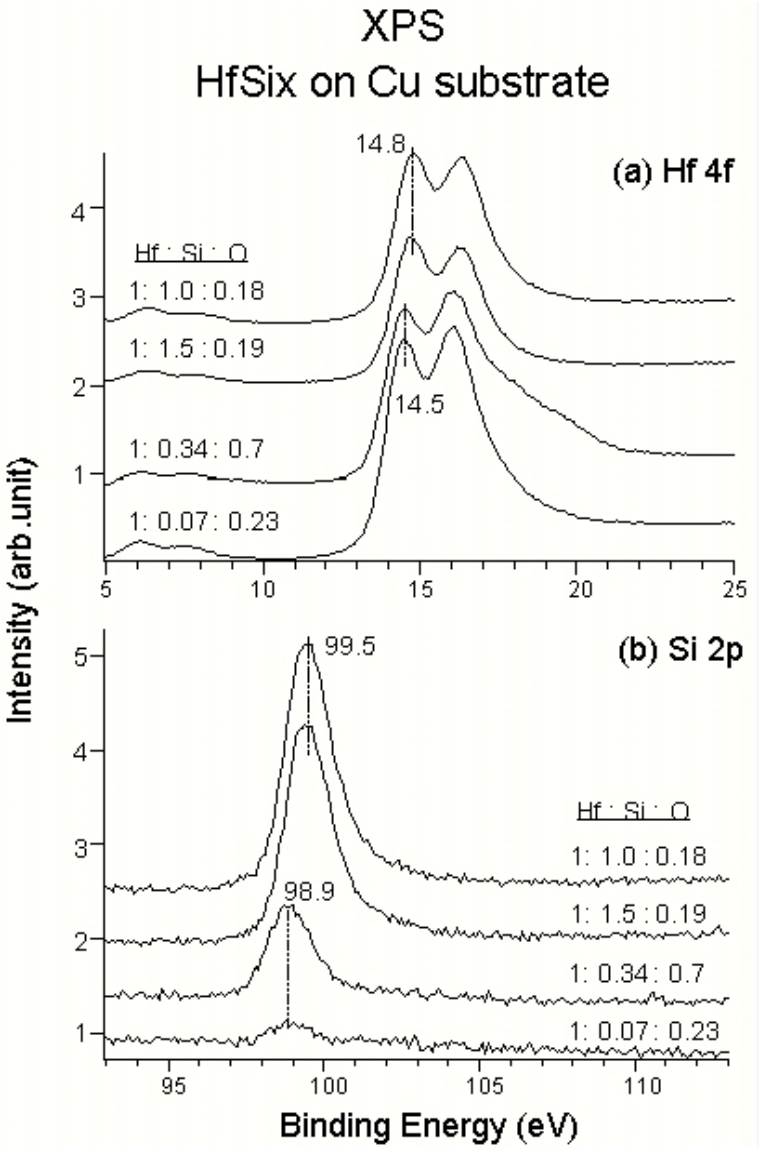

Fig. 4.1 XPS data of Hf 4f and Si 2p from various compositions of hafnium silicide on Cu substrate.

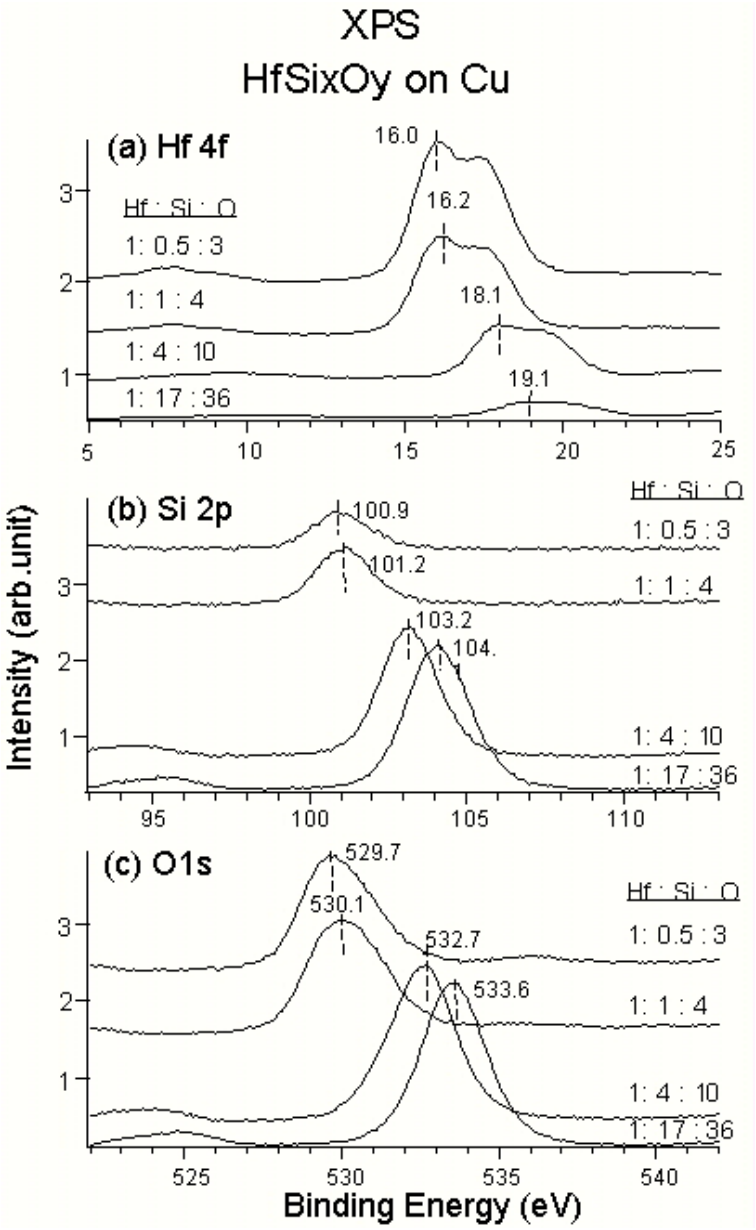

Fig. 4.2 XPS data of Hf 4f, Si 2p, and O 1s from various compositions of hafnium silicate on Cu substrate

4.3.1.2 Hf on Si

To minimize the formation of interfacial silicon oxide during deposition of HfO_2, a thin Hf metal layer was deposited on Si substrate followed by oxidation. To check whether Hf fully covers the Si substrate, LEIS and XPS were used to find the optimum Hf deposition time. Fig. 4.3 shows the LEIS data of Hf on Si as a function of Hf deposition time. The Hf and Si peaks are located at E/E_o = 8.6 and 5.8, respectively. As the deposition time increases from 20 to 60 s, the Si peak is totally depressed and Hf peak intensity increases. This means that Hf fully covers the Si surface.

Fig. 4.4 shows the XP spectra of Hf 4f, Si 2p, and O 1s for the same sample as the one analyzed by LEIS. As the deposition time increases, the Hf 4f peak area did not increase linearly, therefore, the Si 2p peak area did not decreased linearly. Deposited Hf was partially oxidized, as indicated by the higher BE shoulder and the presence of O 1s peak. In addition, the Si surface was also partially oxidized, since the O 1s peak shape is asymmetric, indicating that there is more than one chemical state of oxygen.

Fig. 4.5 shows one example of peak decomposition of Hf 4f, Si 2p, and O 1s from the XPS data shown in Fig. 4.4. Peak decomposition was done using standard least-square fitting procedure and FWHM values from clean Si sample and fully oxidized HfO_2 film. In Hf 4f, (a), there are two sets of peaks attributed to contributions from metallic Hf located at ~ 14.6 eV and nonstoichiometric

HfO_x ($0< x <2$) located at ~ 18.0 eV with one peak. HfO_x peak was difficult to decompose according to spin-orbital coupling since there is no distinguishable feature in the higher binding shoulder (~ 18 eV). In Si 2p, (b), there are two peaks corresponding to contributions from substrate Si located at ~ 99.5 eV and nonstoichiometric SiO_y ($0< y < 2$) located at ~ 101 eV, and there is no silicide peak located at < 99.5 eV. In O 1s, (c), there are also two peaks corresponding to HfO_x located at ~ 531.2 eV and SiO_y located at ~ 533.0 eV. Based on the decomposition of XPS peaks, we suggest that there is no formation of hafnium silicide.

Fig. 4.6 shows the ensemble average Hf thickness and relative ratio of HfO_x and SiO_y as a function of deposition time based on the result of XPS peak decomposition. In Fig. 4.6 (a), the Hf film thickness (including SiO_y) was estimated from the attenuation of metallic Si peak signal using standard attenuation equation [9]. The Hf film thickness increases linearly for deposition time ≤ 40 s and then increases slowly at 60 s. This implies that the growth mode of Hf changes from two-dimensional layer to three-dimensional island formation between 40 and 60 s. In Fig. 4.6 (b) is a plot of the relative ratio of HfO_x peak area to the total Hf peak area, of the SiO_y peak area to the total Si peak area, and the SiO_y peak area to the total O peak area based on the peak decomposition procedure shown in Fig. 4.5. As the Hf deposition time increases from 20 to 60 s, the relative ratio of HfO_x peak area to the total Hf peak area remains constant

within ± 4 %, indicating uniform distribution of HfO_x inside the Hf film. On the other hand, in the case of SiO_y, there are two different trends in Si 2p and O 1s peaks. Between 20 s and 40 s, the relative ratio of SiO_y peak to both total Si and O peak increases, indicating that SiO_y exists at the interface region between the Hf film and the Si substrate. This behavior can be explained by two dimensional growth mode of Hf layer since the area of interfacial SiO_y increases as the Hf deposition time increases. Between 40 s and 60 s, the relative ratio of the SiO_y peak to both total Si and O peak remains constant within ± 3 %. This behavior supports that the growth mode of Hf changes from two-dimensional to three-dimensional mode since the increase in area of interfacial SiO_y is compensated by the attenuation of photoelectrons from SiO_y by three-dimensional Hf islands.

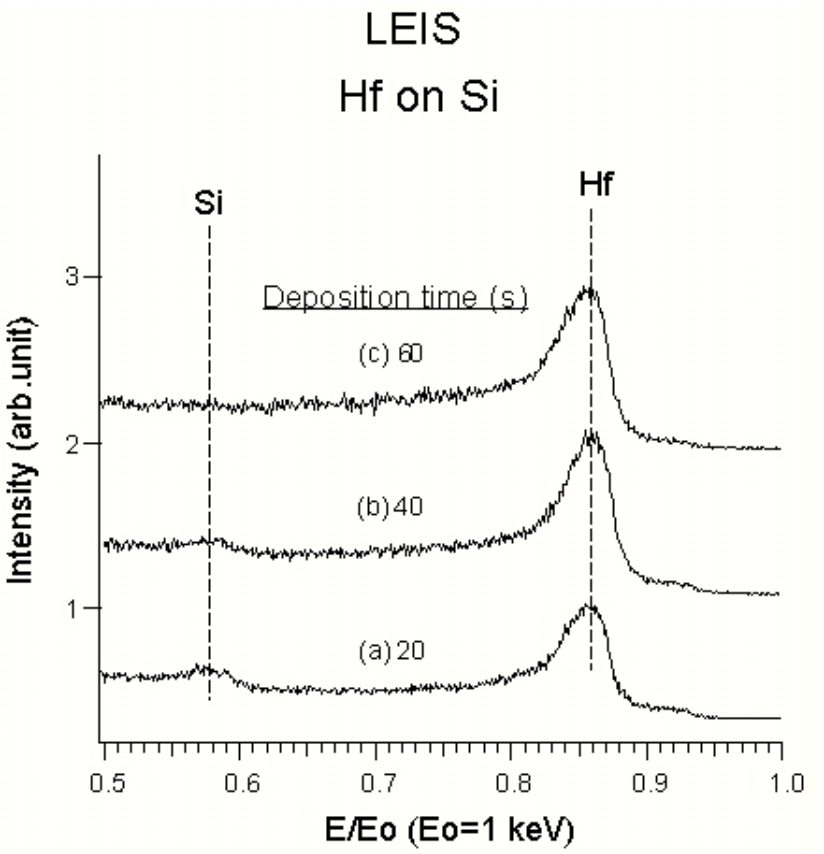

Fig. 4.3 LEIS data of Hf layer on Si substrate as a function of Hf deposition time.

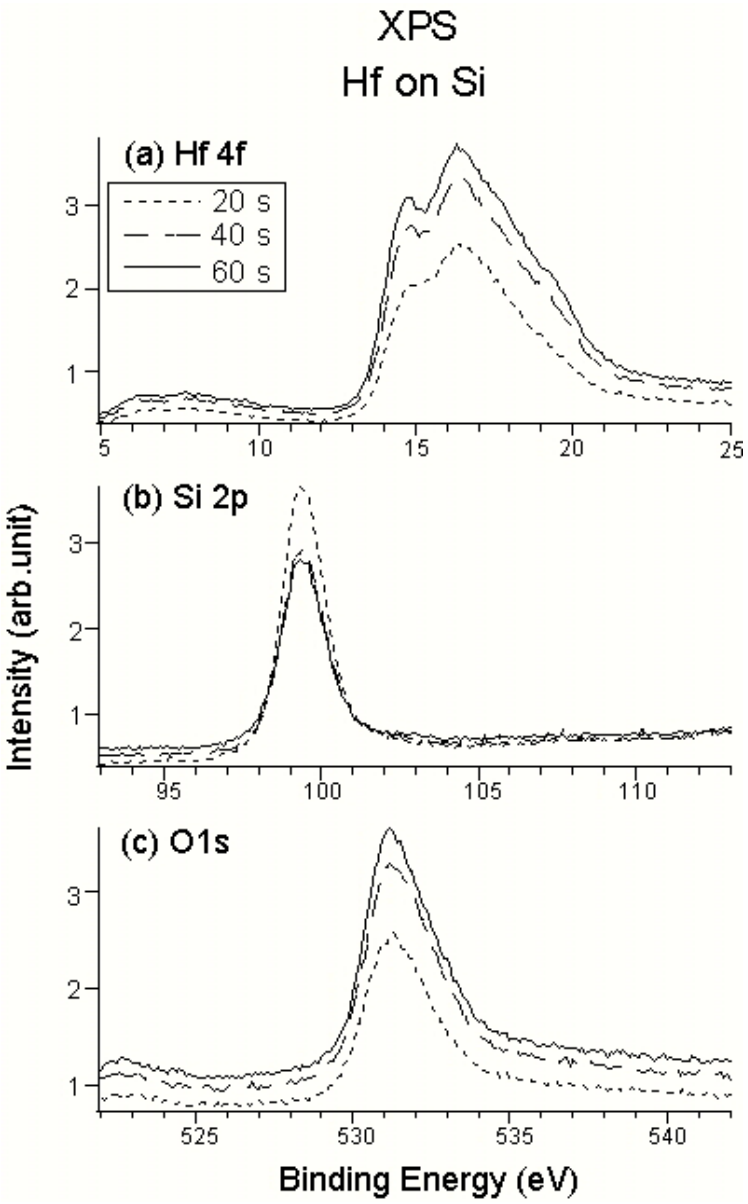

Fig. 4.4 XPS data of Hf 4f, Si 2p, O 1s of Hf layer on Si substrate as a function of Hf deposition time.

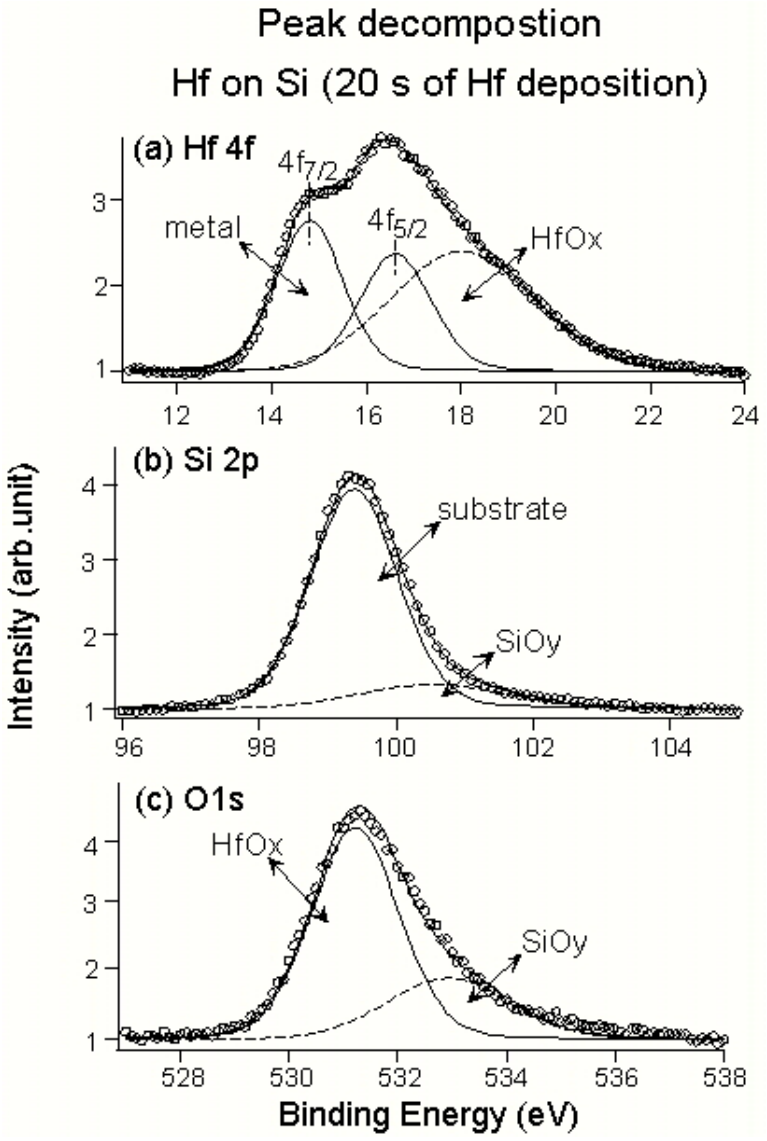

Fig. 4.5 Example of peak decomposition of Hf 4f, Si 2p, and O 1s from XPS data shown in Fig. 4.4

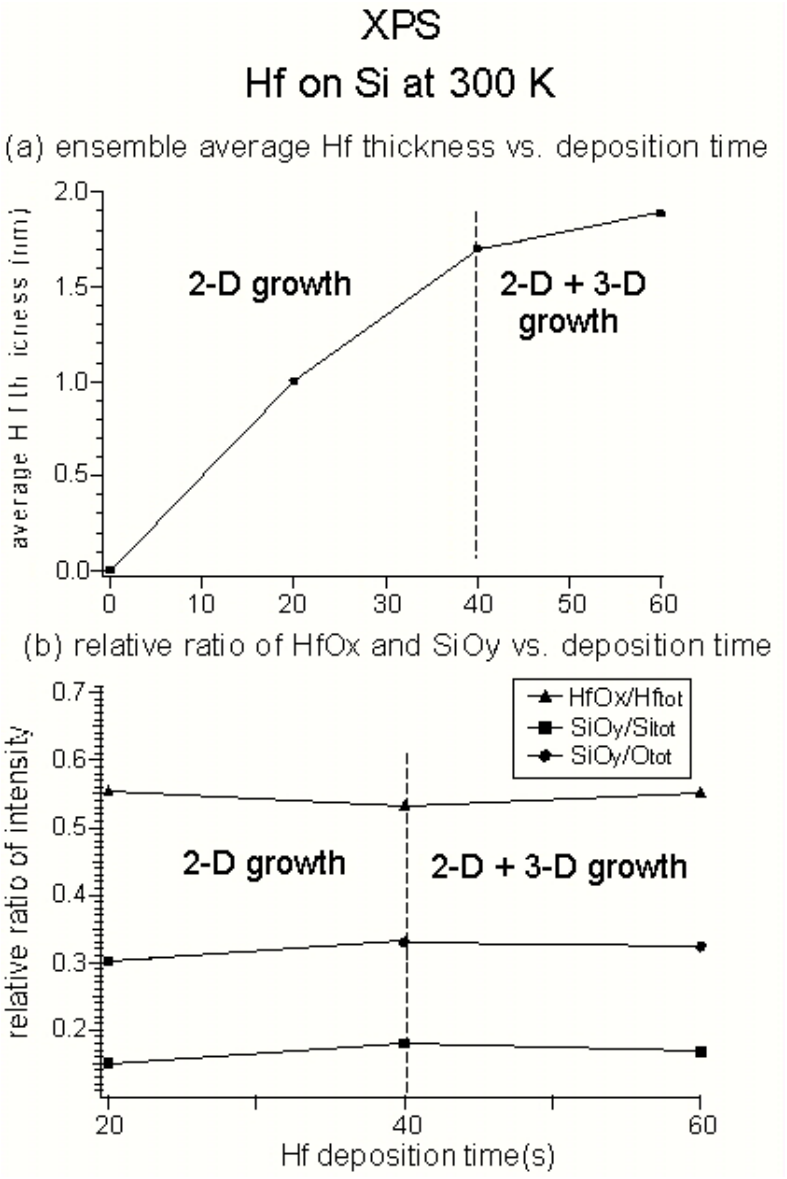

Fig. 4.6 Estimated ensemble average Hf thickness and relative ratio of HfO_x and SiO_y as a function of deposition time based on the result of peak decomposition.

4.3.1.3 HfO_2 on Si

Minimum oxygen plasma power was used to oxidize the Hf layer. The oxidation rate only depends on oxidation time. Fig. 4.7 shows the XP spectra of Hf 4f, Si 2p, and O 1s for various oxidation times. At 15 s, the whole Hf peak shifted toward fully oxidized hafnium but a low BE shoulder (~ 15 eV) remained. As oxidation time increased to 60 s, the low BE shoulder of Hf 4f peak totally vanished while the higher BE shoulder of Si 2p increased, indicating an increase in interfacial silicon oxide. In addition, O 1s peak position shifted toward higher BE.

Fig. 4.8 shows one example of XPS peak decomposition of Hf 4f, Si 2p, O 1 from XPS data shown in Fig. 4.7. The Peak decomposition procedure is same as explained in Fig. 4.5. The Hf 4f peak, (a), was decomposed with two peak sets corresponding to metallic Hf located at ~ 15.0 eV ($4f_{7/2}$) and HfO_2 located at ~ 18.0 eV ($4f_{7/2}$). The Si 2p peak, (b), was decomposed with three peaks corresponding to substrate Si and SiO_y located at ~ 101 eV (SiO_y^{I}) and ~ 102.5 eV (SiO_y^{II}; close to BE of SiO_2). The O 1s peak, (c), was decomposed with two peaks corresponding to HfO_2 located at ~ 531.5 eV and SiO_y located at ~ 533.0 eV. Compared to Hf on Si without oxygen (Fig. 4.5), there is a distinct feature in each spectrum: (1) in the Hf 4f spectrum, stoichiometric HfO_2 peak appears and the metallic peak intensity decreased; (2) in the Si 2p spectrum, an additional higher BE SiO_y peak appears (close to SiO_2) and the total SiO_y peak intensity

increased; and (3) in the O 1s spectrum, the BE of HfO_x shifted toward the higher BE side.

Fig. 4.9 shows the ensemble average HfO_2 thickness and intensity ratio of Hf metal and SiO_x as a function of oxidation time. In Fig. 4.9 (a), the ensemble average HfO_x thickness, including interfacial SiO_y, was estimated using the attenuation of Si substrate XPS peak area as described in Fig. 4.6 (a). In Fig. 4.9 (b), the intenisty ratio of Hf metal peak to total Hf peak area, SiO_y^{tot} (= SiO_y^{I} +SiO_y^{II}) peak area to total Si peak area, $SiOy^{II}$ peak area to SiO_y^{tot} peak area, and SiO_y^{tot} peak area to total O peak area were estimated from peak decomposition procedure as shown in Fig. 4.8. We divide oxidation process in two steps based on the oxidation rate of Hf metal. The first step is fast oxidation process and the second one is slow oxidation process. The first step, during the first 15 s of oxidation, the amount of Hf metal inside HfO_x film decreased from 45 % to 11 %, the amount of $SiOy^{tot}$ to total O peak area decreased from 33 % to 15 %, and another SiO_y^{II} peak appears in Si 2p spectra. The thickness of HfO_x increased from 1.8 nm to 2.8 nm and the atomic ratio of O to Si in SiO_y changed from 1.6 to 1.3. These changes imply that the supplied oxygen oxidized the Hf metal and it also oxidized interfacial Si substrate. The second stage, for the next 45 s of oxidation, the Hf film became fully oxidized and the amount of $SiOy^{tot}$ to both total Si peak and O peak increased by 65 % and 60 %, respectively. The thickness of HfO_2 increased from 2.8 nm to 3.6 nm and the atomic ratio of O to Si

in SiO_y changed from 1.3 to 1.4. Based on the XPS results, we observed that interfacial silicon was oxidized during the oxidation of Hf layer and the $SiOy^{II}$ peak (~ 102 eV) is nonstoichiometric silicon oxide, not from hafnium silicate, since there is no hafnium silicate peak in the Hf 4f spectra.

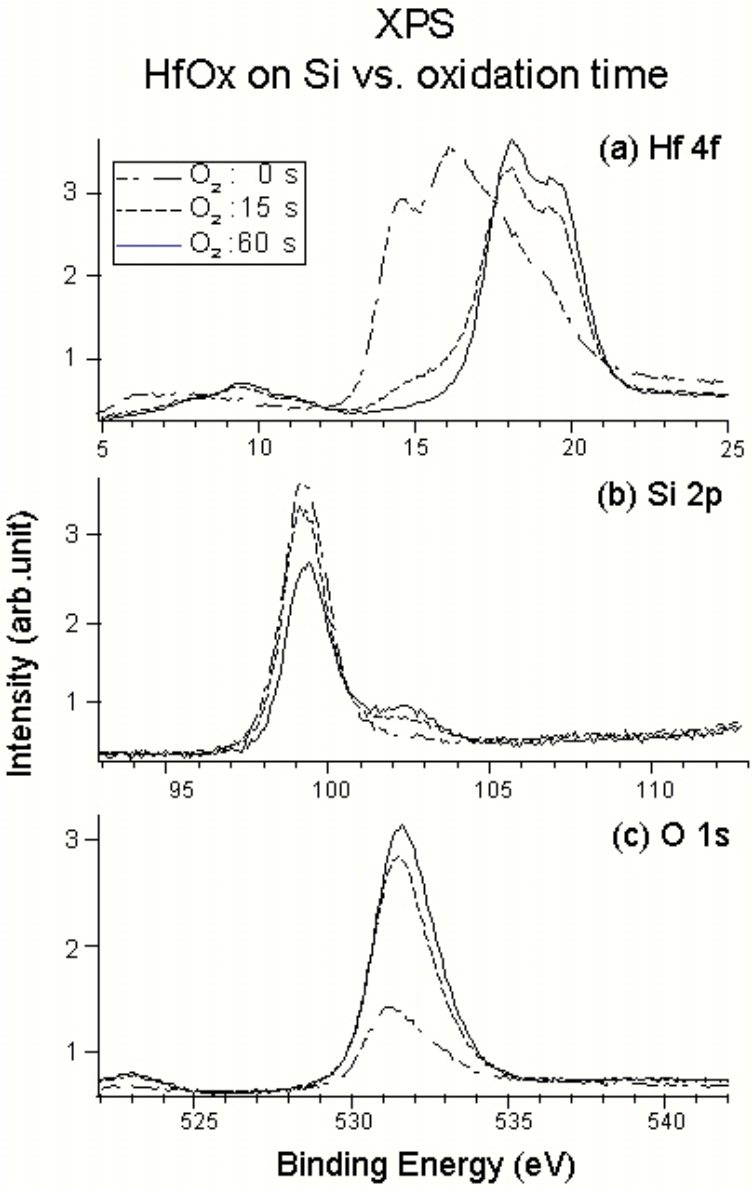

Fig. 4.7 XPS data of Hf 4f, Si 2p, and O 1s of HfO_x on Si for various oxidation times.

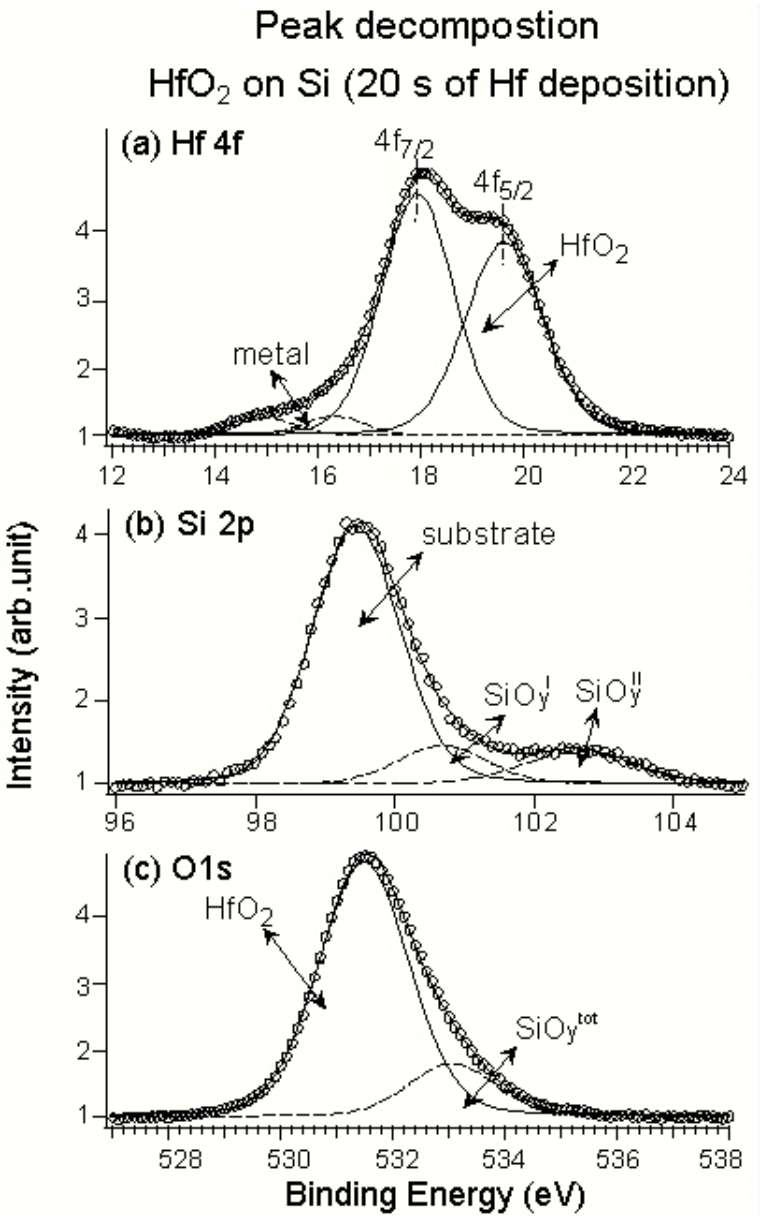

Fig. 4. 8 Example of peak decomposition result of Hf 4f, Si 2p, and O 1s from XPS data shown in Fig. 4.7

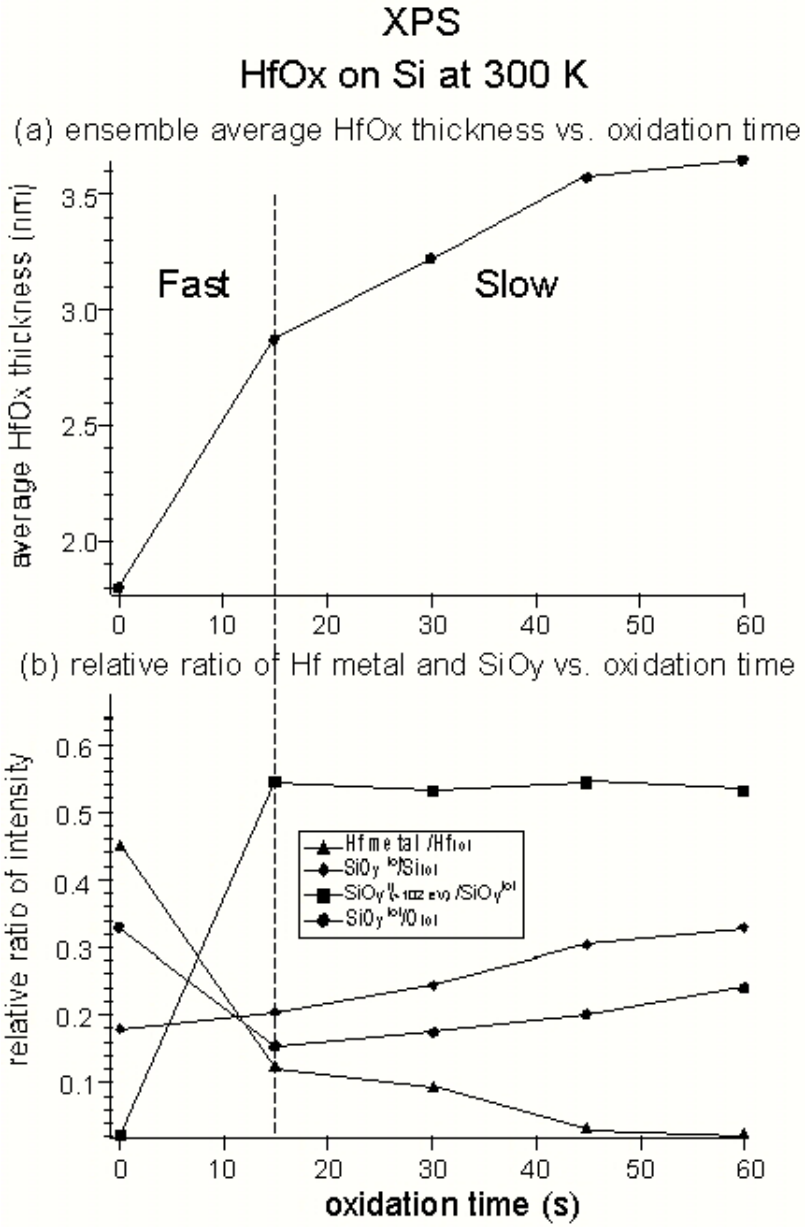

Fig.4.9 Estimated ensemble average HfOx thickness and the intensity ratio of HfO_x and SiO_y as a function of oxidation time based on the result of peak decomposition

4.3.2 At 823 K

To investigate the thermal annealing effect on nonstoichiometric silicon oxide and the formation of hafnium silicate, two different film structures were prepared and then XPS analysis was performed during vacuum annealing at 823 K for 35 min with maximum pressure ($\sim 4 \times 10^{-8}$ torr). In the first sample, A, a thin Hf layer fully covered Si surface; therefore, the Si surface was not exposed directly to oxygen during oxidation of the Hf layer. In the second one, B, the Si surface was not completely covered by Hf; therefore, the Si surface was exposed directly to oxygen during oxidation. In the case of sample A, Fig. 4.10 shows LEIS data of HfO_2 on Si at three stages: deposition of Hf on Si, oxidation of Hf layer, and after thermal annealing. The in-set figure shows the initial structure of Hf on Si before oxidation based on ISS data. Upon deposition of Hf on Si, (a), there is no Si peak, indicating that Hf fully covered the Si surface. After fully oxidation of the Hf layer and thermal annealing, (b) and (c), there is no Si peak but the intensity of the Hf peak decreased after annealing. There are two possible explanations for the decrease in Hf peak intensity: (1) carbon contamination increases, and (2) surface roughness increases. XPS data will help to decide which one is the major factor, since we can not distinguish between the two factors only from LEIS data. Fig. 4.11 shows the XPS data of HfO_2 on Si before and after thermal annealing. First of all, there is no change of FWHM of the Hf 4f peak, indicating that there is no change in chemical states each

element. Second, the peak area of Hf, Si, and O decreased while the C peak area increased. This suggests that the decrease of Hf peak area in LEIS data is due to an increase in surface carbon contamination. The change of peak area of nonstoichiometric silicon oxide in XPS data as a function of annealing time will be discussed with the results from sample B.

In the case of sample B, Fig. 4.12 shows LEIS data of HfO_2 on Si at the same three stages as in Fig. 4.10. The in-set figure shows the initial structure of Hf on Si before oxidation based on ISS data (a). Upon deposition of Hf on Si, (a), there is a Si peak, indicating that Hf did not completely cover the Si surface. After fully oxidation of the Hf layer and thermal annealing, (b) and (c), the Si was still present but the Hf peak intensity decreased after annealing. There are two possible explanations for the decrease of the Hf peak intensity, same as described above for sample A. Fig. 4.13 shows the XPS data of HfO_2 on Si before and after thermal annealing. The XPS data of Hf on Si (is not shown here) shows same features as shown in Fig. 4.4. The Hf layer and the Si substrate were partially oxidized. After oxidation, first, there is no change in FWHM of the Hf 4f peak, indicating there is no change in the chemical state of Hf. Second, the peak area of Hf, Si, and O decreased while the C peak intensity increased. This also suggests that the decrease of Hf peak area in LEIS data is due to increasing surface carbon contamination. The change of peak area of nonstoichiometric

silicon oxide in XPS data as a function of annealing time will be discussed with the result from sample A in the following paragraph.

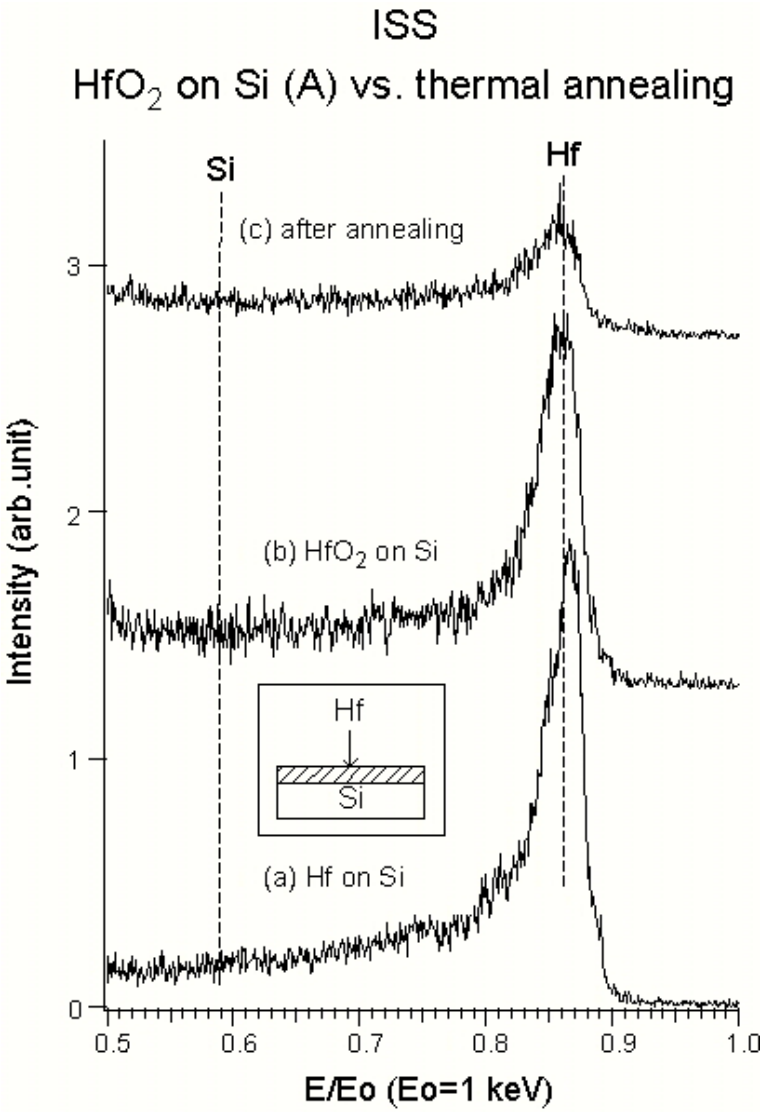

Fig. 4.10 LEIS data of HfO_2 on Si (sample A) corresponding to three steps: Hf on Si, oxidation of Hf layer, and after thermal annealing.

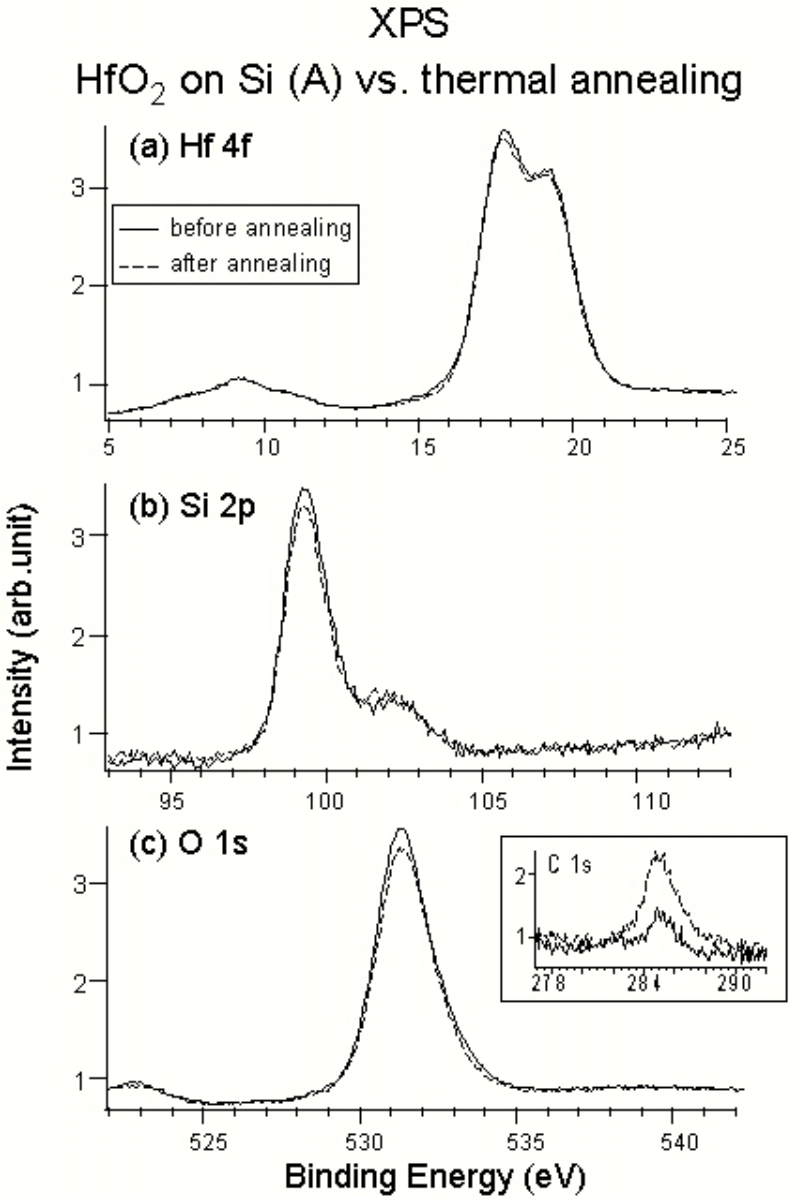

Fig. 4.11 XPS data of Hf 4f, Si 2p, O 1s, and C 1s from sample A before and after thermal annealing at 823 K.

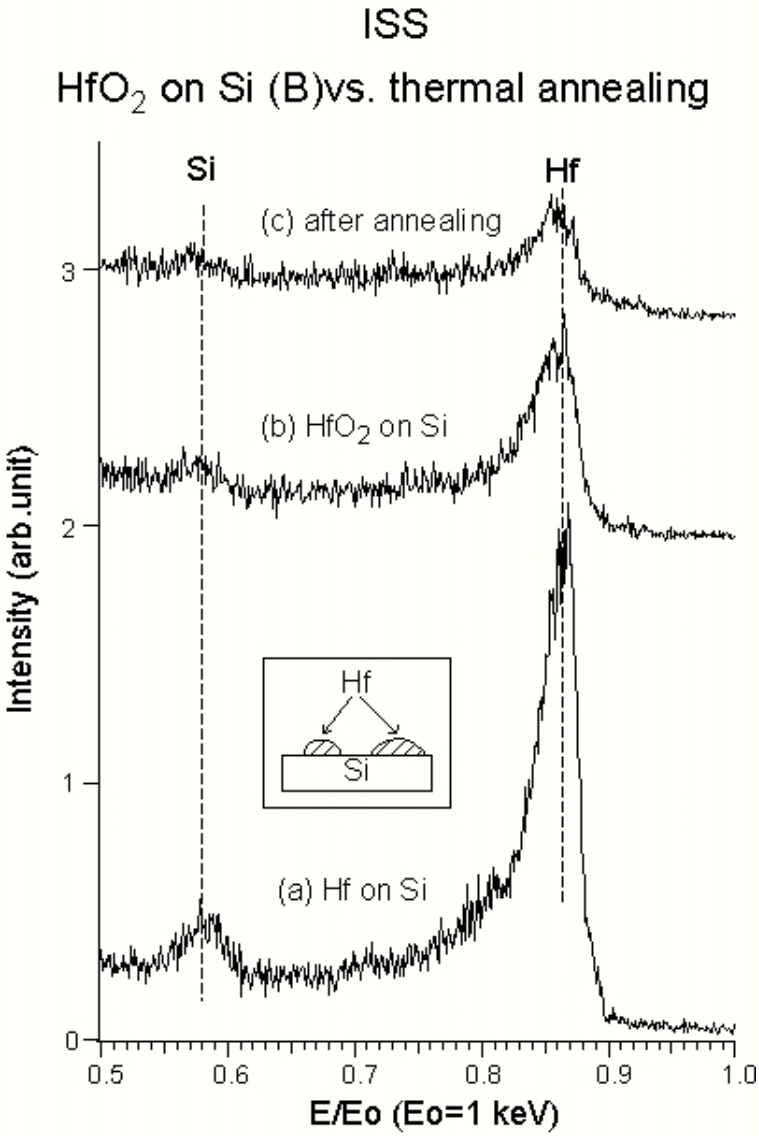

Fig. 4.12 LEIS data of HfO_2 on Si (sample A) corresponding to three steps: Hf on Si, oxidation of Hf layer, and after thermal annealing.

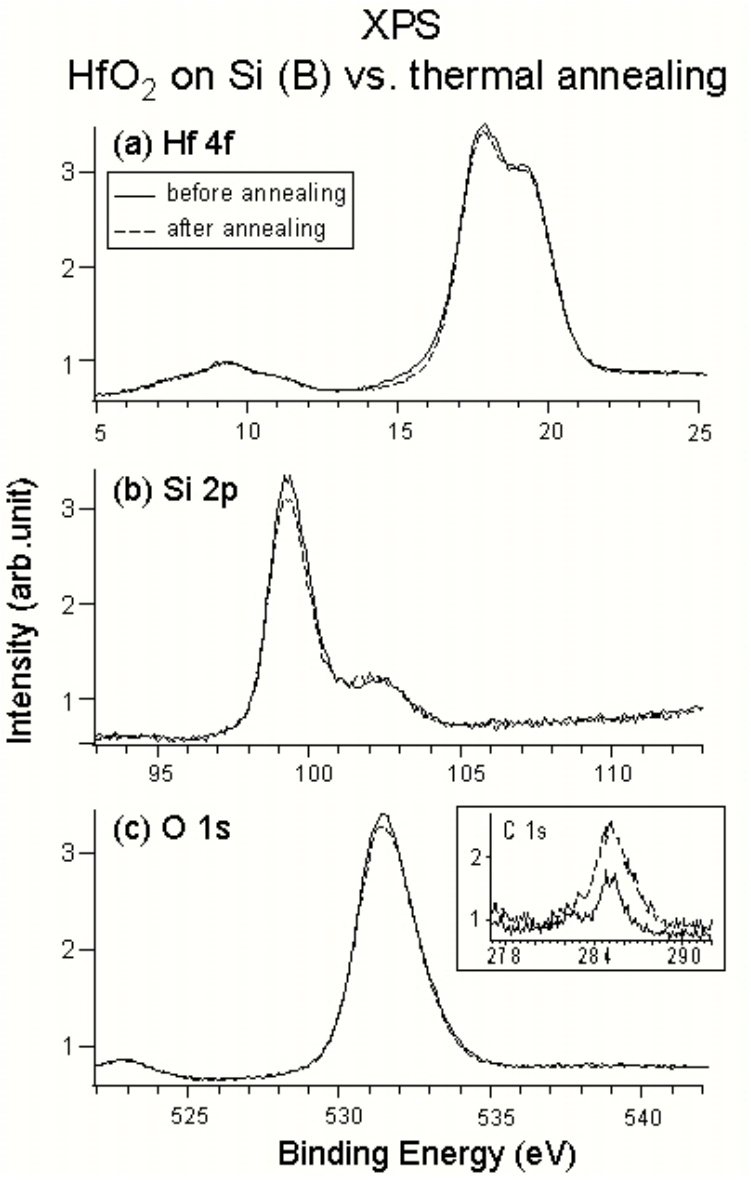

Fig. 4.13 XPS data of Hf 4f, Si 2p, O 1s, and C 1s from sample B before and after thermal annealing at 823 K

Fig. 4.14 shows one example of peak decomposition of Hf 4f, Si 2p, and O 1s from the XPS data shown in Figs 4.11 and 4.13. In Hf 4f spectra, there is no difference between the two samples. This indicates that both two samples are fully oxidized as HfO_2. In the Si 2p spectra, there is a difference between the two samples in SiO_y^{tot}. The relative ratio of SiO_y^{II} to SiO_y^{tot} of sample A is smaller than that of sample B. This difference can be explained by different structure of the two samples. In sample B, the Si substrate can be directly oxidized during oxidation of Hf layer, resulting in more formation of SiO_y^{II} than SiO_y^{I}. In the O 1s spectra, the BE of SiO_y^{tot} of sample A is lower than that of sample B, since the relative ratio of SiO_y^{II} in sample A is smaller than that of sample B.

Fig. 4.15 shows the amount of SiO_y inside HfO_2 film as a function of annealing time based on XPS peak decomposition shown in Fig. 4.14. When the two samples are compared, three distinctive features are observed in Fig. 4.15. First, the percentage of $SiOy^{tot}$ peak area to total Si pear area of sample A (a) and B (b) at 0 min are 31 % and 33 %, respectively. This indicates that the structure of sample A prevents the formation of SiO_y more than in sample B. Second, the percentage of $SiOy^{II}$ peak area to $SiOy^{tot}$ peak area of sample A (a) and B (b) at 0 min are 59 % and 67 %, respectively. This can be explained by different structures of the two samples as described in the previous paragraph. Third, there is an increase in the percentage of SiO_y^{tot} for the fist 9 min of annealing on

both samples while there is no change in the relative percentage of SiO_y^{II} in both samples. This increase in SiO_y^{tot} is due to an increase in carbon contamination. The relative portion of silicon oxide in the XPS detection range (~ 6 nm from the surface) increases since detection range shift upward due to the increase in carbon contamination. From the results of the annealing experiment for the two samples, we suggest that sample A (Si fully covered by Hf) prevents the formation of nonstoichiometric silicon oxide more than sample B (Si partially covered by Hf) and there is no formation of hafnium silicate at the interface between HfO_2 and nonstoichiometric silicon oxide during thermal annealing at 823 K.

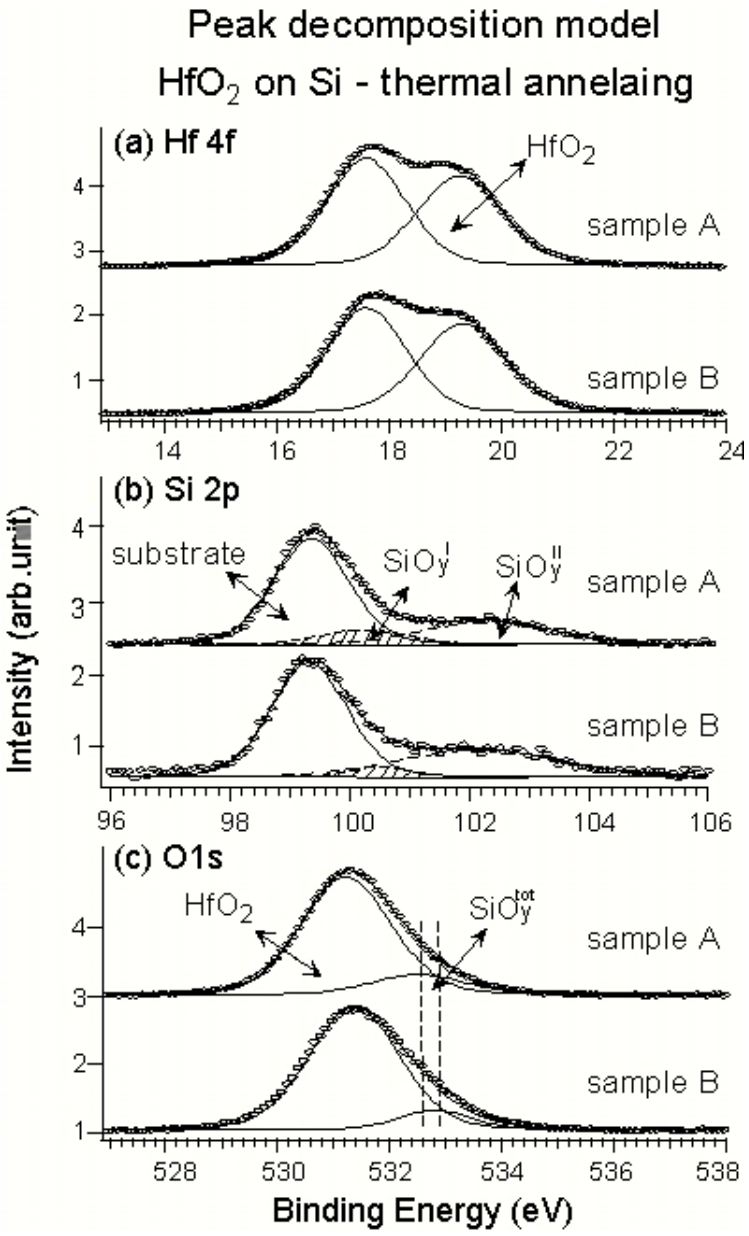

Fig. 4.14 Example of peak decomposition result of Hf 4f, Si 2p, and O 1s from XPS data shown in Figs. 4.11 and 4.13.

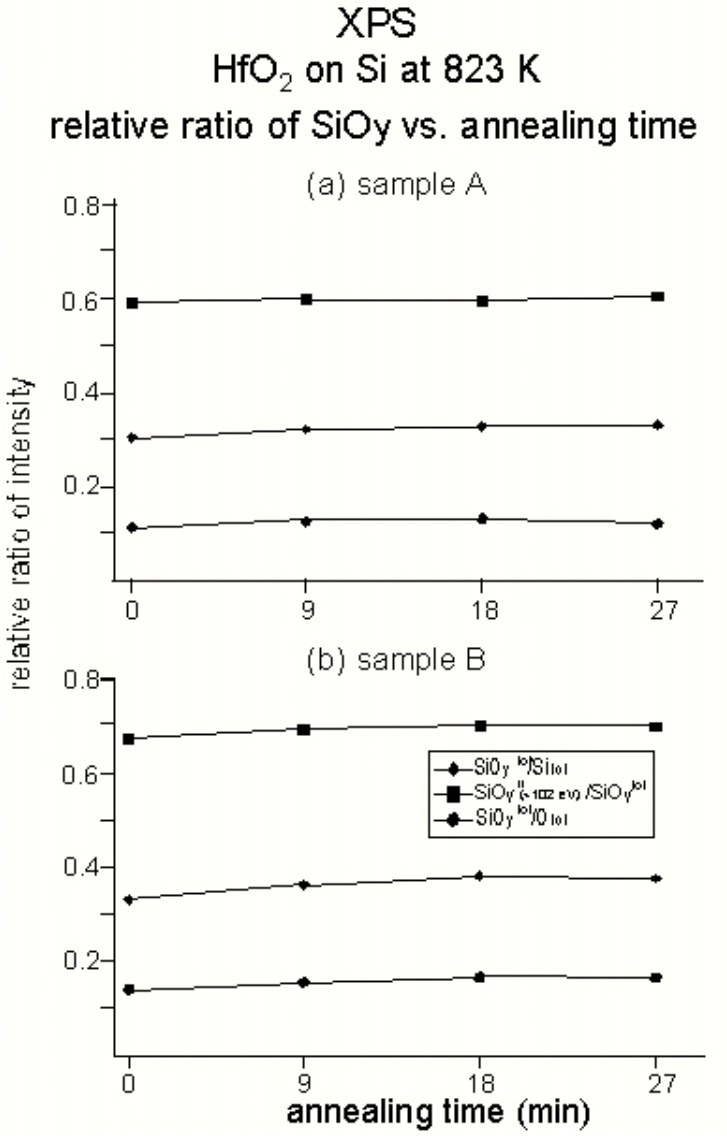

Fig. 4.15 the amount of SiO_y from sample A and B as a function of annealing time at 823 K.

4.3.3 Proposed model

Fig. 4.16 shows the proposed model of growth of HfO_2 on Si at 300 K with two different initial Hf/Si structures based on the XPS and LEIS results. There are two different samples, Hf layer completely covers the Si substrate in sample A and Hf layer partially covers the Si substrate, as shown in Figs. 4.11 and 4.13. Fig. 4.16 (a) shows the growth of Hf layer on Si substrate at 300 K. In both samples, the Hf layer and Si substrate are partially oxidized, i.e., there is formation of nonstoichiometric silicon oxide, SiO_y^I. Importantly, there is no hafnium silicide formation based on the XPS results. Our observation is consistent with previous studies on the initial hafnium silicide formation [10, 11]. Shinkai *et al.* reported that the minimum vacuum annealing temperature for hafnium silicide formation after deposition of Hf film (100 nm) on Si substrate is 693 K [11]. After oxidation of the Hf layer, Fig. 16 (b), the two samples show different interfacial silicon oxide formation. After the oxidation process, in both samples another nonstoichiometric silicon oxide peak (SiO_y^{II}) appears in the Si 2p spectra and its BE is higher than SiO_y^I but lower than SiO_2, as shown in Fig. 4.14. This SiO_y^{II} suggests oxidation of Hf layer and Si substrate during the oxidation process. From the point of view of formation of SiO_y, the ratio of the total amount of SiO_y^{tot} peak area to total Si peak area in sample A is smaller than in sample B, as shown in Fig. 4.15. This indicates that the Hf layer in sample A plays the role of a barrier layer for the oxidation of the Si substrate, although the

Hf layer does not prevent the oxidation of Si substrate totally. In addition, the relative amount of SiO_y^{II} to SiO_y^{tot} in sample A is smaller than in sample B. This also supports that the Si substrate in sample B (not covered by Hf layer) is directly oxidized during the oxidation process.

During vacuum annealing at 823 K, there is no change in the chemical states of Hf, Si, and O in both samples as shown in Figs. 4.11, 4.13, and 4.15. Based on the results from vacuum annealing, we suggest that the interfacial hafnium silicate between HfO_2 and nonstoichiometric silicon oxide / Si (100) was not formed during vacuum annealing at 823 K. This means that HfO_2 is thermodynamically stable upon contact with nonstoichiometric silicon oxide at 823 K.

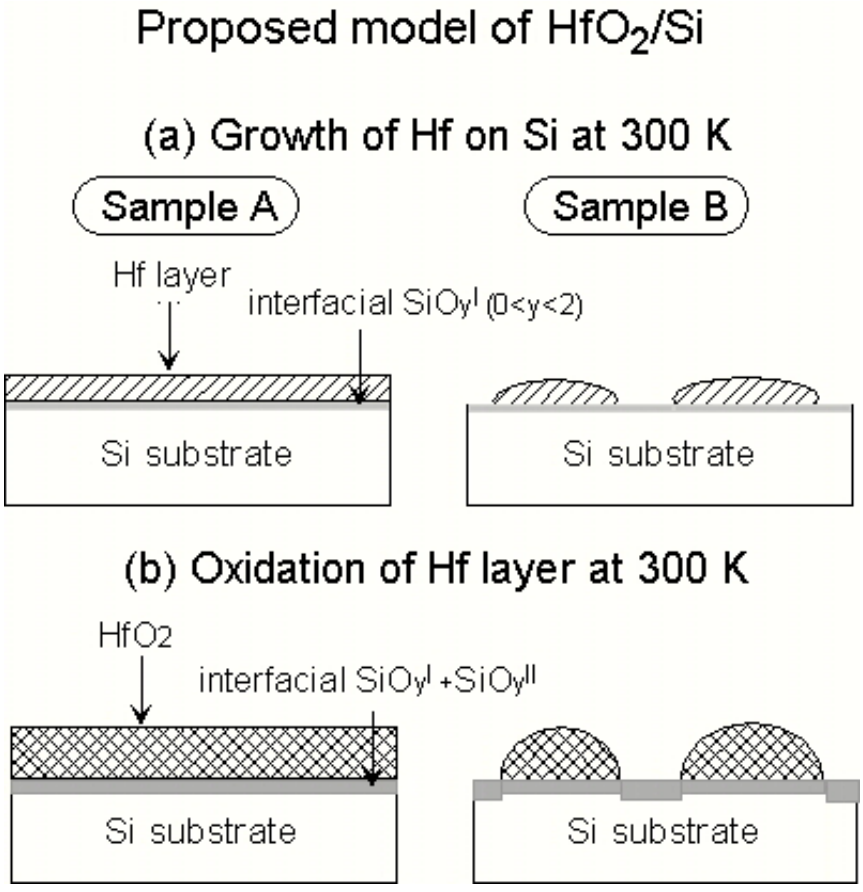

Fig. 4.16 Proposed model of growth of HfO_2 on Si at 300 K according to two different structures.

4.4 CONCLUSION

Various compositions of hafnium silicide and hafnium silicate on Cu substrate, and growth and thermal annealing of HfO_2 on Si (100) were investigated using *in-situ* physical vapor deposition (PVD), *in-situ* X-ray photoelectron spectroscopy (XPS) and *in-situ* low energy ion scattering (LEIS). A CO_2 laser beam was used to heat the sample in order to obtain XPS data at high temperature (823K). XPS spectra of various compositions of hafnium silicide and hafnium silicate were grown on Cu substrate to obtain standard binding energy in XPS spectra with various compositions. The deposition of Hf layer on Si substrate followed by oxidation of the Hf layer was used to minimize the formation of interfacial silicon oxide. There is no hafnium silicide formation during deposition of Hf layer on Si (100). During vacuum annealing at 823 K, there is no change in the chemical states of elements and no evidence for the formation of hafnium silicate at the interface between HfO_2 and nonstoichiometric silicon oxide. Based on the result of thermal annealing, we suggest that HfO_2 is thermodynamically stable upon contact with nonstoichiometric silicon oxide at 823 K

4.5 REFERENCES

[1] K.J. Hubbard and D.G. Schlom. J. Mater. Res. 11(11) (1996) 2757

[2] B. H. Lee, L. Kang, W-J Qi, R. Nieh, Y. Jeon, K. Onishi, and J. C. Lee, IEDM, (1999) 133

[3] S.P. Murarka and C.C. Chang, Appl. Phys. Lett. 37(7) (1980) 639

[4] V. Cosnier, M. Olivier, G. Thrét, and B. André, J. Vac. Sci. Tchnol. A 19(5) (2001) 2267

[5] H.J. Park, A. Mao, D.-L. Kwong, and J. M. White, J. Vac. Sci. Techol. A 18(5) (2000) 2522

[6] Y.-M Sun, J. Lozano, H. Ho, H.J. Park, S. Veldman, J.M. White, Appl. Surf.Sci. 161 (2000) 115

[7] Q. Wang, Y.-M. Sun, W. Zhao, J. Campagna, J. M. White, submitted to Review of Scientific Instruments

[8] J. F. Moulder, W. F. Stickle, P. E. Sobol, and K. D. Bomben, *Handbook of X-ray Photoelectron Spectroscopy* (Physical Electronics, Inc. Eden Prairie, MN, 1995)

[9] A.Y.Mao, K.-A.Son, D.A.Hess, L.A. Brown, J.M.White, D.L. kwong, D.A. Roberts, R.N.Vritis, Thin Solid Films 349 (1999) 230

[10] S. Zaima, N. Wakai, T. Yamauchi, and Y. Yasuda, J. Appl. Phys. 74 (1993) 6703

[11] S. Shinkai, K. Sasaki, Y. Abe, and H. Yanagisawa, Jpn. J. Appl. Phys. 37 (1998) Part 1, 2002.

References

Chapter 1

[1] T. Hori “Gate Dielectrics and MOS ULSIs”, Springer Series in Electronics and Photonics, Vol. 34, Springer, 1997

[2] C.T. Liu, Technical Digest of IEDM, (1998) 747.

[3] D.A. Buchanan, IBM J. Res. Develop., Vol 43, Iss 3, (1999) 245

[4] Y. Wu and G. Lucovsky, IEEE Electron Device Lett. Vol. 19, (1998) 367

[5] X. W. Wang, Y Shi, and T.P. Ma, VLSI Symp. Tech. Dig, (1995) 109

[6] Y. Abe, M. Kawamrua, and K. Sasaki, Jpn. J. Appl. Phys., Vol.36, Part I, (1997) 5175

[7] R.A. Mckee, F.J.Walker, and M.F. Chisholm, Phys. Rev. Lett. Vol. 81, (1998) 3014

[8] H. Luan, S. Lee, S. Song, Y. Mao, Y. Senaki, D. Roberts, and D.Kwong, Technical Digest of IEDM, (1999) 141

[9] D. Wicaksana, A. Kobayashi, and A. Kinbara, J. Vac. Sci. Tchnol. A 10(4) (1992) 1479

[10] W. J. Qi, Nieh, B.H.Lee, L.G. Kang, Y. Jeon, K. Onishi, T. Ngai, S. Banerjee, and J.C. Lee, Technical Digest of IEDM (1999) 145.

[11] L. Kang, B. Hun Lee, W.J. Qi, Y. Jeon, R. Nieh, S. Gopalan K. Onishi, and J.C.Lee, IEEE Electron Dev. Lett., Vol. 21, No. 4 (2000) 181

[12] L. Manchanda, W.H.Lee, J.E. Bower, F.H.Baumann, W.L.Brown, C. J.Case, R.C. Keller, Y.O. Kim, E.J. Laskowski, M. D. Morris, R.L. Opila, R.J. Silverman, T.W.Sorsch, and G.R.Weber, Technical Digest of IEDM (1998) 605

[13] L. Mannchanda, M. Gurvitch., IEEE Electron Dev. Lett. Vol.9 (1988) 180

[14] G.D. Wilk, R.M. Wallace, and J.M. Anthony, J. Appl. Phys., Vol. 87, No. 1 (2000) 484.

[15] M. Balog and M. Schieber, Thin Solid Films, Vol.41 (1997) 247

[16] H. Arashi, J. Am. Cera. Soc., Vol 75, (1992) 844.

[17] H. Treichel, A. Mitwalsky, G. Tempel, G. Zorn, D.A. Bohling, K.R. Coyle, B.S. Felker, M. George, W. Kern, A.P. Lane, N.P. Sandler, Advanced Materials for Optics and Electronics, Vol.5 (1995) 163

[18] J. Li, T. E. Seidel, and J. W. Mayer, MRS Bulletin, August, (1994) 15

[19] Y. Arita, Semiconductor World, December (1993) 158

[20] M. Schick, Les Houches, Session XL VIII, Liquids at Interfaces (1990) 415

[21] U. Diebold, J.-M Pan, T. E. Madey, Surf. Sci. 287/288 (1993) 896

[22] S.H. Overbury, P.A. Bertrand, and G.A.Somorjai, Chem, Rev. 75 (1975) 547.

[23] Q. Wang, Y.-M. Sun, W. Zhao, J. Campagna, J. M. White, submitted to Review of Scientific Instruments

[24] J. F. Moulder, W. F. Stickle, P. E. Sobol, and K. D. Bomben, *Handbook of X-ray Photoelectron Spectroscopy* (Physical Electronics, Inc. Eden Prairie, MN, 1995)

[25] H. Niehus, W. Heiland, and E. Taglauer, Surf. Sci. Rep. 17 (19930 213

[26] D.P.Smith, J. Appl. Phys. 18 (1967) 340

Chapter 2

[1] U. Diebold, J.-M Pan, T. E. Madey, Surf. Sci. 287/288 (1993) 896

[2] D. A. Chen, M. C. Bartelt, R. Q. Hwang, K.F. Macarty, Surf. Sci. 450 (2000) 78

[3] Q. Ge, P. Møller, Thin Solid Films 254 (1995) 10

[4] X. Xu, J.-W. He, D.W. Goodman, Surf. Sci. 284 (1993) 103

[5] Y. Wu, E. Garfunkel, T. E. Maday, J. Vac. Sci. Technol. A 14 (1996) 1662

[6] M-C Wu, D. W. Goodman, J. Phys. Chem. 98 (1994) 9874

[7] Jian Li, Tom E. Seidel, Jim W. Mayer, MRS bulletin/August (1994) 15

[8] M. Balog and M. Schieber, Thin Solid Films 41, 247 (1977)

[9] K.J. Hubbard and D.G. Schlom. J. Mater. Res. 11(11), 2757 (1996)

[10] A. W. Adamson, “Physical Chemistry of Surfaces”, New York (1990)

[11] S. H. Overbury, P. A. Bertrand, G. A. Somorjai, Chem. Rev. 75 (1975) 547

[12] Y. -M Sun, J. Lozano, H. Ho, H. J. Park, S. Veldman, J. M. White, Appl. Surf. Sci. 161 (2000) 115

[13] W. F. Egelhoff, Jr., Surf. Sci. Rep. 6 (1987) 253

[14] Ihsan Barin, Gregor Platzki, "Thermochemical Data of Pure Substances", 3rd edition, VCH Inc., (1995)

[15] A.Y.Mao, K.-A.Son, D.A.Hess, L.A. Brown, J.M.White, D.L. kwong, D.A. Roberts, R.N.Vritis, Thin Solid Films 349 (1999) 230

[16] S. Tanuma, C. J. Powell, Surf. Interface Anal. 17(13) (1991) 911

Chapter 3

[1] U. Diebold, J.-M Pan, T. E. Madey, Surf. Sci. 287/288 (1993) 896

[2] D. A. Chen, M. C. Bartelt, R. Q. Hwang, K.F. Macarty, Surf. Sci. 450 (2000) 78

[3] Q. Ge, P. Møller, Thin Solid Films 254 (1995) 10

[4] X. Xu, J.-W. He, D.W. Goodman, Surf. Sci. 284 (1993) 103

[5] Y. Wu, E. Garfunkel, T. E. Maday, J. Vac. Sci. Technol. A 14 (1996) 1662

[6] M-C Wu, D. W. Goodman, J. Phys. Chem. 98 (1994) 9874

[7] G. D. Wilk, R. M. Wallace, J. M. Anthony, J. Appl. Phys. 87 (2000) 484

[8] H. J. Park, Y.-M. Sun, H. Troiani, P. Santiago, M. J. Yacaman, J. M. White, *submitted to* Surface Science

[9] A. W. Adamson, "*Physical Chemistry of Surfaces*", New York (1990)

[10] S. H. Overbury, P. A. Bertrand, G. A. Somorjai, Chem. Rev. 75 (1975) 547

[11] Y. -M Sun, J. Lozano, H. Ho, H. J. Park, S. Veldman, J. M. White, Appl. Surf. Sci. 161 (2000) 115

[12] Q. Wang, Y.-M. Sun, W. Zhao, J. Campagna, J. M. White, submitted to Review of Scientific Instruments

[13] A. Y. Mao, K.-A. Son, D. A. Hess, L. A. Brown, J. M. White, D. L. Kwong, D. A. Roberts, R. N. Vritis, Thin Solid Films 349 (1999) 230

[14] W. F. Egelhoff, Jr., Surf. Sci. Rep. 6 (1987) 253

[15] S. Tanuma, C. J. Powell, Surf. Interface Anal. 17(13) (1991) 911

Chapter 4

[1] K.J. Hubbard and D.G. Schlom. J. Mater. Res. 11(11) (1996) 2757

[2] B. H. Lee, L. Kang, W-J Qi, R. Nieh, Y. Jeon, K. Onishi, and J. C. Lee, IEDM, (1999) 133

[3] S.P. Murarka and C.C. Chang, Appl. Phys. Lett. 37(7) (1980) 639

[4] V. Cosnier, M. Olivier, G. Thrét, and B. André, J. Vac. Sci. Tchnol. A 19(5) (2001) 2267

[5] H.J. Park, A. Mao, D.-L. Kwong, and J. M. White, J. Vac. Sci. Techol. A 18(5) (2000) 2522

[6] Y.-M Sun, J. Lozano, H. Ho, H.J. Park, S. Veldman, J.M. White, Appl. Surf.Sci. 161 (2000) 115

[7] Q. Wang, Y.-M. Sun, W. Zhao, J. Campagna, J. M. White, submitted to Review of Scientific Instruments

[8] J. F. Moulder, W. F. Stickle, P. E. Sobol, and K. D. Bomben, *Handbook of X-ray Photoelectron Spectroscopy* (Physical Electronics, Inc. Eden Prairie, MN, 1995)

[9] A.Y.Mao, K.-A.Son, D.A.Hess, L.A. Brown, J.M.White, D.L. kwong, D.A. Roberts, R.N.Vritis, Thin Solid Films 349 (1999) 230

[10] S. Zaima, N. Wakai, T. Yamauchi, and Y. Yasuda, J. Appl. Phys. 74 (1993) 6703

[11] S. Shinkai, K. Sasaki, Y. Abe, and H. Yanagisawa, Jpn. J. Appl. Phys. 37 (1998) Part 1, 2002.

VITA

Hyun Jung Park was born in Seoul, Republic Korea, on September 5, 1970, a daughter of Moontae Park and Moonja Hong. She received the Bachelor of Science degree and the Master of Science degree both in Physics from Ehwa Woman's University in February 1994 and February 1996, both in Seoul, Republic of Korea, respectively. She worked at Science and Technology Center of Ewha Woman's Universtiy from 1996 to 1997 as research assistant. She entered the Ph. D program of Materials Science and Engineering program at the University of Texas at Austin in Fall, 1997. She worked at Physical Science Research Laboratory at Motorola for summer internship in 2000. During her Ph.D. studies, she contributed the following research publications:

[1] "Interfacial silicon oxide formation during synthesis of ZrO_2 on Si (100)", Y. Sun, H. Ho, S. Veldman, J. Lozano, H. J. Park, and J.M white, Appl. Surf. Sci**.** 161 (2000) 115

[2] "Interfacial silicon oxide formation during oxygen annealing of Ta_2O_5 thin films on Si: Oxygen isotope labeling", H. J. Park, A. Mao, D.-L. Kwong, and J. M. White, J. Vac. Sci. Technol. A 18(5) (2000) 2522

[3] "Growth and thermal annealing of Cu on HfO_2", H. J. Park, Y.-M Sun, H. Troiani, P.Santiago, M.J.Yacaman, J. M. White, accepted to be published in Surface Science

[4] "Growth and thermal annealing of Cu on $HfSiO_4$ ", H. J. Park**,** Y.-M Sun, J. Lozano, J. M. White, in preparation

[5] “ Growth and thermal annealing of HfO_2 and Si (100)”, H. J. Park, Y.-M Sun, J. M White, in preparation

Permanent address: Sechogu Jamwongdong Shinbanpo Apt. 338-702, Seoul, Republic of Korea

This dissertation was typed by Hyun Jung Park